

Copy No. _____



Defence Research and
Development Canada Recherche et développement
pour la défense Canada



Estimating Drag Forces on Submarine Hulls

*Christopher Baker
University of New Brunswick*

*University of New Brunswick
Department of Mechanical Engineering
PO Box 440, Fredericton, NB
E3B 5A3*

Contract Number: W7707-03-2135

Contract Scientific Authority: George D. Watt (902) 426-3100 ext 381

The scientific or technical validity of this Contract Report is entirely the responsibility of the contractor and the contents do not necessarily have the approval or endorsement of Defence R&D Canada.

Defence R&D Canada – Atlantic

Contract Report
DRDC Atlantic CR 2004-125
September 2004

Canada

This page intentionally left blank.

Estimating Drag Forces on Submarine Hulls

Christopher Baker
University of New Brunswick

University of New Brunswick
Department of Mechanical Engineering
Box 440, Fredericton, NB
E3B 5A3

Contract number: W7707-3-2135

Contract Scientific Authority: George D. Watt, 426-3100 Ext. 381

The scientific or technical validity of this Contract Report is entirely the responsibility of the contractor and the contents do not necessarily have the approval or endorsement of Defence R&D Canada.

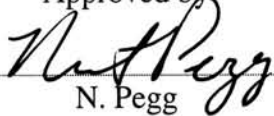
Defence R&D Canada – Atlantic

Contract Report

DRDC Atlantic CR 2004-125

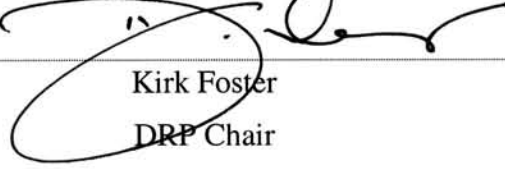
September 2004

Approved by


N. Pegg

Head/Warship Performance

Approved for release by


Kirk Foster
DRP Chair

University of New Brunswick Disclaimer

The following is a student report prepared for partial academic credit in the senior Project course ME4853. Its content is entirely the responsibility of the student and in no way do the findings or conclusions represent the opinion of the University.

- © Her Majesty the Queen as represented by the Minister of National Defence, 2004
- © Sa majesté la reine, représentée par le ministre de la Défense nationale, 2004

Abstract

This report describes a methodology for completing simulations of flow around a standard bare submarine hull using CFX-5. The simple case of zero yaw is used to demonstrate the process used to set up, run and analyze a simulation. The process of creating the geometry, mesh generation, boundary condition application, solution control and post processing is described. Particular emphasis is placed on building a high quality unstructured mesh for resolving boundary layer flows. Subsequently images of the mesh and results are shown to further the understanding of how to model a domain effectively and efficiently. Efforts to ensure a mesh insensitive solution are shown. Final values are validated against wind tunnel testing.

Résumé

Ce rapport décrit une méthode visant à achever les simulations de l'écoulement autour d'une coque de sous-marin standard nue à l'aide du programme CFX-5. Le cas simple correspondant à zéro embardée est utilisé afin de démontrer le procédé utilisé pour établir, mettre à l'essai et analyser une simulation. Le procédé de création de géométrie, de production de treillis, d'application de conditions limites, de contrôle de solution et de post-traitement est décrit. On accorde une attention particulière à la construction d'un treillis non structuré de haute qualité pour résoudre le problème des écoulements dans les couches limites. Par la suite, des images du treillis et des résultats seront indiqués afin de mieux comprendre comment modéliser un modèle de manière efficace. Des efforts visant à obtenir une solution ne tenant pas compte du treillis sont indiqués. Les valeurs finales sont validées et comparées aux résultats des essais en soufflerie.

Cette page est laissée vide délibérément.

Executive summary

Introduction

DRDC Atlantic is collaborating with UNB on developing a method for estimating the hydrodynamic forces on unappended submarine hulls. These forces are highly viscous and nonlinear in nature and no satisfactory method exists for quickly estimating their magnitudes with reasonable accuracy. The objective of this collaboration is to devise such an estimation method using the Reynolds Averaged Navier-Stokes (RANS) code CFX-5 to rapidly investigate the physics associated with the problem.

Principle Results

This report represents preliminary work carried out to investigate some of the basic problems associated with the RANS calculations. Grid generation and the sensitivity of the results to the grid has been well studied for the zero incidence problem.

Significance of Results

This work paves the way for more advanced calculations that will take place during the author's master's degree program.

Future Plans

The author will continue this work over the next couple of years, refining and validating the RANS calculations and extending them to nonzero flow incidence angles and, possibly, rotation problems. Another student will use these calculations as the basis for developing the force estimation method.

Baker, C., 2004; Estimating Drag Forces on Submarine Hulls; DRDC Atlantic CR 2004-125; Defence R&D Canada – Atlantic.

Sommaire

Introduction

Le RDDC Atlantique collabore actuellement avec l'UNB dans le but d'élaborer une méthode d'estimation des forces hydrodynamiques appliquées sur des coques de sous-marins sans surveillance. Ces forces sont par nature hautement visqueuses et non linéaires et il n'existe actuellement aucune méthode satisfaisante permettant d'estimer rapidement leur importance avec une exactitude raisonnable. L'objectif de cette collaboration consiste à concevoir une méthode d'estimation utilisant le programme CFX-5 avec des équations de Navier-Stokes à moyenne de Reynolds (RANS) afin de pouvoir examiner rapidement les aspects physiques du problème.

Principaux résultats

Ce rapport représente les travaux préliminaires réalisés dans le but d'étudier certains des problèmes associés aux calculs RANS. La génération d'un grillage a été bien étudiée pour ce qui est du problème à incidence nulle.

Importance des résultats

Ces travaux poseront les premiers jalons des calculs plus approfondis qui feront l'objet du programme de maîtrise de l'auteur.

Plans à venir

L'auteur poursuivra ces travaux au cours des deux prochaines années environ, de manière à perfectionner et à valider les calculs RANS et à les adapter aux angles d'incidence dans des conditions d'écoulement non nulles et possiblement dans des conditions de rotation. Un autre étudiant utilisera ces calculs comme fondement pour l'élaboration de la méthode d'estimation des forces.

Baker, C.; 2004; *Estimating Drag Forces on Submarine Hulls*; RDDC Atlantique CR 2004-125; R & D pour la défense Canada – Atlantique.

ACKNOWLEDGMENTS

I would like to extend my thanks and appreciation to Dr. Andrew Gerber for his help and guidance while acting as my Advisor. His direction in the use of CFX-5 and help with the fluid dynamics aspect of the problem has been of paramount importance in completing this project.

I would also like to extend to my thanks and appreciation to Dr. Gordon Holloway for his insight into the fluid dynamics aspect of the problem while acting as my Advisor. His direction was invaluable to relating this project to fluid flow theory.

To finish I would like to thank my family, Ray, Betsy, Tracey and Mike, and to Michelle Wheaton, Shaun Lingley, Shaun Nadeau and Marc Duguay for their help throughout this project.

TABLE OF CONTENTS

ABSTRACT	i
ACKNOWLEDGMENTS	v
TABLE OF CONTENTS.....	vi
LIST OF FIGURES	viii
LIST OF TABLES	x
Chapter 1	1
INTRODUCTION.....	1
1.1 Computational Fluid Dynamics in Research and Development	2
1.2 Project Objectives.....	2
Chapter 2	4
THEORY	4
2.1 Reynolds Number and Fluid Dynamics Basics	4
2.2 Drag Forces and Dynamic Similarity	5
2.3 Flat Plate Boundary Layer Theory and Viscous Drag.....	6
2.4 Boundary Layer Modeling in CFD.....	8
2.5 Surface Pressure Gradients, Flow Separation and Form Drag.....	9
2.6 The Case of Zero Yaw	11
Chapter 3	13
METHODOLOGY	13
3.1 CFX-5	13
3.2 CFX-Build – Overview	14
3.3 CFX-Build – Geometry	15
3.4 CFX-Build – Meshing	17
3.5 CFX-Pre – Overview	20
3.6 CFX-Pre – Domain	22
3.7 CFX-Pre – Boundary Conditions.....	23
3.8 CFX-Pre – Solver Control.....	24
3.9 Project Parameters Set in Pre.....	25
3.10 CFX-Solver Manager – Overview.....	26
3.11 CFX-5 – The “Out” File	27
3.12 CFX-Post – Overview	28
Chapter 4	30
MESH RESULTS AND DISCUSSION	30
4.1 Mesh	30
4.2 Side Mesh	31
4.3 Inflated Boundary	32
4.4 Tail Section	34
4.5 Front Section	36
4.6 DREA Submarine Hull Mesh and y^+ Sensitivity Analysis.....	37
4.7 y^+ Visualization	42
Chapter 5	49
FLUID MECHANICS RESULTS AND DISCUSSION	49
5.1 Overview	49
5.2 Pressure Plots	49
5.3 Velocity Plots.....	52

5.4 Wall Shear Plots	54
5.5 Turbulence Kinetic Energy Plots	56
5.6 Comparison with Experimental Data	58
Chapter 6	60
CONCLUSIONS	60
Chapter 7	61
RECOMMENDATIONS.....	61
References	62
Appendix A - Boat Hull	64
Appendix B - Axisymmetric Mesh and y^+ Sensitivity Analysis	71
Appendix C – Simulations	76
Appendix D – Sample calculations	122
Appendix E – DREA Standard Hull.....	130

LIST OF FIGURES

Figure 1 – DREA Bare Submarine Hull and Axes Label	1
Figure 2 - Flat Plate Boundary Layer Development [1]	7
Figure 3 – Displacement Effect of Boundary Layers [1].....	7
Figure 4 – Flow Through a Converging-Diverging Duct [1]	10
Figure 5 - CFX-5 Simulation Set-up Flow Chart.....	13
Figure 6 - CFX-Build Menu Path	14
Figure 7 - Bare DREA Submarine Hull Domain in CFX-5.....	15
Figure 8 - CFX-Pre Menu Path.....	21
Figure 9 - RMS Residual Plot for Example Simulation (u, v, w Momentum and Mass Conservation).....	25
Figure 10 - Naming Convention for CFX-5 Simulations	30
Figure 11 - View of Entire Domain of Bare DREA Submarine Hull 556G-Mesh.....	31
Figure 12 - Centreline Side View of Bare DREA Submarine Hull 556G-Mesh	32
Figure 13 - Top View of Side Section of DREA Submarine Hull 556G-Mesh	33
Figure 14 - Centreline Side View of Side Section of Bare DREA Submarine Hull 556G-Mesh.....	34
Figure 15 - Centreline Side View of Tail Section of DREA Submarine 556G-Mesh.....	34
Figure 16 - Top View of Tail Section of Bare DREA Submarine 556G-Mesh.....	35
Figure 17 - Close Up Top View of Tail Section of Bare DREA Submarine Hull 556G-Mesh.....	35
Figure 18 - Top View of Front Section of Bare DREA Submarine Hull 556G-Mesh	36
Figure 19 - Top View of Front Section of Bare DREA Submarine Hull 556G-Mesh	37
Figure 20 - Centreline Top View of Front Section of Bare DREA Submarine Hull 556G-Mesh.....	37
Figure 21 - Standard DREA Hull Drag Values with Changing Mesh Size (Preliminary)	39
Figure 22 - Standard Bare DREA Hull Drag Values with Changing Mesh Resolution (Final).....	41
Figure 23 - Standard Bare DREA Hull Maximum y^+ Values with Changing Inflated Boundary Parameters	42
Figure 24 - y^+ Values for DREA Submarine Hull at $Re = 23$ Million (3.42 m/s) 556G-Mesh.....	43
Figure 25 - y^+ Values for Front of DREA Submarine Hull at $Re = 23$ Million (3.42m/s) 556G-Mesh	44
Figure 26 - y^+ Values for Tail of DREA Submarine Hull at $Re = 23$ Million (3.42 m/s) 556G-Mesh	45
Figure 27 - DREA Submarine Hull y^+ Values with Changing Reynolds Number	47
Figure 28 - DREA Submarine Hull Drag Values with Changing Reynolds Number	48
Figure 29 - Drag Coefficient Vs. Log Reynolds Number.....	48
Figure 30 - Top View Pressure Plot for DREA Submarine Hull at $Re = 23$ Million (3.42 m/s) 556G-Mesh	50
Figure 31 - Top View Pressure Plot of Front Section for DREA Submarine Hull at $Re = 23$ Million (3.42m/s) 556G-Mesh	50
Figure 32 - Centreline Side View Pressure Plot of DREA Submarine Hull at $Re = 23$ Million (3.42 m/s) 556G-Mesh	51

Figure 33 - Centreline Side View Velocity Plot of DREA Submarine Hull at Re = 23 Million (3.42 m/s) 556G-Mesh	52
Figure 34 - Top View Velocity Plot of Front Section of DREA Submarine Hull at RE = 23 Million (3.42 m/s) 556G-Mesh	53
Figure 35 - Top View Velocity Plot of Tail Section of DREA Submarine Hull at Re = 23 Million (3.42 m/s) 556G-Mesh	53
Figure 36 - Centreline Side View “v” Direction Velocity Plot of DREA Submarine Hull at Re = 23 Million (3.42 m/s) 556G-Mesh	54
Figure 37 - Top View Wall Shear Plot of DREA Submarine Hull at Re = 23 Million (3.42 m/s) 556G-Mesh	55
Figure 38 - Top View Wall Shear Plot of Front Section of DREA Submarine Hull at Re = 23 Million (3.42 m/s) 556G-Mesh	55
Figure 39 - Top View Wall Shear Plot of Tail Section of DREA Submarine Hull at Re = 23 Million (3.42 m/s) 556G-Mesh	56
Figure 40 - Centreline Side View Turbulent Kinetic Energy Plot of DREA Submarine Hull at Re = 23 Million (3.42 m/s) 556G-Mesh	57
Figure 41 - Centreline Side View Turbulent Kinetic Energy Plot of DREA Submarine Hull at Re = 23 Million (3.42 m/s) 556G-Mesh	57
Figure 42 - Standard Bare DREA Hull Drag Values with Changing Mesh Resolution (Final) & Wind Tunnel Tests Error Inclusive Range.....	58
Figure 43 - Side View of Example Boat Hull – Modified Yacht	64
Figure 44 – Side View of Mesh for Example Boat Hull.....	65
Figure 45 – Top View of Mesh for Example Boat Hull	65
Figure 46 – y_+ Side View Plot for Example Boat Hull	66
Figure 47 – Wall Shear Side View Plot for Example Boat Hull	66
Figure 48 – Pressure Side View Plot for Example Boat Hull	67
Figure 49 – Velocity v Top View Plot of Example Boat Hull.....	67
Figure 50 – Velocity v Side View Plot or Rear of Example Boat Hull	68
Figure 51 – Velocity Side View Plot of Rear Section of Example Boat Hull	68
Figure 52 – Turbulence Kinetic Energy for Example Boat Hull	69
Figure 53 – Streamlines Along Example Boat Hull	69
Figure 54 – Streamlines at Rear of Example Boat Hull.....	70
Figure 55 - Axisymmetric Shape Modeled For Trials (Bulbous Front with Tail).....	71
Figure 56 - Example y_+ Value Plot for Axisymmetric Shape With No Mesh Control....	74
Figure 57 - Example y_+ Value Plot for Axisymmetric Shape With Mesh Control.....	74
Figure 58 - Axisymmetric Bulbous Front Shape Drag with Changing Mesh Size (at 50 m/s)	75

LIST OF TABLES

Table 1 - Preliminary Mesh Sensitivity Analysis on Bare DREA Submarine Hull	38
Table 2 - Preliminary Mesh Sensitivity Analysis Changes for Bare DREA Submarine Hull	38
Table 3 - Final Mesh Sensitivity Analysis on Bare DREA Submarine Hull Run at 3.5 m/s	40
Table 4 - Final Mesh Sensitivity Analysis Changes for Bare DREA Submarine Hull....	40
Table 5 - Drag Sensitivity to Reynolds Number Using 556G-Mesh	46
Table 6 - Velocity Related to Reynolds Number (Re) and Upstream Pressure (Q)	47
Table 7 - Preliminary Mesh Sensitivity Analysis on Axisymmetric Shape (at 50 m/s) ...	72
Table 8 - Preliminary Mesh Sensitivity Analysis Changes for Axisymmetric Shape (at 50 m/s)	73
Table 9 - Comparison of Axisymmetric Bulbous Front Shape Values at 50 m/s and 3.5 m/s.....	75

CHAPTER 1

INTRODUCTION

This report details the use of Computational Fluid Dynamics (CFD) software to analyze flow around a submersible body. The submersible body used for this purpose is a standard DREA (Defence Research Establishment Atlantic) bare submarine hull seen below:

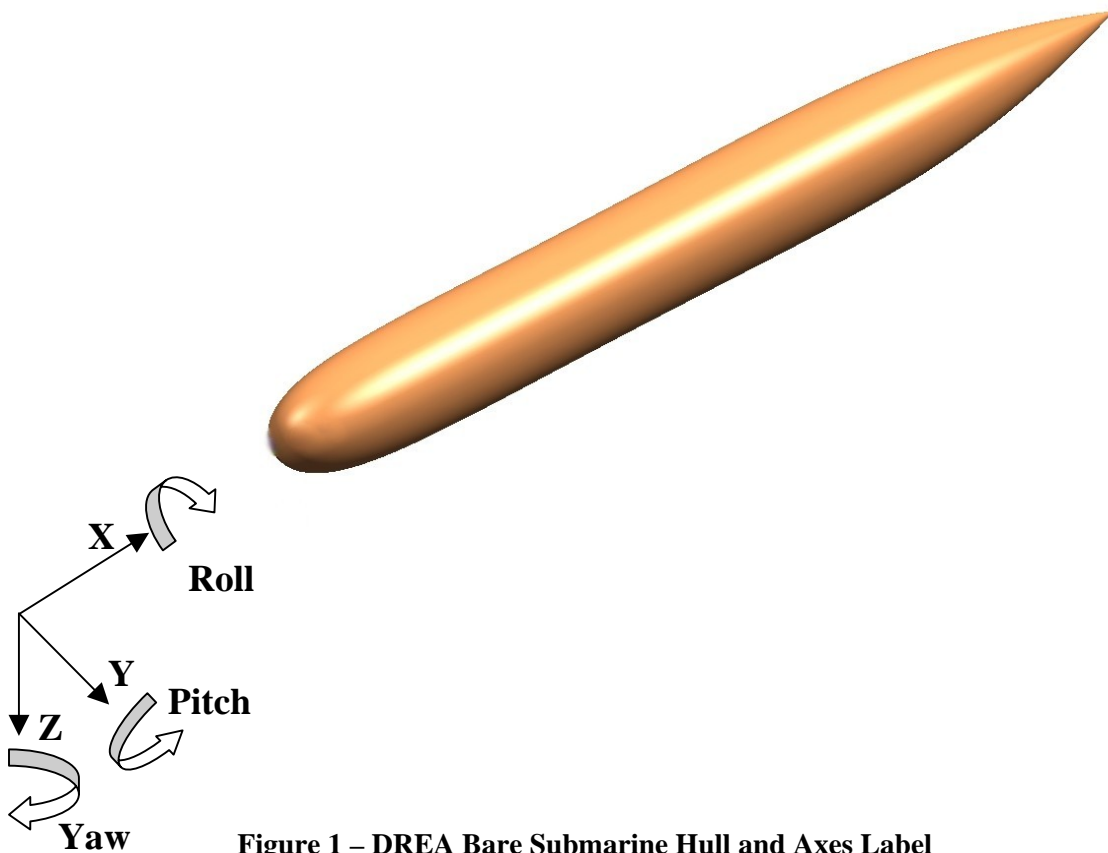


Figure 1 – DREA Bare Submarine Hull and Axes Label

DREA is now known as Defence Research and Development Canada – Atlantic, or DRDC-Atlantic, and is an Agency of the Canadian Department of National Defence. The CFD software used was the ANSYS software CFX-5.6. CFX-5 is a finite volume Reynolds Averaged Navier-Stokes (RANS) equations based software [11]. The geometry construction was done using a standard Computer Aided Drafting (CAD) software package while all other aspects of the project were completed using the CFX-5 software.

1.1 Computational Fluid Dynamics in Research and Development

Whether in the private or public sector, research into fluid flow problems is necessary for the development of new fluid based systems. CFD has the power to model fluid flow and heat transfer in an abundance of situations. With the advent of more powerful computers and more comprehensive computer codes, CFD has come to the forefront as a legitimate and effective research tool. CFD analysis can be much more cost effective compared to experimental models since changes can be made quickly and easily to almost any characteristic of the simulation. Simulations can also be set up more quickly and easily than experimental methods. However, since it is a computer based solution technique, the results must be verified against experimental data. This seems counter intuitive since no profitable company or agency has the money to duplicate their experimentation. This is not entirely the case. Not every simulation needs to be compared with experimental values. Only a few base cases are compared for validation purposes and then it is assumed safe to say that the other CFD simulations in that range are valid. Oftentimes this data previously exists, as is the case for this report. Even if some simulations are analyzed both experimentally and numerically, CFD is still beneficial since it has the ability to offer more information to researchers about the flow. CFD not only gives the overall values that experimentation offers, but gives a value at every node in the domain. If the overall values match, it can be assumed that all the detail described by the CFD solution is legitimate, giving researchers the ability to investigate small but important regions of the flow more closely [2].

1.2 Project Objectives

The goal of this report is twofold. First the report aims to assist anyone who is beginning to work with CFX-5 by shortening the traditionally long and steep learning curve. There is a great deal of learning about geometry creation, meshing, simulation set-up, solution control and post processing that goes on during a CFD simulation. Currently, a very limited body of knowledge at the University of New Brunswick exists to guide those starting with a CFD program such as CFX-5. This report will focus on the procedure used for this particular project, but much of the procedure can be extrapolated to other simulations. The second part of this report deals specifically with the analysis of the standard submarine hull.

All CFD simulations must be properly constructed and then validated against some other form or measurement to ensure accurate results. This simulation will be compared against the experimental wind tunnel testing done in 1988 by DRDC on the same geometry. Hopefully this report will be helpful in preventing some of the lost time due to the frustration and wrong turns that come with learning such a complex and expansive software package.

In the future, it is hoped that the entire experiment done in 1988 by DRDC can be compared using CFD with the ultimate goal of developing a set of force and moment coefficients that researchers can use in the development of new submarine control estimation tools. This will be done using the most advanced turbulence modeling and a super-computing cluster able to handle the massive solution set required to model such situations. This is beyond the scope of this project, but it is important to note that the information learned here will be used for this purpose.

CHAPTER 2

THEORY

2.1 Reynolds Number and Fluid Dynamics Basics

In order to understand the results of this report, one must first understand the basics of fluid flow concepts including viscosity (μ), density (ρ), turbulent and laminar flow and Reynolds number. Firstly, all fluids, whether they are liquids or gasses, have a certain density and viscosity. While the definition of density is widely understood as the weight of set volume of material, the definition of viscosity is much less widely known. Viscosity is a measure of a fluids resistance to flow. When a fluid is sheared (a force is applied), it begins to strain at a rate inversely proportional to the viscosity [1,4]. Accordingly, a high viscosity translates to a slower moving fluid. Together with the geometry and velocity of the flow situation a value known as the Reynolds number can be assigned. Reynolds number is shown as follows in *equation 1*.

$$\text{Re} = \frac{\rho UL}{\mu} \quad (1)$$

U is the free stream flow velocity and L is the length value suited for the situation, typically the length of a surface or the diameter of a pipe. Reynolds number is a dimensionless value describing the viscous behaviour of all Newtonian fluids. It is necessary to understand the nature of Reynolds number since it will be a governing factor for the research done in this report.

Refreshing what the definition of viscosity is and how the Reynolds number is determined is also necessary for discussing the difference between laminar and turbulent flow. Laminar flow is orderly in nature and follows smooth streamlines. Turbulence is a random phenomenon of flow disorder paradoxically due to the destabilizing effects of viscosity [1]. Reynolds number is used as a measure of when or where turbulent flow will occur. In confined flows such as pipe flow, turbulence occurs at a Reynolds number of approximately of 2300 based on pipe diameter. In open flow, such as flow over a flat plate,

turbulence transition occurs at Reynolds number of $5(10)^5$ based on plate length. The laminar to turbulence transition point in either flow situation is based on the disturbance from the leading edge of the plate or pipe by the boundary layer growth [4]. Working out the math accordingly, it can be shown that water at room temperature and pressure reaches the criteria for turbulent flow in a 10 cm diameter pipe at only 0.023 m/s, or 0.5 m/s over a flat plate one meter long. These numbers are not exact and it is not possible to predict exactly when the transition from laminar to turbulent flow will occur since factors such as free stream mixing and environmental noise levels influence the transition. Realistically, most engineering problems are in the turbulent domain. Understanding the difference between these two types of flow is critical in analyzing a fluid dynamics problem, since much different answers can be determined based on the flow condition.

2.2 Drag Forces and Dynamic Similarity

Flow past an immersed body causes forces to be applied to that body, which are dependent on its shape and the nature of the flow. With regard to submarines, the submarine moves through the fluid, while the fluid is more or less stationary. However, analyzing flow patterns past a moving body with stationary fluid is dynamically equivalent to analyzing the flow patterns around a stationary body as the flow moves. For ease of CFD simulation the later frame of reference is employed to determine the forces.

In order to compare data between experimental tests run using different speeds or even fluids one can make use of dynamic similarity. With drag values this common ground is found using a dimensionless coefficient C_D , which is determined using *equation 2*.

$$C_D = \frac{DRAG}{\frac{1}{2} \rho U^2 A} = \frac{DRAG}{QA} \quad (2)$$

As shown, the drag force is made non-dimensional by dividing by the dynamic pressure Q and the area. The particular area used depends on the shape involved. As a general rule, the frontal area is used for bluff bodies, the planform area is used for wings and the wetted area is used for surface ships and barges [1]. In this particular case, to stay consistent with the experimental data from the wind tunnel testing, the arbitrary area l^2 was used. The square of

the length has no physical meaning, but it serves the purpose. The *DRAG* value in the above equation is the drag force on the body, which is caused by both viscous (frictional) and pressure (form) effects.

2.3 Flat Plate Boundary Layer Theory and Viscous Drag

The viscous effects are a result of the friction between the fluid and the body and are generated in the boundary layer. Fluid near the body is in a no slip condition, meaning the flow directly next to the body wall is at zero velocity relative to the velocity of the wall. This causes shear stresses to be introduced to the flow. Turbulence kinetic energy builds up as the flow passes over the body creating swirling vortices that eventually dissipate into heat energy. This viscous effect accounts for nearly all of the drag on a flat plate. Much more detail is available from other resources [1], but the most beneficial feature of flat late theory is its relationship for viscous drag [17]:

$$D_V(x) = \int^S \tau_w dA \quad (3)$$

For this equation D_V is the drag force, τ_w is the wall shear and the integral is over the surface.

The influence of viscous effects on wall shear and hence drag cannot be fully understood until boundary layer development is understood. As flow passes over a body a layer of fluid grows next to the body called the boundary layer. The simplest case for comparison is flow over a flat plate with a sharp front. Flat plate boundary layer theory tells us that at low Reynolds number (< 1000) the boundary layer is large and extends far in front of and around the plate. This creates a large effect on the flow. However, for most practical situations the Reynolds number is high. Boundary layer development over a flat plate at high Reynolds number is much different, and much more amenable to flow over an immersed body. Initially the boundary layer is laminar and begins at the edge of the plate. The boundary layer grows until the Reynolds number (changing because of the changing L value) reaches a point where the flow will transition to turbulence. The turbulent region of the boundary layer then increases its thickness more. An image of the boundary layer development can be show below in *Figures 2 and 3*.

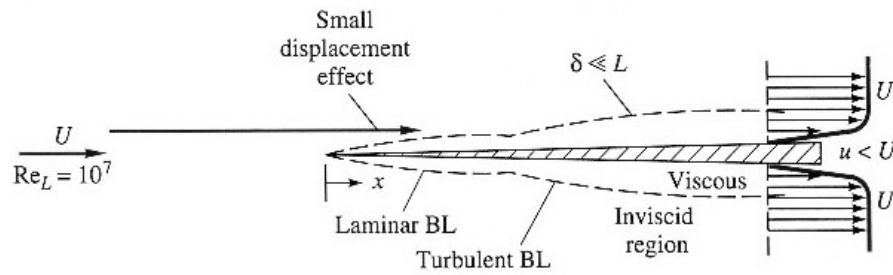


Figure 2 - Flat Plate Boundary Layer Development [1]

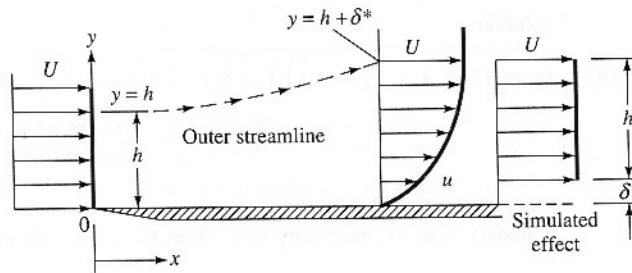


Figure 3 – Displacement Effect of Boundary Layers [1]

Figure 3 shows the presence of a boundary layer can have an effect on the outer streamlines by moving them outward from the plate. Boundary layers with high Reynolds numbers are very thin and in comparison to the size of the body they could be considered negligible with respect to the displacement thickness effect (δ^*). The effect of the boundary layer displacement on the outer flow would only be of interest in low Reynolds number flow and only in certain instances where this might affect something important. In most practicable CFD analyses this is not a point of interest. However, it is beneficial to know the approximate boundary layer thickness. The boundary layer thickness can be predicted via a relationship with the Reynolds number at that point. Equations 4 and 5 were put forth by Blasius in 1908 and follow:

$$\frac{\delta}{x} = \frac{5.0}{\text{Re}_x^{1/2}} \quad \text{laminar} \quad (4)$$

$$\frac{\delta}{x} = \frac{0.16}{\text{Re}_x^{1/2}} \quad \text{turbulent} \quad (5)$$

Re_x is the Reynolds number at the point of interest (x) while δ is the thickness of the boundary layer at the point of interest. Flat plate theory can be used to get an idea some of the mesh parameters necessary for a valid simulation. Blasius was also able to determine the skin friction coefficient of the flat plate, which relates to viscous drag. Equations 6 and 7 follow:

$$c_f = \frac{0.664}{\text{Re}_x^{1/2}} \quad \text{laminar} \quad (6)$$

$$c_f = \frac{0.027}{\text{Re}_x^{1/7}} \quad \text{turbulent} \quad (7)$$

C_f is the skin friction coefficient and is a measure of the wall shear on the flat plate. It can be used to determine if CFD results are at least in the right range for its final results. Based on flat plate calculations, the viscous drag coefficient is equal to twice the skin friction coefficient over the surface. Again, this is only an approximation since an ideal flat plate is rare in practical applications. More information regarding flat plate theory and the derivations of these equations can be found by consulting a fluid dynamics textbook such as Fluid Mechanics by Frank M. White [1].

2.4 Boundary Layer Modeling in CFD

In order to accurately predict the viscous and pressure drag via CFD analysis the boundary layer must be accurately resolved. This can be done two ways. First, nodes surrounded by control volumes can be placed in abundance next to the object to resolve the boundary layer. Unfortunately this generally requires a prohibitively large number of nodes and computation time. A widely used alternative is to place a node close enough to the

surface that the remainder of the boundary layer (between that node and the surface) can be predicted by the flat plate velocity profile.

Reasonably accurate predictions can be made because turbulent boundary layers under zero or modest pressure gradients follow a logarithmic profile [1]. This means that a relationship between wall shear, free stream velocity and velocity at a point at the edge of the boundary layer can be found. The relationship is shown in *equations 8, 9, and 10*.

$$u^+ = \frac{U_t}{u_\tau} = \frac{1}{k} \ln(y^+) + C \quad (8)$$

$$y^+ = \frac{\rho \Delta y u_\tau}{\mu} \quad (9)$$

$$u_\tau = \left(\frac{\tau_w}{\rho} \right)^{1/2} \quad (10)$$

In these equations y^+ is a dimensionless distance from the wall that shows where the point of interest is relative to the size of the boundary layer, u^+ is a dimensionless near wall velocity, U_t is a known velocity tangent to the wall at a distance Δy from the wall, u_τ is the friction velocity, and C and k are constants dependent on the fluid. A CFD solution can then determine the flow values at a point close enough to the boundary layer to extrapolate the wall shear stress. It is interesting to note though, that this procedure is only valid for a set range of y^+ values (generally between 20 and 100 [16]), and the exact y^+ value for near surface nodes can not be determined until the solution has been converged since it is dependent on the wall shear value. It is helpful to use the flat plate theory to get an estimate of the boundary layer thickness and hence an approximate value for how close the nearest node must be (Δy).

2.5 Surface Pressure Gradients, Flow Separation and Form Drag

Determining the boundary layer thickness from flat plate theory can only act as an approximation since flat plate boundary layer development is not affected by pressure gradients. In most practical cases there will be pressure gradients that very much affect the

boundary layer thickness. Negative pressure changes, or where pressure is decreasing and velocity is increasing, are known as favourable pressure gradients (front section of *Figure 4*) and lead to a thinner boundary layer. Positive pressure changes, or where pressure is increasing and velocity is decreasing, are known as adverse pressure gradients (rear section of *Figure 4*) [1] and lead to a thicker boundary layer.

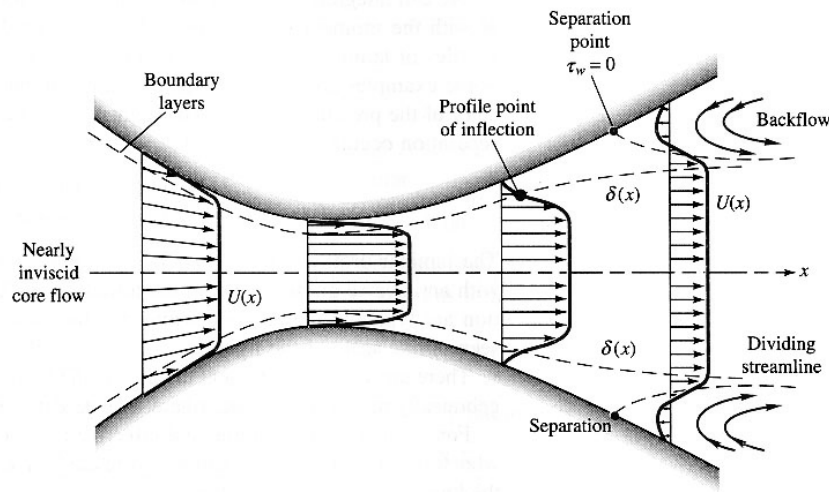


Figure 4 – Flow Through a Converging-Diverging Duct [1]

Flow separation describes the phenomenon of boundary layers separating from the body and often recirculating back towards the flow. Flow separation cannot occur under favourable pressure gradient, only under an adverse pressure gradient. For the case of a submarine hull facing directly into the flow, there is a favourable pressure gradient at the front of the hull, near zero pressure gradient along the body of the hull and an adverse pressure gradient along the rear of the hull. Naturally, there is a potential for the flow to separate at the rear of the hull. If the adverse pressure gradient is too high the fluid near the wall will stall and separation will occur. A very interesting and useful point to note about separation is that at the separation point the wall shear equals zero, and hence there is no

viscous drag contribution. A zero wall shear condition can be looked for to determine if flow separation has occurred.

Pressure effects are dependent on the perturbation that a body makes on the flow. As fluid moves around an object, there exists a pressure difference between the front and the rear of that object. At the front of the submarine hull exists a stagnation point, where high pressure is the result of a near stop in fluid flow. Surrounding the stagnation point there is a favourable pressure gradient with higher velocities. At the rear there is an adverse pressure gradient with low velocity and the possibility of separation. The effects of pressure differences appear in the general equation for pressure drag see in *equation 11* [17].

$$D_p = \int_S p dA \quad (11)$$

The effects of boundary layer displacement, separation and viscous losses contribute to a pressure difference between the front and the rear of an object. It is the pressure difference over the area of the shape that makes up the pressure drag. Streamlined objects have relatively little pressure difference between the front and the rear and hence the viscous drag is dominant. Bluff bodies induce flow separation at the rear, which increases the pressure difference, thus making the pressure drag dominant.

2.6 The Case of Zero Yaw

By studying the drag on a submersible body such as a submarine hull, only one of the three forces acting on the body is being considered, the others being lift and side force. This is ok if you are simulating a flow situation where the flow approaches directly to the body with no angle of attack or yaw angle. Angle of attack refers to the angle made between the flow and a horizontal plane while yaw angle refers to the angle made between the flow and a vertical plane. The reference set of axes is illustrated in *Figure 1*.

In more realistic cases of flow around a submarine hull, the flow is rarely direct to the body. This means that there is not only a drag force but a side force and lift force.

Accompanying these forces are moments acting about the three axes. Together these forces and moments form the six degrees of freedom available in a CFD analysis of this nature.

For this report only the simple case of direct flow with no angle of attack or yaw angle will be considered. In this instance the forces in the y and z directions will be zero since symmetry is present. It should be noted that the axis scheme described above is not consistent with current published CFD works where the x and y directions are swapped. This was a default labelling of the drafting program used to create the geometry.

CHAPTER 3

METHODOLOGY

3.1 CFX-5

CFX-5 has four subprograms that each represents a step in creating a CFD simulation. These four sub-programs are called CFX-Build, CFX-Pre, CFX-Solver Manager, and CFX-Post. The process of creating a CFD simulation involves working through the first two components. The Solver Manager then runs the simulation and Post allows the final results to be examined. This process is shown in *Figure 5*.

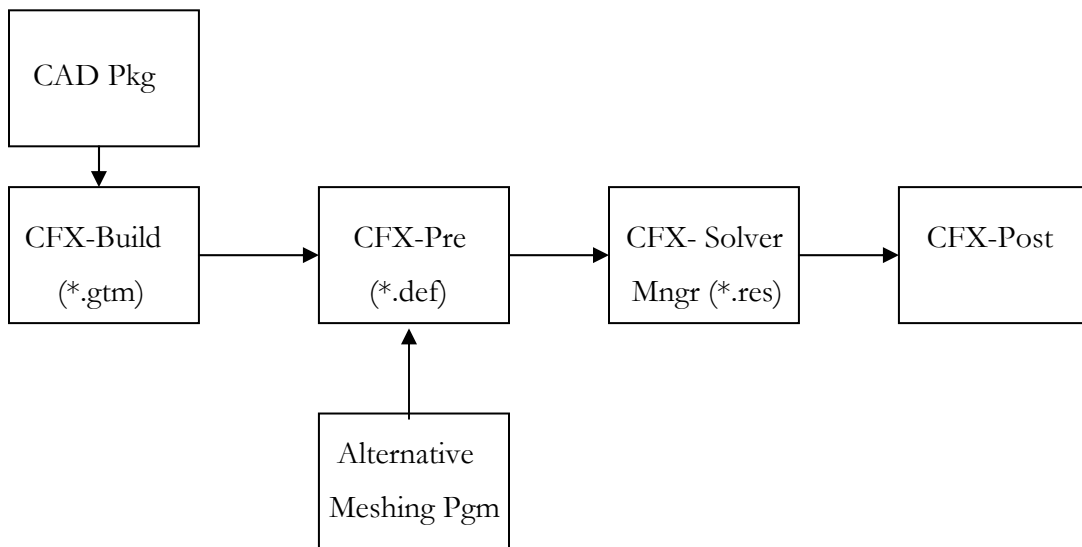


Figure 5 - CFX-5 Simulation Set-up Flow Chart

As shown in the figure the geometry can be created using either Build or another CAD package. The latter was done for this project. Also, an alternative meshing program could have been used to eliminate Build from the process altogether.

To better understand the logic behind these steps it is important to understand the concept of solving a fluid dynamics problem numerically. For every problem there are governing partial differential equations that apply. Generally there are four equations, one to conserve mass and three to conserve flow momentum in the x, y and z directions (u, v and w momentum). These equations, and any others that are applicable to the situation, are

discretised and applied to small control volumes. The control volumes must be small enough to adequately resolve the flow but large enough as to allow for a reasonable solution time. Build has the ability to create geometry and then generate control volumes (called a mesh or a grid), which determines where the discretised governing equations are applied. From there, the mesh is used in Pre where the boundary conditions are applied. After the simulation is set up to best model the real situation a definition file is written. This definition file contains the mesh, boundary conditions and simulation commands and is loaded in the Solver Manager. The Solver Manager allows the convergence of the run to be monitored and controls when the run is complete. The Solver Manager outputs a results file that is used in Post. Post allows visualization of the flow as well as the output of quantitative values that are of interest.

3.2 CFX-Build – Overview

As with all subsections of the CFX-5 program, fulfilling all the requirements of the Build portion of the simulation follows a logical path. The operator simply follows the menus located along the top of the screen, skipping those that are optional and do not apply. The menu titles for Build are located in *Figure 6*.



Figure 6 - CFX-Build Menu Path

Geometry is the CAD menu used for building and altering the geometry, **3D regions** assigns the solid that represents the flow domain a name, **2D regions** is an optional menu that assigns surfaces names, **mesh** sets the mesh parameters and **write file** writes the mesh file (gtm file).

3.3 CFX-Build – Geometry

In this case half the hull was modeled to take cut down on the computation time by taking advantage of symmetry. A duct-like domain was established with the hull indented into one face. This can be seen in *Figure 7*.

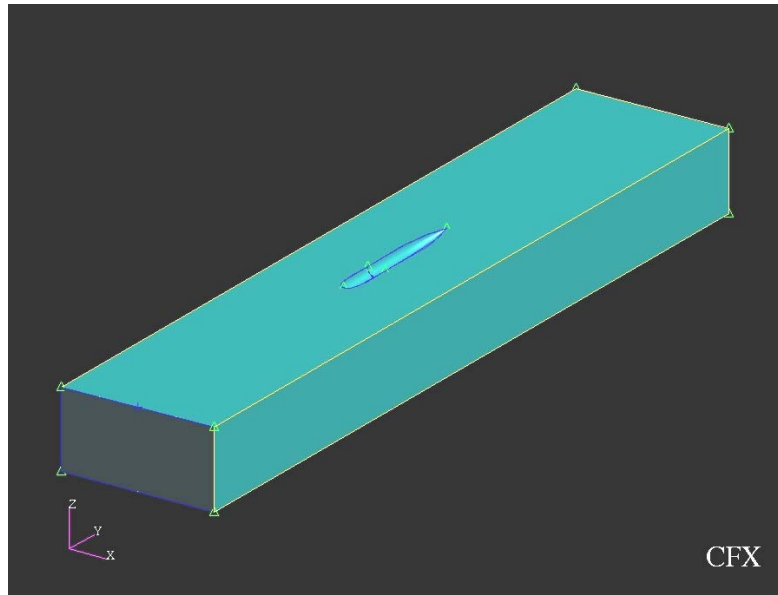


Figure 7 - Bare DREA Submarine Hull Domain in CFX-5

The first step in creating a CFD simulation is the creation of the fluid domain. Typically this can be done two ways; geometry can be created in CFX-5 or geometry can be created in a commercial CAD package. To create the geometry in CFX-5, CFX-Build is used. Build has a full range of CAD tools including surfaces, solids, scaling, mirroring and most of the tools common to all CAD packages. However, since a good working knowledge of a high quality CAD package already existed, Build was not used for this part of the project. Geometry was constructed using the Solids option in a CAD package and exported as an IGES file. IGES is a baseline generic file type that is widely available, but is not ideal for maintaining geometric integrity. The IGES file is then imported into Build using the import option. This is a simple process but some modifications do have to be made in Build. IGES does not

maintain solids so the geometry must be converted back into one. This is done using the Boundary Represented (B-Rep) method in the Solid-Create window. B-rep solids must be defined by surfaces that completely enclose to make a solid. If the geometry was created as a solid in the CAD package, the surfaces should close to make a solid without a problem. However, problems can arise with the congruency of the surfaces. If the edges do not match to within a specified tight tolerance, there can be problems with meshing. This can be examined using the Verify-Surface-B-Rep option; it will show any edges that are not within tolerance. If there is an edge match problem then the Edit-Surface-Edge Match option can be used to make the boundaries coincident. Problems stemming from surface edges not matching are the major problems with using IGES files to import geometry.

In the submarine case it was necessary to import the hull only and then create a wireframe box around it representing the domain using Build. Flat surfaces were created from the wireframe using the Create-Surface-Trimmed-Four Curves. Then the Edit-Surface-Hole option was used to create a hole in the top surface to fit the half-hull. Solid B-rep method was then used to convert the surfaces to a solid. It was also necessary to cut the hull in half because IGES represents surfaces with four curves and the hull only had two. This meant there were two curves with zero length at either end, causing problems with meshing. By cutting the hull in half, the problem was resolved.

A much better way to import geometry is to use the Parasolid method. Parasolid is widely available in CAD packages and maintains the solid form from the CAD package into Build. Using this method, all work can be done in the CAD package in solid form, so the potential edge matching problems are avoided. However, this import option is not currently available in CFX-5 at UNB as it requires a separate license key.

As a general rule, the geometry should not contain too much detail. Too much detail will present a plethora of problems when it comes time to apply the mesh. It is best to look at the flow situation critically and remove any components that are not significant. An example of this might be the modeling an automobile in a wind tunnel. It would be possible to model the radio antenna, the windshield wipers and the license plate but details this small could not be resolved by the mesh engine and would not appreciably alter the results. At this point it would be beneficial to understand just how the Build mesh engine works. Once the meshing parameters are set the meshing can begin. This starts when the definition file is

written. First, a surface mesh is generated over the entire domain. The more detailed the geometry, the finer the mesh has to be to resolve it. After the surface mesh is created, the entire domain has to be filled with volume elements. Finite volume elements are generated based on the surface mesh. The program generates elements of different sizes so that different areas are more resolved than others, based on the initial parameters and how complex the geometry is. As the mesh becomes finer due to the parameters or in order to resolve the fineness of the geometry, the size of the problem goes up, therefore increasing the solution time. Also, as geometry becomes more complex the mesh engine can fail, again making it beneficial to have a simple geometry.

3.4 CFX-Build – Meshing

Meshing in CFX-Build can be a very frustrating process, especially during the learning phase. There are a large number of parameters that control the mesh generation process. This section will try to give some insight into what parameters control what aspect of the meshing, but each problem is different and will require different meshes. Care should be taken to increase mesh density in areas of concern, and reduce the mesh in areas of little change such as free stream flow. For example, this problem aims to estimate the drag on the hull. The flow around the hull is most important while flow at the edge of the domain is of the least importance. For that reason the mesh will be fine near the hull and coarser at the outer domain.

Generally in CFD, there are two types of control volumes, node centred control volumes and node defined control volumes. In the case of the former, there is one control volume surrounding the node, and hence there is the same number of nodes as control volumes. In the case of the latter, the nodes are placed at the vertices of the control volume. This allows for one node to be used for many control volumes and thus cuts down on computation time. CFX-5 uses node defined control volumes.

There are three types of meshing in CFX-Build, namely: Advancing Front and Inflation, Patran Volume Meshing and Paving and Isomeshing. Advancing Front and Inflation is the default and was used for this project. The advancing front is a surface mesh of triangles and the inflation is a volume mesh of tetrahedral elements. Prismatic and Pyramidal elements are

also used when an inflated boundary is used. Inflated boundaries will be discussed later. Before the mesh creation step begins it is a good idea to perform a check on the geometry. This can be done via the tool menu after the domain has been labelled as a 3D region. This tool checks for sliver faces and edges that do not match to within tolerance. Sliver faces are surfaces that come to a sharp angled point. This check will identify portions of the geometry that will nearly always cause problems meshing, especially if the mesh is fine.

The mesh density is controlled by setting parameters with high and low bounds and then created by simply letting the mesh engine do its work. For this reason it is very important to know what parameters control what aspects of the mesh. When you enter the set-mesh parameters window you are presented with the maximum volume edge length control and multiple surface meshing controls. One important thing to note is that all of these parameters are in an absolute form, therefore the value inputted is in meters and not as a percentage of the domain size. This means that it is important to understand the size of your domain and the nature of your problem when inputting these values. It is sometimes beneficial to do some rough calculations by using some known theory, such as the flat plate theory previously described, to get a rough idea of what range you should be in. This also means it may be necessary to scale down your CFD geometry size, even though it is only a virtual CFD geometry, in order to cut down on computation time. Large-scale models of submarines in CFX take an extraordinary amount of time to generate a mesh for and to solve. For instance, modeling a prototype size hull 30 meters in length in CFX-5 would be prohibitively computationally intense due to its size. For this reason it makes much more sense to use a smaller geometry for the CFX simulation.

For the hull shape, the maximum volume edge length was set to 0.3 meters. In this case it was acceptable to use such a high maximum since it only came into effect at the very edge of the domain where there was not much change in the flow and a coarse mesh was not detrimental to the overall solution. The next control is the type of surface meshing. There are fewer controls for the volume meshing because the volume mesh is constructed based on the surface mesh. There are four types of surface meshing control, namely: use volume spacing, angular resolution, relative error and constant. Angular resolution and relative error are very similar in their ability to control the mesh while volume spacing and constant are similar in they both offer less control. For this project, angular resolution was used. This

method requires an angle, a minimum edge length, a maximum edge length and an expansion factor. The maximum edge length controls the maximum size the triangular surface mesh can be, while the minimum edge length controls the minimum size of the surface mesh. The expansion factor controls how much the size of the volume elements increase as they are inflated out from the surface mesh, since the volume mesh is generated from the surface mesh. For example, this project has an angle of 7° , a minimum edge length of 0.0003 meters, a maximum of 0.3 meters and an expansion factor of 1.03. Therefore, the curve of the hull wall is resolved with elements that move in 7° increments. The smaller this angle is the finer the mesh is. Areas where 7° can resolve a large area are bound by the maximum edge length so the control volume size is not too large. Areas where 7° resolves only a small element size are bounded by a minimum as to avoid elements that are so small they have effectively no volume as well as to cut down on unnecessary computation time. Visual representation of the mesh will be shown in the results section.

Since the flow near the hull was the most important part of the flow it was beneficial to use an inflated boundary. An inflated boundary is a way to place prisms and pyramids next to the wall. This works well because the elements are aligned with the flow producing better results and the prisms and pyramids are much more efficient at resolving these areas than tetrahedrals. An inflated boundary can be set up in two different ways. First, it can be generated the same way normal volume elements are, based on the surface mesh. This involves setting the maximum number of inflation layers, the geometric expansion factor and the inflation thickness multiplier. The mesh engine then takes the size of the surface mesh, multiplies it by the inflation thickness multiplier and sets that as the first prism height. The first layer is made, and the second is added on top of the first, but the second layer is thicker than the first by a factor of the inflation thickness multiplier. This continues until the outer layer has the same thickness as the tetrahedral based mesh that would have existed in that region, or the maximum number of layers is met. This allows for a smooth transition between the inflation layer prisms and the normal mesh tetrahedrals. However, this method requires a fine surface mesh to get a fine inflated boundary. This may over refine the volume mesh outside of this region as it still depends on this surface mesh.

To avoid over refining the mesh it is possible to set the first prism height. This means that the first prism height is a parameter set by the operator and not by the surface mesh.

This is useful in cases where the $y+$ value is important and it is necessary to control how close the nodes get to the surface. In the case of the submarine hull it was necessary to set a first prism height of 0.0003 meters with a geometric expansion factor of 1.3 and a maximum number of layers of 32. A first prism height this low allowed the nearest node to be close enough to the surface to get a valid $y+$ value, while an expansion factor this high reduced the number of nodes by quickly increasing the size of the control volumes back to a size comparable with the rest of the mesh. The maximum number of layers is often not reached as this maximum is based on the maximum edge length. It is set so that in the worst-case situation, where the volume mesh outside the inflated boundary is at its maximum size, the inflated boundary has enough space to reach a size where the transition from one element type to the other is smooth. If this criterion is reached before the 32 layers have been reached then the transition just simply occurs at that point.

Another way to control the density of the mesh in a certain portion of the domain is to use a Mesh Control. A mesh control does exactly what its name says it does, it controls the density of the mesh. This can be added to a point, a line or a surface. It allows the operator to apply different mesh parameters to that area. The actual parameters are dependent on what option is chosen. A mesh control was not necessary for the submarine hull but, as will be discussed later, it was necessary for a test case. The test case had a bulbous front that required a point mesh control at the outermost point of the bulb. The different length scale was interconnected to the normal mesh by using an expansion factor to control how quickly the transition between the two mesh scales progressed. Stipulating a radius for which the length scale would remain constant allowed for a large enough mesh control to control the entire trouble area. This will be illustrated in the results section, but as with any topic discussed, more information is available in the help files.

3.5 CFX-Pre – Overview

CFX-Pre is where the simulation boundary conditions, solution control, initialization and expert parameters are applied. The menu path is shown in *Figure 8*.

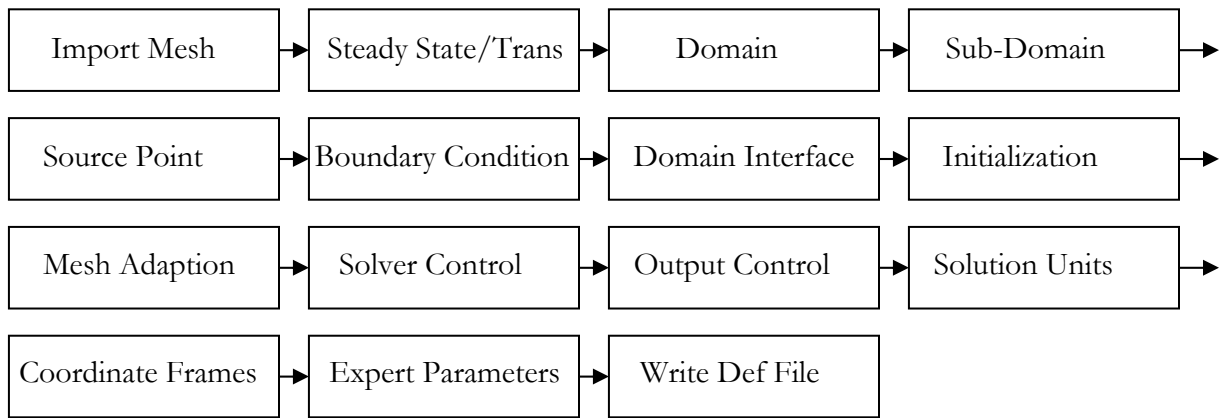


Figure 8 - CFX-Pre Menu Path

Import mesh is how the mesh file created in Build or another meshing program is imported. **Steady state/transient** is where the simulation is set to either a steady state solution or a transient solution. This is a simply choice based on the problem being simulated but is important since it affects how the other menus are displayed. Pre is clever in the way it displays the menus; it displays only the options required based on previous menu choices. For instance, if steady state is chosen as the simulation type, none of the options for a transient simulation will ever appear. The **domain** menu assigns 3D regions to different fluid domains. The **sub-domain** menu is used to assign sub-domains in the domain, which is optional and is used in more complex situations such as ones with multiphase flow or sources such as combustion.

The **boundary conditions** menu is used to apply walls, openings, inlets, outlets and symmetry planes to the domain. The **domain interface** menu is optional and is used to link two mesh regions together. This option is also only used in more complex situations where meshing is complex and must be done in separate regions. **Initialization** is where the initial conditions are set. This menu has the default setting of using automatic initial conditions calculated based on the boundary conditions and other parameters. **Mesh adaption** is another optional menu. This is a clever option where after the simulation is solved, the program looks at where the largest changes in a set of values are and regenerates the mesh adding more nodes in that region, hopefully improving the results. **Solver control** is where the convergence control, convergence criteria and advection control schemes are set.

Output control is used to control how the output is stored and backed up. **Solutions units** is where the units are set for the simulation. This simulation is solved using the metric units meter, kilogram and second. **Coordinate frames** is used in situations where the coordinate frame of reference influences the results. **Expert parameters** allows for alternative options for expert users. For this project ‘output equation flows’ was set to true to allow for quantitative force values in post processing. **Write definition file** is where the definition file is written for use in the Solver Manager.

3.6 CFX-Pre – Domain

Setting the domain in Pre sets the environment for the simulation. Questions about buoyancy, turbulence, phase, fluid type and reference pressure are answered here. With regards to buoyancy, if the non-buoyant option is chosen all buoyant effects are simply eliminated. If the flow does experience buoyancy effects then the menu to input the nature of this effect appears. In this case the flow was non-buoyant. The fluid type was chosen as water at 25°C and a 0 Pa reference pressure was chosen. The choice of reference pressure is irrelevant for this simulation because the flow is incompressible and a relative pressure is used in the solution of the equations to reduce round off error. Choosing a turbulence model will have the most effect on a flow simulation of this type. First the choice of laminar flow or turbulent flow must be decided upon. Current turbulent models are not advanced enough to account for the initial laminar region and the transitions zone. A choice must be made stipulating that the entire surface is laminar or the entire surface is turbulent. In some cases where enough is known about the turbulent transition behaviour it may be beneficial to stipulate a laminar region and a turbulent region. For this case the flow should be entirely turbulent at the 0.13 meter mark from the tip of the hull. This allows for a safe assumption that the entire hull is turbulent.

For this simulation the k- ϵ turbulence model was used. Examples of other choices were the k- ω model and the Shear Stress Transport (SST) model. The k- ϵ turbulence model is a relatively simple and widely tested working model for CFD calculations. Both the k- ϵ model and the k- ω based models solve equations of turbulence generation and dissipation to account for turbulence. The SST model is reportedly the best for accurate boundary layer

simulations and involves placing node close enough to the surface to resolve the boundary layer [2]. The k- ω formulation is used in the boundary layer region and the k- ϵ is used in the outer region. In this case, scalable wall functions were used to predict the boundary layer influence with the k- ϵ model since it requires less computational effort. The stipulation for accurate results with this model was to have a y^+ value between 20 and 100 [16]. A lower y^+ value was not as much of an issue because CFX will scale nodes that are too close to a more appropriate y^+ value by effectively ignoring the fluid flow in that region [16, 2]. Since there is no or very little separation expected in this flow, the k- ϵ model should be sufficient.

3.7 CFX-Pre – Boundary Conditions

Every surface in the domain must have a boundary condition associated with it, either explicitly through a set condition or implicitly through a default setting. All boundary conditions are applied by selecting the surface that it will apply to. This process is made easier if common regions are given a common name in the 2D Regions menu in Build. For instance, the two surfaces that made up the hull shape (solid 1.1 and solid 1.2) were named “shape” using the 2D regions menu, thus making the application of the boundary conditions more intuitive.

By far the most common boundary condition is the wall. Walls can be stipulated to be smooth walls or can have a set surface roughness. The surface roughness is set using an absolute length value. For this project the hull was considered a smooth surface. Walls can also be given a free slip condition as opposed to a no slip condition. The free slip condition is a wall that contains the flow but does not retard it through the development of a boundary layer. This was useful in the analysis of the ship hull because free slip walls bounded the domain. A symmetry plane is another type of wall. A flat symmetry plane is nearly identical to a flat free slip wall. There is a difference with regards to curved walls since a free slip wall only bounds the flow with no regards to what is going on in the domain, whereas a symmetry plane will replicate the exit condition of one symmetry plane to the entrance of another, thus maintaining symmetry.

An inlet condition was also used for this project. Inlet conditions can be set as a constant total pressure, a mass flow, a normal velocity or as Cartesian or cylindrical velocity

components. For this case a normal velocity condition was applied at the inlet. The outlet conditions can be static pressure, normal velocity, Cartesian or cylindrical velocity components, average static pressure or mass flow rate. For this project the static pressure was set relative to the entrance at a value of zero. Another type of boundary condition is an opening. This is a combination of an inlet and an outlet. Pressure conditions in these regions must be specified and fluid will flow in the required direction based on the solution.

3.8 CFX-Pre – Solver Control

Criteria must be set to establish when the simulation is considered converged and what timescale the simulation is going to operate on. These criteria are set using the solver control menu. Since the nature of a CFD solver is that it is solving a combination of discretised equations using a guess and correct algorithm, there will always be a residual that represents how far the current values are from satisfying the equations. The simulation will be considered converged when the residuals are below a set target. The residuals can be denoted in two ways, as the Root-Mean-Square (RMS) residual or the maximum (MAX) residual. The RMS residual is the summation of the square of the residuals at every node, square rooted and then divided by the number of nodes. With this method it is possible for certain nodes to be well converged and others to be less so, since it is an average value. The alternative method is to use the MAX residual. This ensures that every node within the domain has a residual below a certain value.

Output control is also where the advection scheme is controlled. The default setting for CFX-5 is the High Resolution advection scheme. This scheme alters the effect of diffusion and momentum based on the flow. Faster flow means more influence from momentum and less from diffusion while slower flow leads to the opposite. The alternative is the upwind differencing scheme. In this scheme the momentum effect from the downwind control volume is reduced in influence since it is assumed that the upwind momentum will dominate [3]. This option was used because it is a unidirectional flow and the scheme is more robust. This choice will be revisited in the recommendations section.

Timestep control was also an issue for this simulation. At lower node densities the automatic option was sufficient to converge the simulation. As node density increased it became necessary to stipulate a lower timestep to in essence “get the simulation off the

ground” and then it was possible to raise it to decrease the time to convergence. A general way to determine what a timestep should be set at is to look at the physics of the flow [3]. For this simulation the time for a fluid particle to traverse the shape is of interest. For example, with a fluid flow of 3.42 m/s and a six meter long hull a particle would take approximately 1.75 seconds to traverse the hull. A number slightly lower but on the same scale was chosen as the timestep. If problems with convergence present themselves an often-used trick is to reduce the timestep by a factor of ten [2]. Continuing the example, a timestep of 0.05 seconds was used for the first 50 iterations after which it was raised to 0.5 seconds. A display of the residuals from such a simulation can be see bellow in *Figure 9*.

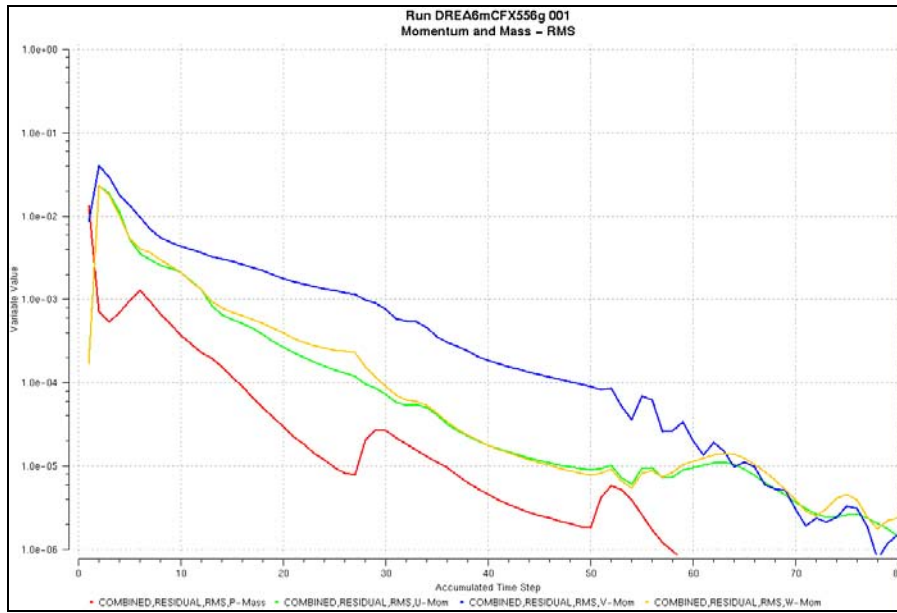


Figure 9 - RMS Residual Plot for Example Simulation (u, v, w Momentum and Mass Conservation)

3.9 Project Parameters Set in Pre

The domain for this project was shown in *Figure 7*. The entire length of the box was 30 meters with the hull situated 12 meters from the front and 12 meters from the rear. The x direction width of the hull was 6 meters and the z direction depth was 3 meters. The coordinate axis was located at the intersection of the inlet and top plane, at the centre of the

line. From here the front tip of the hull was located at (12, 0, 0). The domain was double checked for size using a volume comparison once imported into CFX-5.

Mesh parameters changed with the different trials and are catalogued in Appendix B. The simulation was set up as steady state. The domain was the entire duct like geometry shown in *Figure 7* with no sub-domains. No source points were necessary, nor any domain interfaces. Initialization was set to all automatic and mesh adaption was not necessary. The front vertical surface in *Figure 7* was set as an inlet with a normal inlet velocity dependent on the Reynolds number required. For a Reynolds number of 23 million, based on a tip to tail length of six meters, the inlet velocity was set to 3.422 m/s. The inlet was placed far enough upstream that the pressure at the inlet was constant; indicating the disturbance cause by the shape did not propagate to the inlet. The opposite surface to the inlet was set as an outlet with zero relative static pressure, so the static pressure at the entrance was relative to the static pressure at the exit. The two side and one bottom surfaces were set as free slip walls. The top surface with the cut out for the hull was set as a symmetry plane. The two surfaces that represent the surface of the hull were set as a wall with a no-slip condition and a smooth surface. The solution was set to converge at a maximum residual of $1(10^{-4})$. The physical timestep was determined based on the inlet velocity and often increased one order of magnitude after 50 iterations to decrease convergence time, as discussed above. The advection scheme was set to upwind differencing. The solution units were set to meter-kilogram-second. The coordinate frame was left in the default position and the expert parameters “output equation flows” was set to true to allow for quantitative values of force to be available in Post.

3.10 CFX-Solver Manager – Overview

CFX-Solver Manager shows the solutions progress through presentation of a residual plot and the “out” file. The manager can be used to stop divergent runs or modify selected criteria during a run. Runs can be restarted if they have reached their maximum number of iterations before reaching convergence, a very important point which can be determined from the out file. If a run were converging at a very slow rate it would not be sensible to simply restart the run with the same parameters. In this case it is often beneficial to raise the

physical timestep and then restart the run. As stated earlier, a low physical timestep is sometime necessary at the beginning of a run to ensure robustness, but it does not make sense to use it for the entire simulation.

3.11 CFX-5 – The “Out” File

The out file is a text document that stores the residuals from each iteration, the command code that summarizes all the parameters of the simulation and some final results. Learning to read and understand the out file is important for understanding the results the CFD simulation is producing. The out file is created as soon as a simulation run is started. The first thing written to an out file is the information about the run. This information includes the library values for the fluid used, such as the density and viscosity. The boundary conditions, advection scheme, convergence control and everything else outline in Pre is summarized here in a command code format. From here some information about the run is produced. The total number of nodes and elements is determined, as well as the Reynolds number and the memory allocation for the computer. Next, the physical timestep for the run is shown. If this is set to automatic, this value is updated every six iterations by default. If an equation is used such as in this case, the physical timestep is calculated at each iteration. Following this step the iterations begin. Both RMS and MAX residuals and the convergence rate for each governing equation are outputted after an iteration.

After convergence or the maximum number of timesteps is reached, the results are exported in a results file for use in Post. The out file summarizes the run by displaying the domain imbalance and location of maximum residuals. It also outputs the general viscous and pressure forces on the shape and walls. If the coordinate axis is in the right location the drag, lift, side force and their respective moments can be determined from, this part of the out file. The last part of the out file is a summery of how much computer time and how much wall clock time elapsed for the run to complete. For the final run of this project the simulation took over 20 hours on a 500 Mhz UNIX computer with 1 Gigabyte of RAM. Available memory and computer speed both play a large role in the solution completion time.

3.12 CFX-Post – Overview

CFX-Post is the engine that allows the data calculated in the Solver Manager to be presented in an understandable and clear way. Post allows visualization of the flow and the different values as well as the output of these values. For example, there are streamline plots, vector plots, contour plots and others available in Post. Using these tools is really quite easy. To make a plot you simply follow the menu options. The face location of the plot is set, the variable of interest is set, and the control parameters are set. The control parameters control how many streamlines or how many contour levels to use. With small scale problems these plots take very little time to be produced, but with large problems care must be taken to not oversize the plots. For instance, when a streamline plot is generated in a large problem care must be taken to set the reduction factor correctly. A reduction factor is a measure of how many streamlines there are related to how many nodes there are. Where a small problem might be able to use a reduction factor of one, a large problem might require a reduction factor of 500 to produce a useful plot in a reasonable amount of time. Contour plots are useful for displaying various types of data. They can be used to show pressure, velocity, turbulent kinetic energy and y^+ values as well as many others. Contour plots show bands of colour to represent ranges of values. A nice alternative to this method is to change the colour of the plane or object of interest via the object manager. The options of each object allow for a colour to be applied. If the variable colour option is chosen then the parameter to vary the colour can be chosen as one of the same variables available for a contour plot. The variable plot is a smooth contour plot representing the changing values, rather than an abrupt change from one band to another.

Post also has a function calculator. This allows quantitative values to be extracted from the simulation. For example, an area summation of the shear stress can be applied to the hull and the viscous drag can be calculated. This function calculator can also be used to find maximum and minimum values as well as averages, summations and area averages. There is also a mesh calculator that produces statistics on the quality of the mesh. Ranges of acceptable limits for the mesh statistics can be found in the help files. Users of CFX-5 are strongly urged to utilize the help files early and often. It is sometimes difficult to understand

what the help files are saying without actually doing it. For this reason it is beneficial to work through some of the tutorials or to work with the help files while learning by doing.

CHAPTER 4

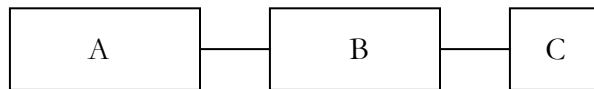
MESH RESULTS AND DISCUSSION

4.1 Mesh

The mesh generation procedure for this project was trial and error complemented by what could be learned from the help files. The mesh must be fine enough to produce grid independent solutions but coarse enough to have a reasonable computation time.

Completing a mesh sensitivity analysis is how this balance is achieved. In essence, a mesh sensitivity analysis is an iterative process of refining the mesh and checking the results until the results no longer change by an appreciable amount. A mesh sensitivity analysis was done on two different shapes. First, an axisymmetric shape with a bulbous front and a tapered rear was used to understand the interaction between y^+ values and the mesh. This was actually completed at a free stream velocity of 50 m/s. The reason for this stems from the initial intention of the project, where a 30-meter long hull was arbitrarily used. The results of this initial study can be found in Appendix B. After the interaction between y^+ and mesh (specifically the inflated boundary) was understood, the knowledge was applied to the bare DREA submarine hull. A further study was done focusing on the other parameters to determine when a mesh insensitive solution was found.

In order to accurately track how each mesh was generated, the parameters were recorded and the files assigned a specific name. A naming convention was established to document the type of shape, the version of CFX used and the mesh label. The convention can be found below in *Figure 10*:



Naming convention:

A – Type of Shape, either DREA6m or AXI6m

B – Version of CFX-5 used, either CFX55 for CFX-5.5, CFX556 for a file created in CFX-5.5 and converted to CFX 5.6 or CFX56 for CFX-5.6

C – Mesh name - a letter of the alphabet

Figure 10 - Naming Convention for CFX-5 Simulations

Each trial is catalogued in Appendix B and the results summarized in the following sections. The final mesh was DREA6mCFX556g since an increase in the mesh density did not change the values appreciably.

4.2 Side Mesh

The following is a visual representation of the mesh used for the final results. The image is a side view of the centre plane. *Figure 11* is a view of the entire domain. The image is simply a slice through the control volumes and since the grid is unstructured is not an image of the full size of every node. As discussed earlier, the increased mesh density near the hull can be noted. The outer domain has the coarsest mesh since there are fewer changes in that region of the flow.

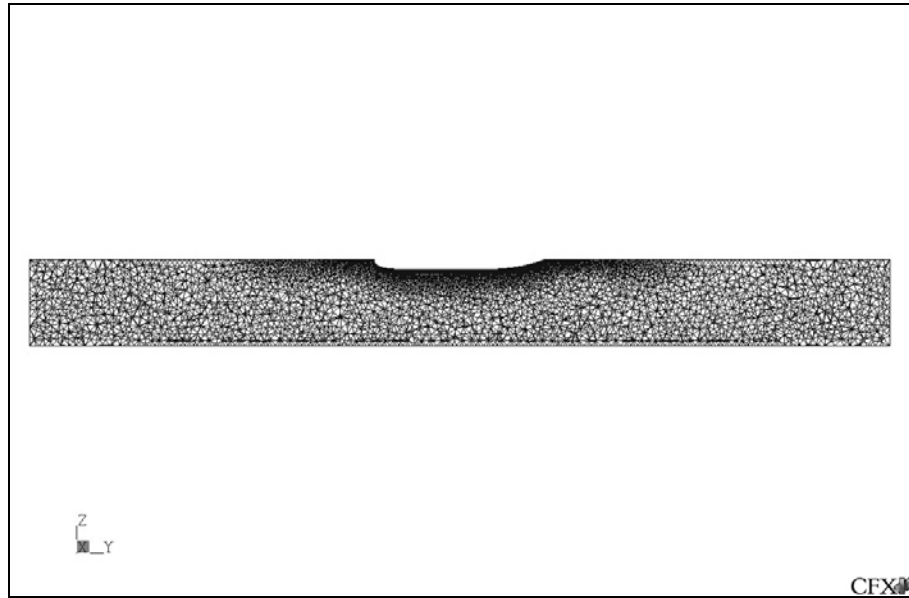


Figure 11 - View of Entire Domain of Bare DREA Submarine Hull 556G-Mesh

Figure 12 is a closer look at the mesh near the submarine hull. Here the inflated boundary can be observed. It is the region of the mesh near the hull made of prismatic (prism) shapes. More will be discussed about inflated boundaries in the Inflated Boundary section. The tetrahedral mesh just outside this region is based on the surface mesh generated from the parameters applied. At this time it would be beneficial to reiterate how the mesh is constructed, which was discussed previously. The mesh engine uses the parameters chosen

in Build to generate a surface mesh to resolve the geometry. These parameters, based on the angular resolution type of meshing, are the angular resolution angle, the maximum edge length, the minimum edge length and the expansion factor. The volume mesh is then generated based on the surface mesh using the expansion factor to increase the control volume size as the mesh propagates from the surfaces. The inflated boundary is also created at this time.

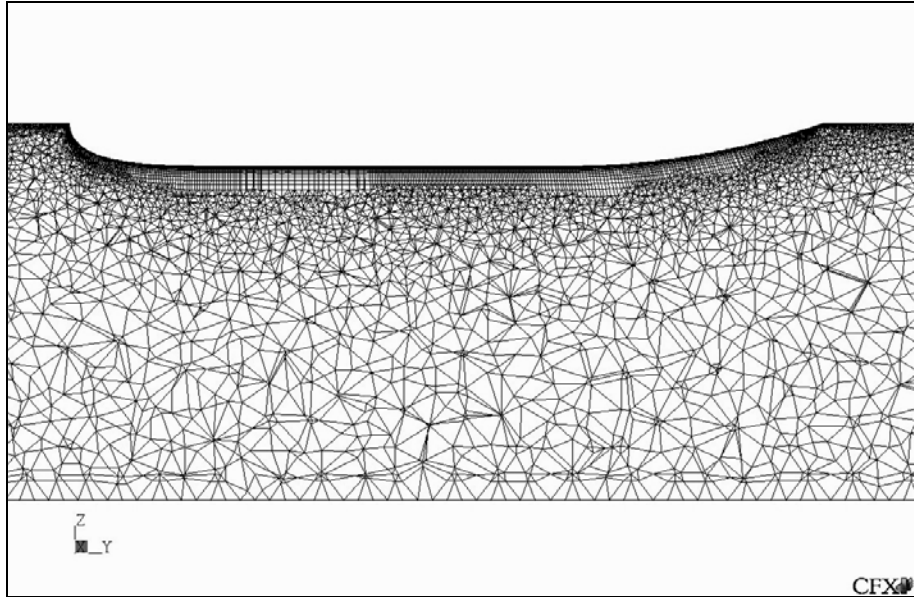


Figure 12 - Centreline Side View of Bare DREA Submarine Hull 556G-Mesh

4.3 Inflated Boundary

Figures 13 and 14 show the mesh along the side of the hull more closely. *Figure 13* is a top view while *Figure 14* is a centreline side view, although both show the same thing since the inflated boundary is radial around the hull. *Figure 13* shows how the inflated boundary grids start small near the hull and increase in size as the number of layers increases. This happens until the edge length of the prism mesh matches the edge length of the tetrahedral mesh and a smooth transition is afforded.

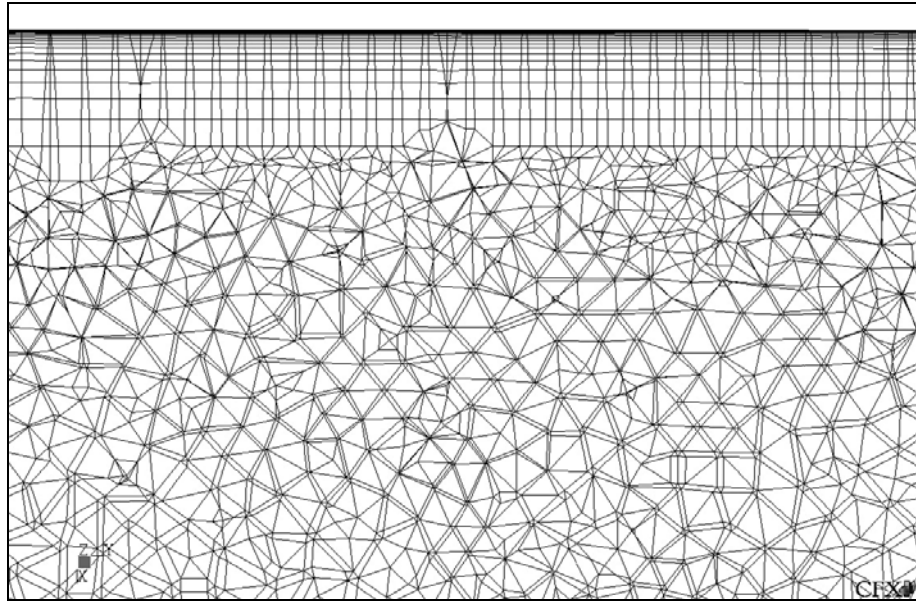


Figure 13 - Top View of Side Section of DREA Submarine Hull 556G-Mesh

Figure 14 shows a closer view of the inflated boundary. The extent of how small the prism mesh near the surface is when compared to the rest of the mesh is shown in this figure. The prisms near the surface are not visible in this view and only appear as a dark line. The rapid expansion from such a small mesh size back to a size comparable to the tetrahedral mesh can also be noted. This expansion is a result of choosing such a high geometric expansion factor in the inflated boundary parameters.

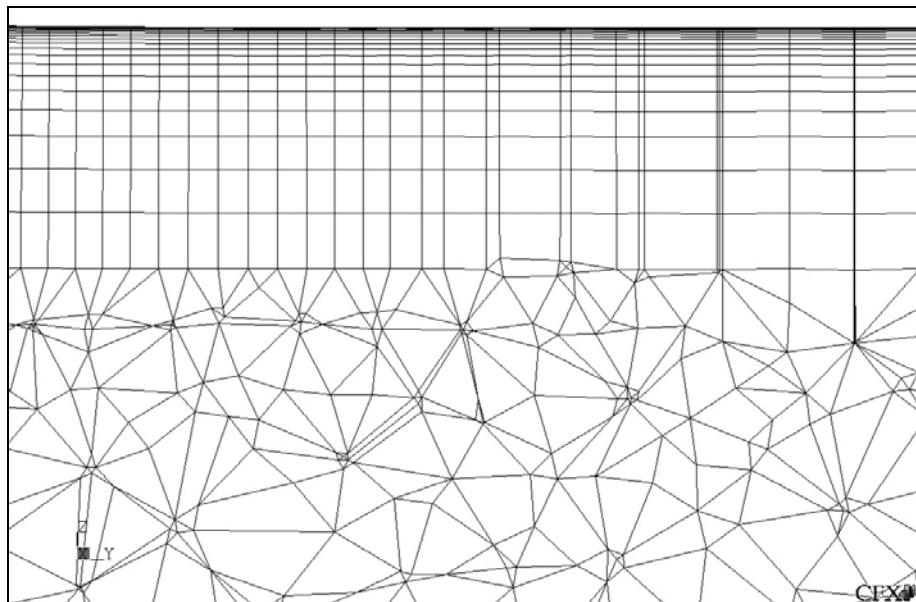


Figure 14 - Centreline Side View of Side Section of Bare DREA Submarine Hull 556G-Mesh

4.4 Tail Section

The following *Figures 15, 16 and 17* are images of the mesh in the tail section of the ship. In *Figure 15* the side view of the centreline profile is shown. Since the tail section is the most complex part of the geometry it required a much finer surface mesh to resolve it. This translates into a finer volume mesh at the tail. Since the inflated boundary only grows until it reaches the same edge length as the tetrahedral mesh, the inflated boundary is markedly thinner than in the rest of the hull. This effect can be seen in *Figure 15*.

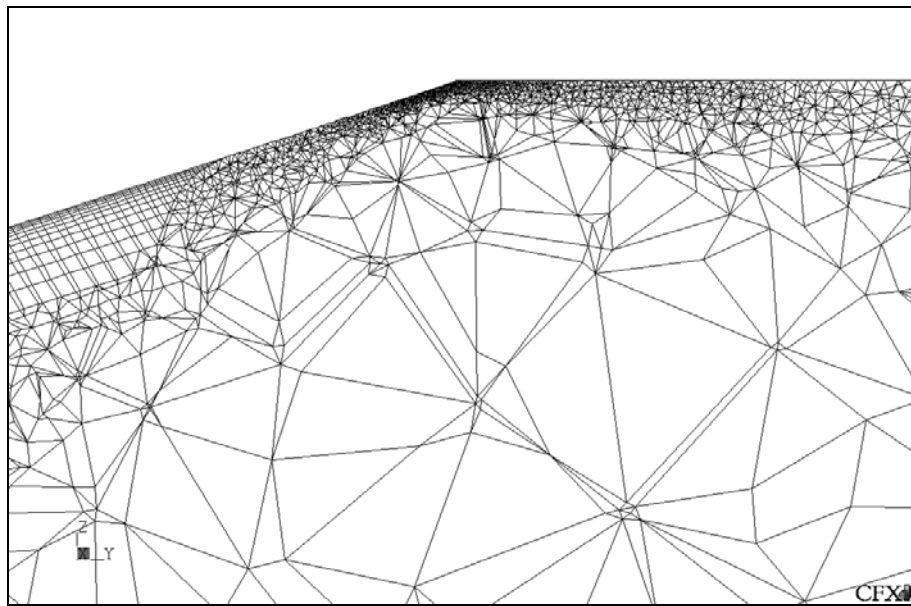


Figure 15 - Centreline Side View of Tail Section of DREA Submarine 556G-Mesh

Figure 16 shows a top view of a larger scale picture. Again, this is another good example of how finer mesh is required to resolve more complex geometry.

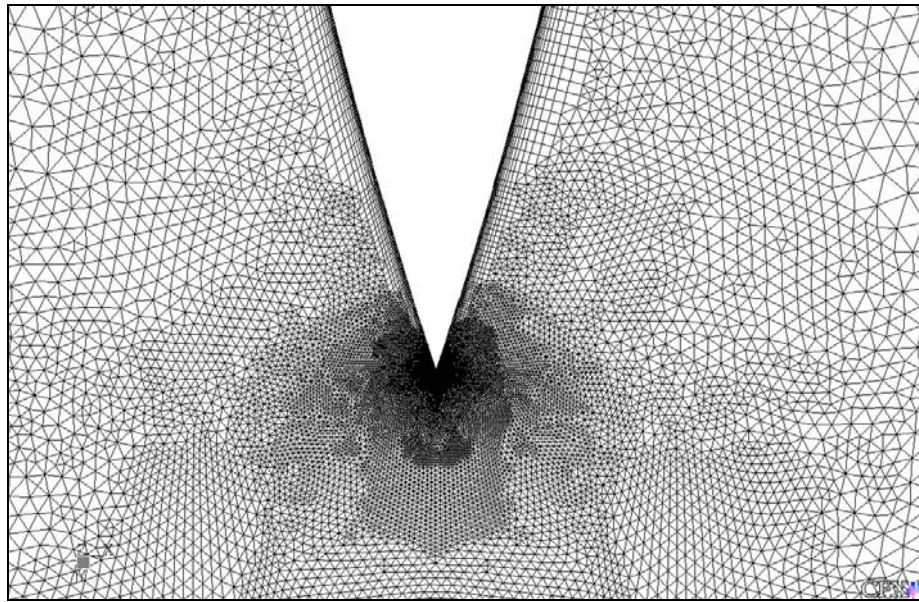


Figure 16 - Top View of Tail Section of Bare DREA Submarine 556G-Mesh

Figure 17 is a close up of the top view of the tail section's inflated boundary. Although the inflated boundary is much smaller at the tail in total thickness, this shows that it still exists near the surface allowing the surface shear to be predicted via the wall functions.

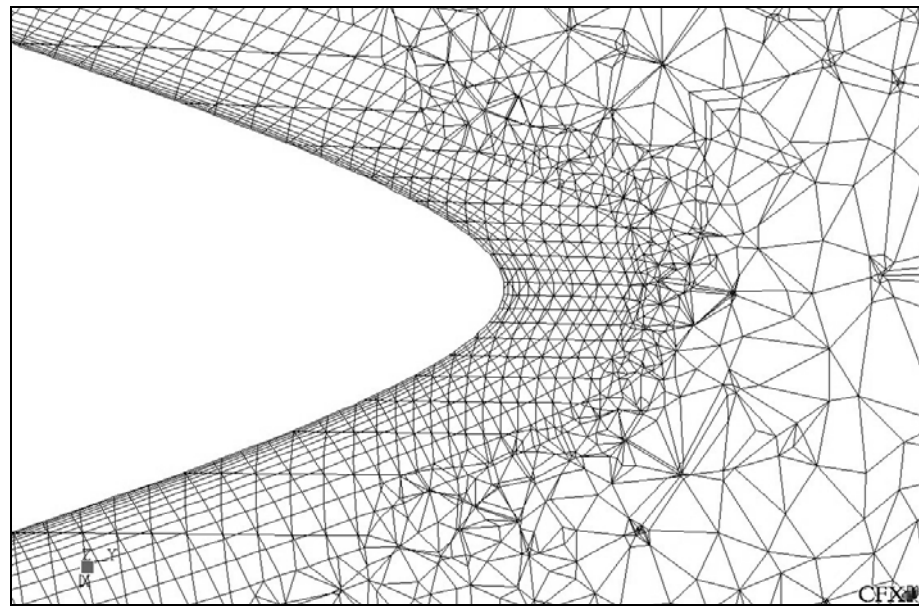


Figure 17 - Close Up Top View of Tail Section of Bare DREA Submarine Hull 556G-Mesh

4.5 Front Section

Figures 18, 19 and 20 show the mesh at the front section of the hull. *Figure 18* shows how the mesh engine increases the mesh density near the tip of the hull, which helps to resolve the stagnation point. It is also interesting to note that the mesh is not symmetric around the symmetric hull. *Figures 19 and 20* show the front section of the hull more closely and in two different views. *Figure 19* is a top view while *Figure 20* is a centreline side view. Upon closer inspection it can be seen that the inflated boundary is nearly none existent at the tip. This means the tetrahedral mesh is so dense that the inflated boundary generation is terminated upon creation since the criterion for conversion from one mesh type to another was met.

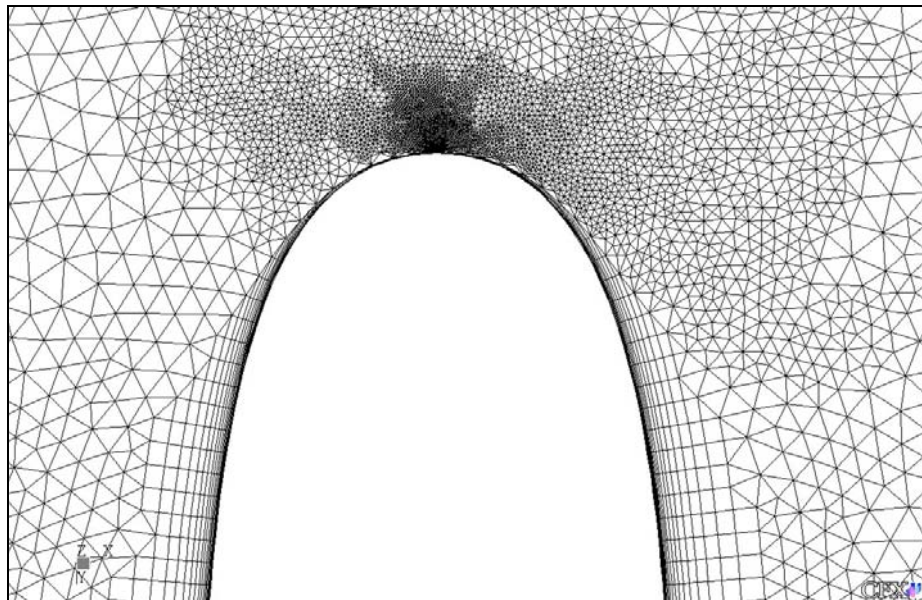


Figure 18 - Top View of Front Section of Bare DREA Submarine Hull 556G-Mesh

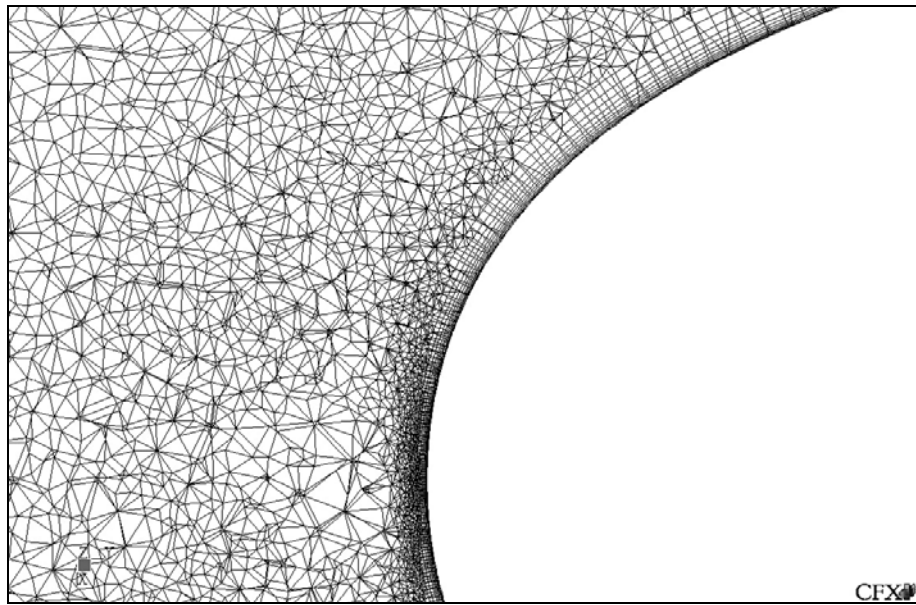


Figure 19 - Top View of Front Section of Bare DREA Submarine Hull 556G-Mesh

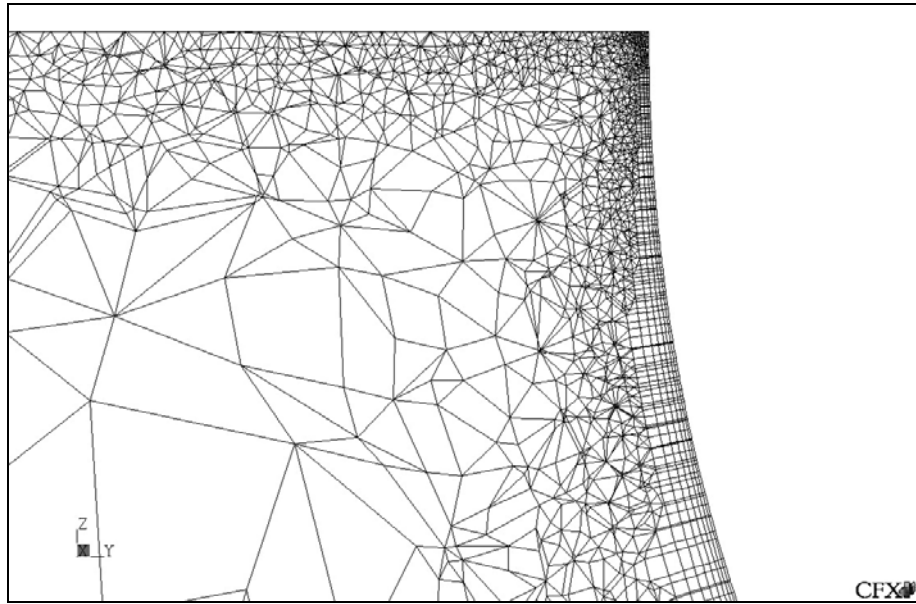


Figure 20 - Centreline Top View of Front Section of Bare DREA Submarine Hull 556G-Mesh

4.6 DREA Submarine Hull Mesh and $y+$ Sensitivity Analysis

A mesh sensitivity analysis was completed for the DREA submarine hull. *Table 1* shows the preliminary mesh sensitivity analysis. A lot of the parameters applied during the

preliminary mesh sensitivity analysis are the same as the parameters applied to the axisymmetric shape and hence appear as a duplication of trials. To one extent this is true and is related to the learning process, but it is also important to note that each mesh sensitivity analysis is different. The axisymmetric shape had a bulbous front and a tapered rear while the submarine hull had a bulbous front, a flat body and a tapered rear. These geometries are markedly similar but it is still important to appreciate the difference between the two, and thus try different mesh settings to determine what best suits that particular situation.

<u>Name</u>	<u>Number of Nodes</u>	<u>Number of Elements</u>	<u>Pressure Drag (N)</u>	<u>Viscous Drag (N)</u>	<u>Total Drag (N)</u>	<u>Maximum y+</u>
55A	101140	405 358	233.5	182.2	415.7	900
55B	163856	530496	228.7	186.9	415.6	60
55C	403090	1867774	210.9	185.4	396.3	60
55D	158176	520731	229.8	186.5	416.3	80
55E	172164	546859	232.6	187.7	420.3	40
55F	191872	605547	228.3	186.6	414.8	60

Table 1 - Preliminary Mesh Sensitivity Analysis on Bare DREA Submarine Hull

<u>Name</u>	<u>Change</u>
55A	First prism height of 0.005 m
55B	First prism height of 0.0003 m
55C	Maximum edge length reduced to 0.15 m
55D	First prism height of 0.0004 m
55E	First prism height of 0.0002 m
55F	Angular resolution changed to 6 degrees

Table 2 - Preliminary Mesh Sensitivity Analysis Changes for Bare DREA Submarine Hull

As can be noted from *Table 2*, the main focus of the preliminary mesh sensitivity analysis was to get the $y+$ values in the correct range while at the same time experimenting to better understand the relationships involved. The main relationship in effect here is the one between the first prism height of the inflated boundary and the $y+$ values, which has been well documented so far in the report. *Figure 21* shows the results of the preliminary

mesh analysis in a graphical fashion. The general trend at this stage of the analysis is the more nodes, and thus denser the mesh, the more consistent the values.

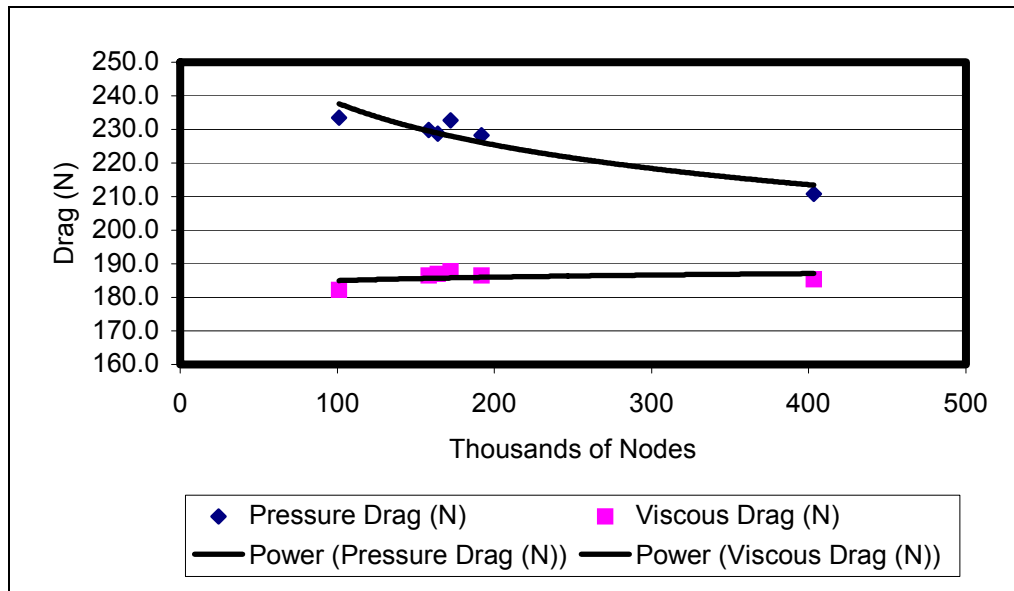


Figure 21 - Standard DREA Hull Drag Values with Changing Mesh Size (Preliminary)

Tables 3 and 4 show the second stage of the mesh sensitivity analysis. At this stage the focus shifts from the inflated boundary to the other mesh parameters. This can be noted by the lack of any change in the maximum $y+$ values from simulation to simulation. The actual changes are outlined in Table 4. Simulation 556B was set to the same parameters as 55B to show that there is no difference between working with CFX-5.6 and CFX-5.5, the previous version of CFX-5 in which some of the simulations were run. At this stage of the analysis the drag values are not changing by much but are still changing. This final mesh was found by varying the maximum edge length and the expansion factor. Varying the expansion factor increases the influence of the fine surface mesh around the hull on the volume mesh just outside the inflated boundary. The minimum edge length alters the size of the control volumes in the outer domain. Simulation 556C is a good example of a mesh with a large number of nodes, which would generally indicate a better solution, but the increased nodes do not further resolve the domain. The maximum edge length was reduced but the expansion factor was left at 1.20. In this case the extra 900 000 nodes were placed in the outer domain and not near the hull where the flow is changing the most and thus affects the

results the most. Simulations D, E, F and G alter the expansion factor to increase the number of nodes near the shape but just outside the inflated boundary, playing off the fact that the surface mesh is finer in that area. Just to prove that more nodes do not necessarily assure a better answer, simulation 556H is a combination of the reduced expansion factor and the reduced maximum edge length. Comparing it to simulation 556G which has only the reduced expansion factor, and one quarter of the number of nodes, the results are nearly identical.

<u>Name</u>	<u>Number of Nodes</u>	<u>Number of Elements</u>	<u>Pressure Drag (N)</u>	<u>Viscous Drag (N)</u>	<u>Total Drag (N)</u>	<u>Maximum y+</u>
556A	151161	465259	229.9	184.4	414.3	60
556B	163856	530496	228.7	187.0	415.7	60
556C	1030017	5441004	210.9	185.4	396.3	60
556D	218932	798143	210.4	181.1	391.5	60
556E	272889	1036615	199.3	182.1	381.4	60
556F	272889	1036615	199.3	182.1	381.4	60
556G	435537	1723342	183.2	183.1	366.3	60
556H	1238502	6286636	181.9	183.0	364.9	60

Table 3 - Final Mesh Sensitivity Analysis on Bare DREA Submarine Hull Run at 3.5 m/s

<u>Name</u>	<u>Change</u>
556A	Maximum edge length increased to 0.5 m
556B	First prism height of 0.0003 m (compares with 55B)
556C	Maximum edge length reduced to 0.1 m
556D	Expansion factor reduced to 1.075
556E	Expansion factor reduced to 1.05
556F	Same as 556E (Illustrates reason for recording all parameters)
556G	Expansion factor reduced to 1.03
556H	Expansion Factor at 1.05 and max edge length at 0.1 m

Table 4 - Final Mesh Sensitivity Analysis Changes for Bare DREA Submarine Hull

Figure 22 shows the trends in the final mesh sensitivity study. The off trend node at approximately one million nodes is simulation 556C. Again, this figure follows the same trend as the others with the only change being the significance of the change in drag values as the mesh parameters are changed. This is an example of how y^+ values are not the only indication of how adequate the mesh is for the simulation.

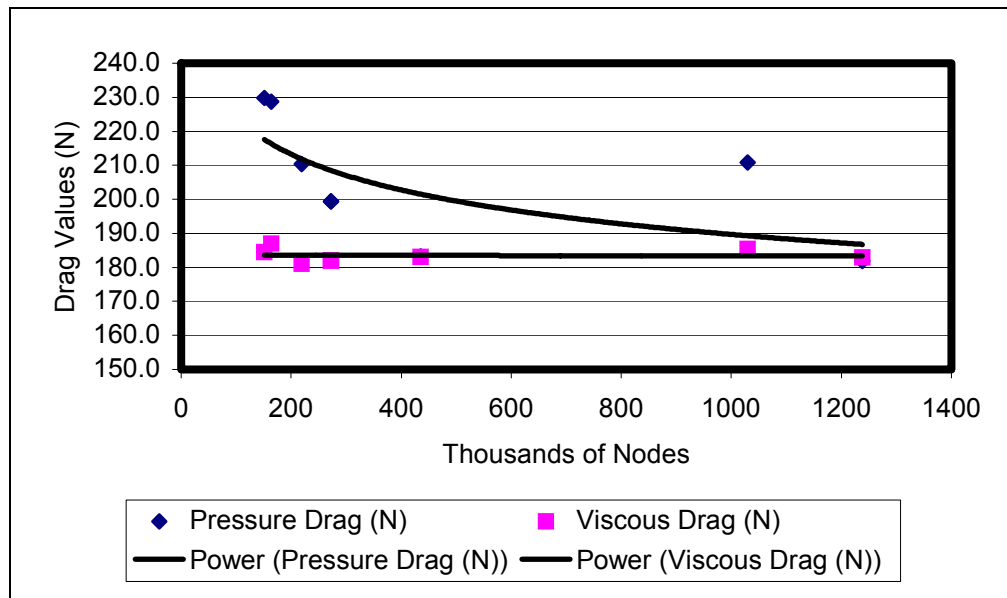


Figure 22 - Standard Bare DREA Hull Drag Values with Changing Mesh Resolution (Final)

Figure 23 shows the relationship between the changing prism height of the inflated boundary and the maximum y^+ value. Any one of the three values could have been used given the criterion that the y^+ values had to be between 20 and 100, but the middle value of 0.0003 meters was used because it offered the lowest values over the general shape with the fewest instances of the y^+ values dropping below 20. As noted in the mesh theory section this is not as much of a problem as having y^+ values that are too high because CFX-5 has built in scaling functions that can account for the lower values.

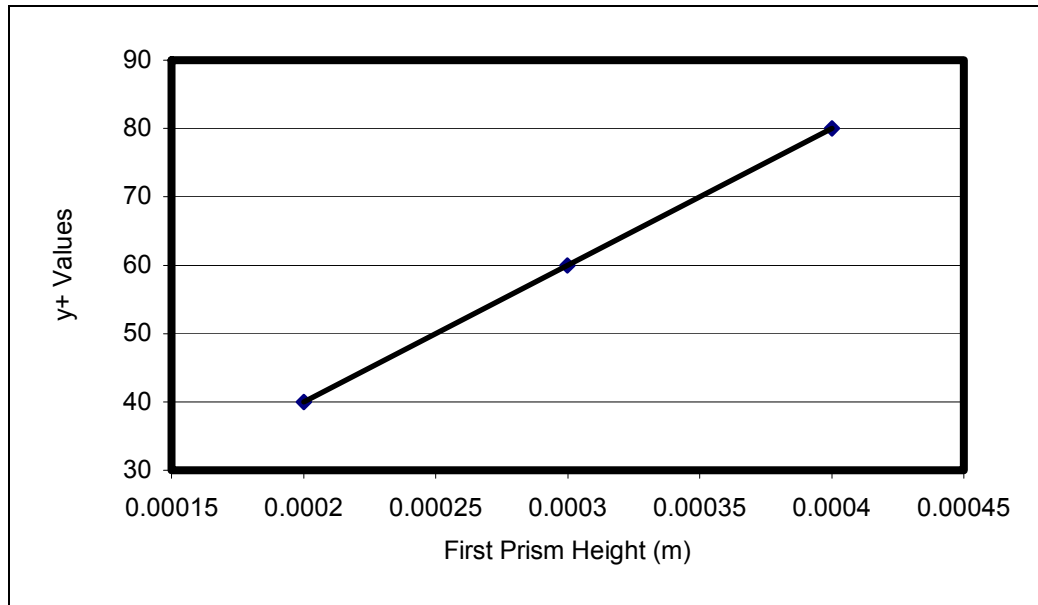


Figure 23 - Standard Bare DREA Hull Maximum $y+$ Values with Changing Inflated Boundary Parameters

4.7 $y+$ Visualization

Figure 24 shows a variable colour plot of the $y+$ values along the entire length of the submarine hull. The majority of the $y+$ values are in the range of 30 to 60. There is a slight increase to values of approximately 65 at the front section of the hull and a slight decrease to values of approximately 20 at the tail section of the hull. This makes sense physically since the $y+$ value is depended on the nearest node to the surface and the actual boundary layer thickness. At the front section of the hull there is a favourable pressure gradient, which makes the boundary layer thin. The $y+$ values at the tail of the hull are lowest because there is an adverse pressure gradient, which causes the boundary layer to thicken.

The $y+$ values are nearly constant across the flat part of the hull. This is the region that best compares to flat plate boundary theory. It is suspected that a change in the $y+$ values as the boundary layer grows over this region is not seen because the boundary layer growth is entirely outside the nearest node. From flat plate theory a flat plate has a boundary layer thickness of 0.0183 meters at the one-meter mark based on turbulent flow. This thickness increases to 0.0729 meters at the five-meter mark. The nearest node was set to be on the order of 0.0003 meters which means the outer region of the boundary layer is outside

of this node and we are only estimating the shape of a small portion of the total boundary layer. This can also be related to the wall shear since y^+ value is dependent on the wall shear at that point. At the front section there is a high wall shear value, which can be seen in *Figure 39* in section 5.4. Noting *equations 9 and 10*, as the wall shear increases the y^+ values increase. At the tail section the wall shear is decreasing because of the adverse pressure gradient and hence the y^+ values decrease.

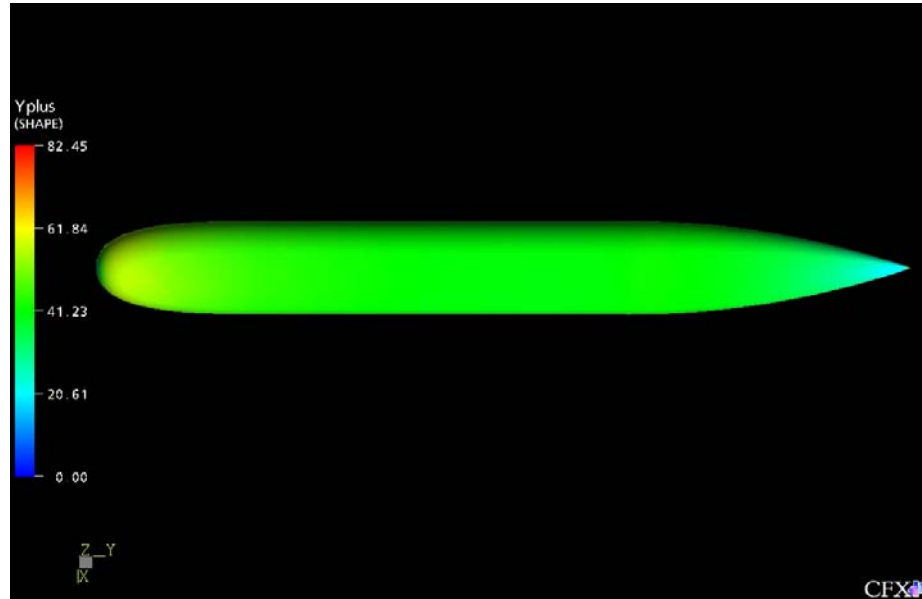
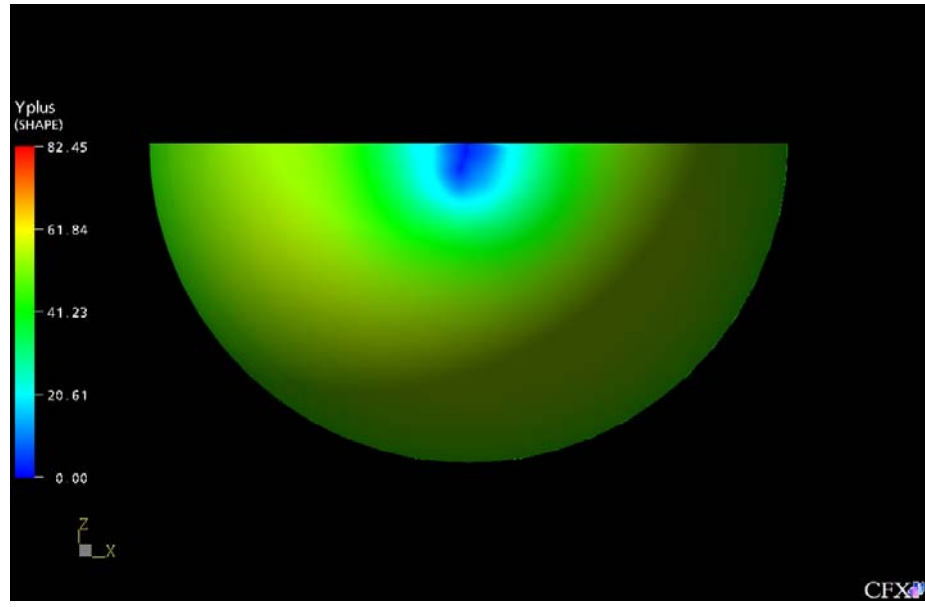


Figure 24 - y^+ Values for DREA Submarine Hull at $Re = 23$ Million (3.42 m/s) 556G-Mesh

Figure 25 shows a front view of the y^+ values at the front section of the hull. The slight yellow increase shows the increase in y^+ values discussed above. The blue circular region shows an area where the y^+ values slip below the lower limit of 20. This is only a small region and should not have too much affect on the final results.



**Figure 25 - $y+$ Values for Front of DREA Submarine Hull at $Re = 23$ Million (3.42m/s)
556G-Mesh**

Figure 26 shows a top view of the tail section of the $y+$ plot. The light blue indicates the region where the $y+$ values went down as expected. The small region at the outermost tip shows how $y+$ values are very much dependent on the mesh. Consulting *Figure 15* showing the mesh at the tail section we can see that the inflated boundary does not work well in regions of complex geometry and is thence replaced by tetrahedral elements. This results in the variation in $y+$ value through this extremely small region. It also should be noted that the values are still within the valid range

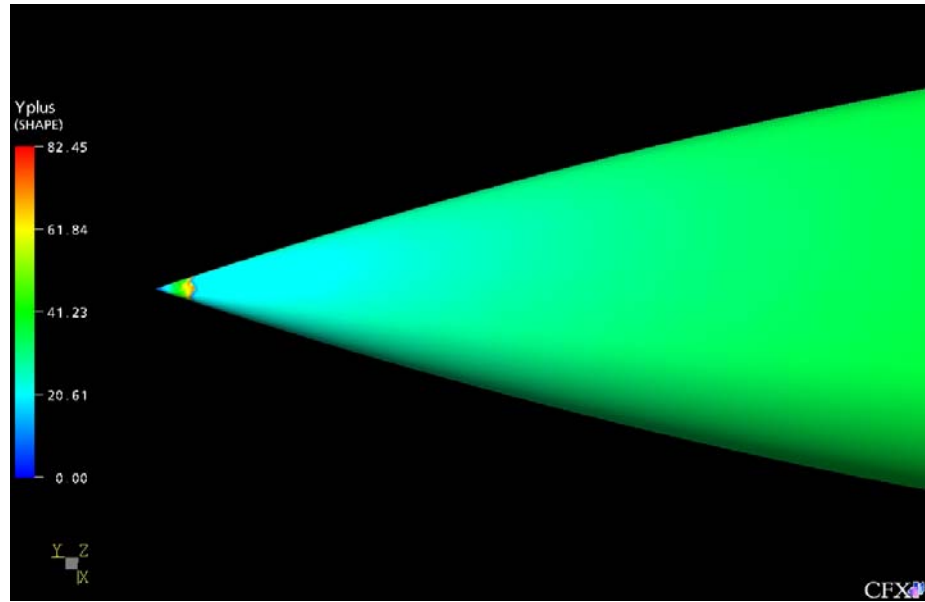


Figure 26 - y^+ Values for Tail of DREA Submarine Hull at $Re = 23$ Million (3.42 m/s) 556G-Mesh

Table 5 shows an investigation into the relationship between y^+ values and the free stream velocity or Reynolds number. The results make sense physically since as the velocity increases, the wall shear increases and hence the y^+ values increase and the drag increases. From this we can recognize that the mesh is only valid for a range of flow speeds. This particular mesh produces acceptable y^+ values up to 4.5 m/s. However, it is important to reiterate that ensuring the y^+ values are in the proper range is only one criterion for ensuring the mesh is adequate for producing acceptable results.

<u>Velocity (m/s)</u>	<u>Pressure Drag (N)</u>	<u>Viscous Drag (N)</u>	<u>Total Drag (N)</u>	<u>Maximum y+ Value</u>	<u>Majority y+ Value</u>	<u>Reynolds Number</u>
1.00	15	18	33	27	20	6722104
2.50	94	98	192	62	45	16805259
3.00	135	138	273	73	50	20166311
3.422	175	176	351	82	60	23003039
3.50	180	183	363	84	63	23527363
4.50	302	291	593	105	80	30249466
10.00	1479	1285	2764	218	163	67221036
25.00	9164	7110	16275	509	300	168052590
40.00	23394	17140	40534	788	600	268884144

Table 5 - Drag Sensitivity to Reynolds Number Using 556G-Mesh

Table 6 shows the relationship between the free stream inlet velocity, the Reynolds number and the upstream dynamic reference pressure (Q). The reference pressure is shown in *Equation 12*.

$$Q = \frac{1}{2} \rho U_{ref}^2 \quad (12)$$

The upstream dynamic pressure Q is often used in wind tunnel testing since it is used in many dimensionless coefficients and is the total pressure read from the measurement devices [4].

Velocity (m/s)	Reynolds Number	Q (Pa)
1.0	672,210	499
2.5	1,680,526	3,116
3.0	2,016,631	4,487
3.422	2,300,304	5,837
3.5	2,352,736	6,107
4.5	3,024,947	10,095
10.0	6,722,104	49,850
25.0	16,805,259	311,563
40.0	26,888,414	797,600

Table 6 - Velocity Related to Reynolds Number (Re) and Upstream Pressure (Q)

Figure 27 shows the trends of the y^+ values as the Reynolds number increases. This appears to be a linear relationship. *Figure 28* shows the relationship between the final drag values and the Reynolds number. This is not a linear relationship, in fact it resembles a logarithmic relationship as can be seen in *Figure 29*. The nonlinearities are a result of the fact total drag is a combination of the viscous drag and the pressure drag. As the flow increases in speed separation can occur and the pressure drag can increase more than if separation was not involved.

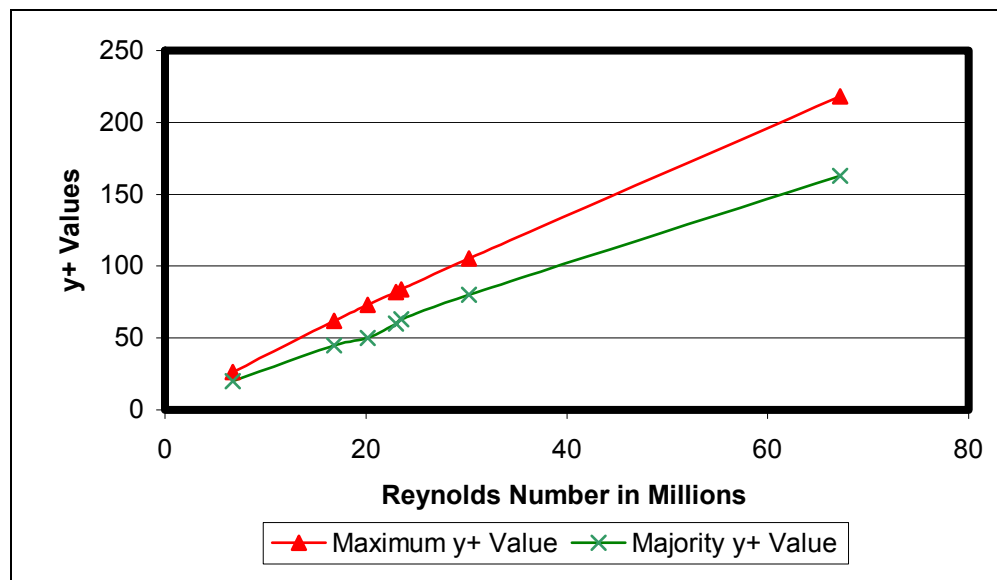


Figure 27 - DREA Submarine Hull y^+ Values with Changing Reynolds Number

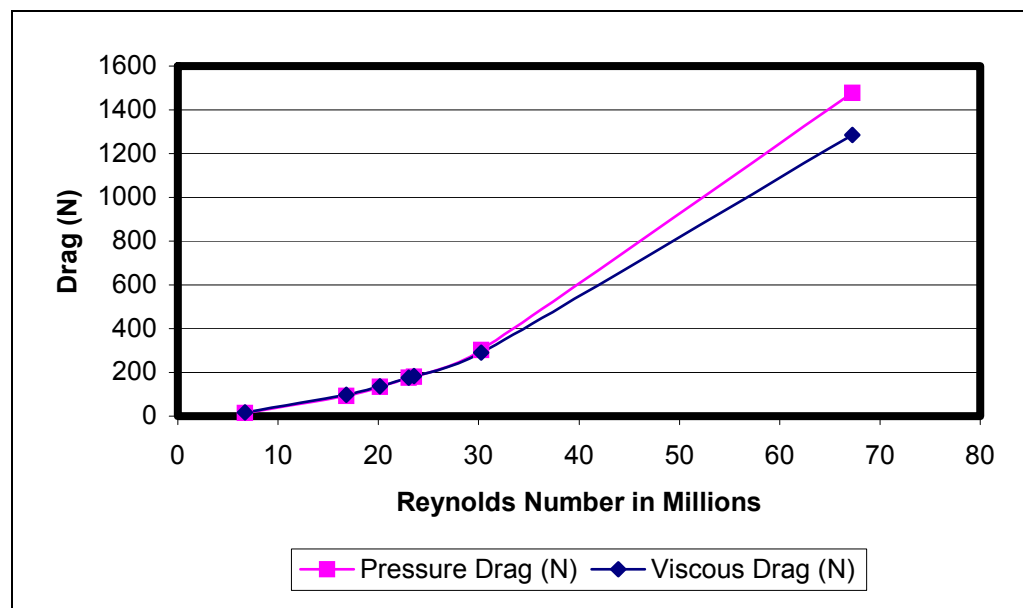


Figure 28 - DREA Submarine Hull Drag Values with Changing Reynolds Number

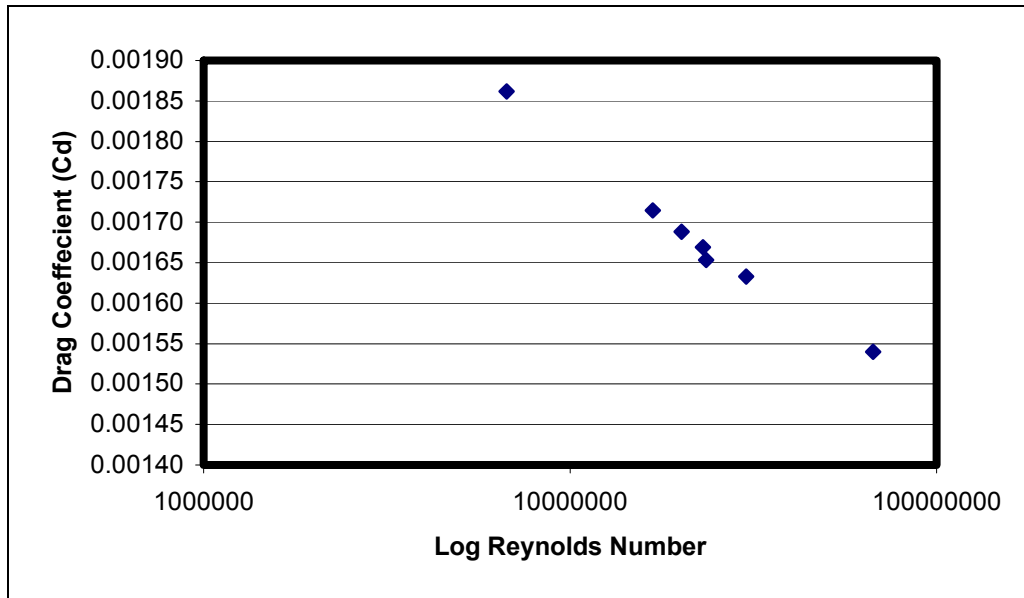


Figure 29 - Drag Coefficient Vs. Log Reynolds Number

Figure 29 is also an example of the changing drag coefficient (C_D) with changing Reynolds number. This trend of decreasing drag coefficient with increasing Reynolds number compares well with trends exhibited in flow over a sphere or wing [1,2].

CHAPTER 5

FLUID MECHANICS RESULTS AND DISCUSSION

5.1 Overview

One of the greatest advantages of CFD over experimentation is the ease and availability of flow visualization. The following chapter shows some of the more relevant flow parameters. It is important when first learning to use CFD that these images can be produced despite having not completely converged a simulation or not having a mesh insensitive solution. It is possible to investigate trends in flow without completing such an exhaustive mesh sensitivity analysis as long as the operator realizes that little stock can be placed in the quantitative values. Generally, with a reasonable grid and a reasonable level of convergence, the results outputted from these simulations will not look much different than one that is fully converged and deemed mesh insensitive.

5.2 Pressure Plots

Figure 30 shows a top view of the pressure plot around the submarine hull at an inlet velocity of 3.422 m/s. We can note the stagnation point of high pressure at the front tip of the hull, the favourable pressure gradient at the front section and the adverse pressure gradient at the rear section of the hull. Since the reference pressure was set to zero the pressures shown are relative.

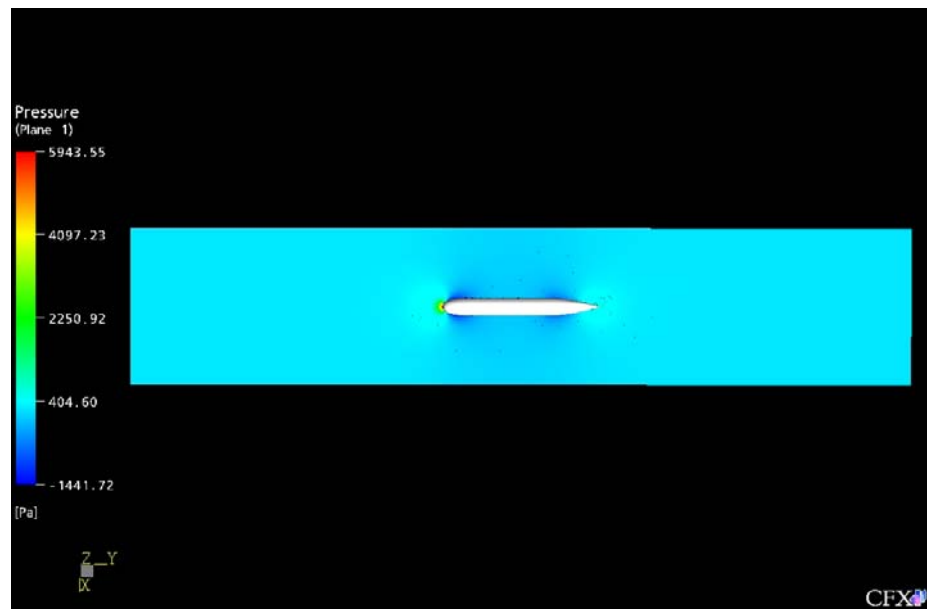


Figure 30 - Top View Pressure Plot for DREA Submarine Hull at $Re = 23$ Million (3.42 m/s) 556G-Mesh

Figure 31 shows a close up of the front section of the hull. Here the stagnation point and the favourable pressure gradient are even more visible.

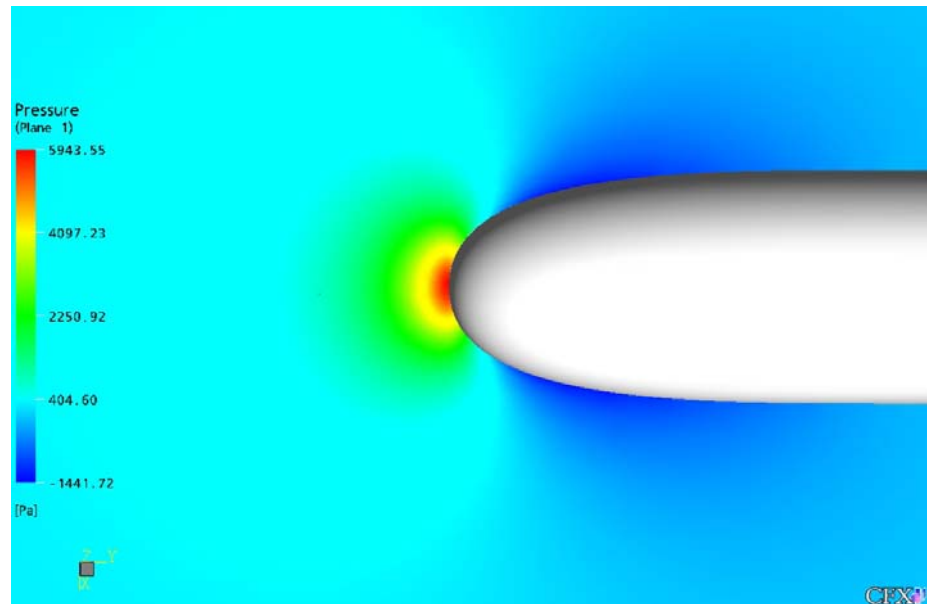


Figure 31 - Top View Pressure Plot of Front Section for DREA Submarine Hull at $Re = 23$ Million (3.42m/s) 556G-Mesh

Figure 32 shows the pressure plot from the centreline side view. This shows a different perspective but looks identical to *Figure 30* which is as expected since the bare submarine hull is axisymmetric.

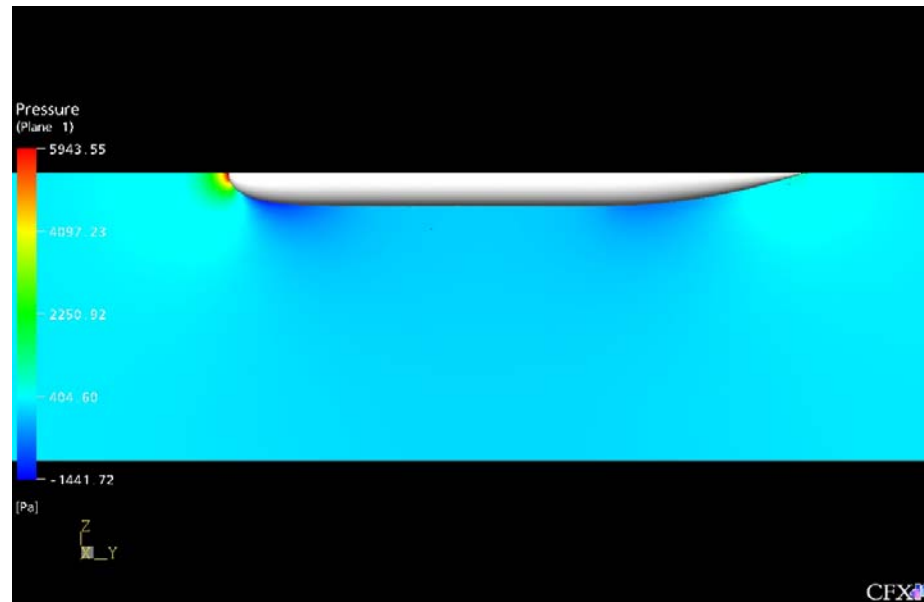


Figure 32 - Centreline Side View Pressure Plot of DREA Submarine Hull at $Re = 23$ Million (3.42 m/s) 556G-Mesh

5.3 Velocity Plots

Figure 33 shows a centreline side view of the velocity plot for the submarine hull run at 3.422 m/s. When compared to the pressure plot we can see the stagnation point of high pressure corresponds to the low velocity point at the front, the favourable pressure gradient in the front section corresponds to a high velocity and the adverse pressure gradient at the rear corresponds to a lower velocity. These trends are as expected since they correspond with the Bernoulli equation.

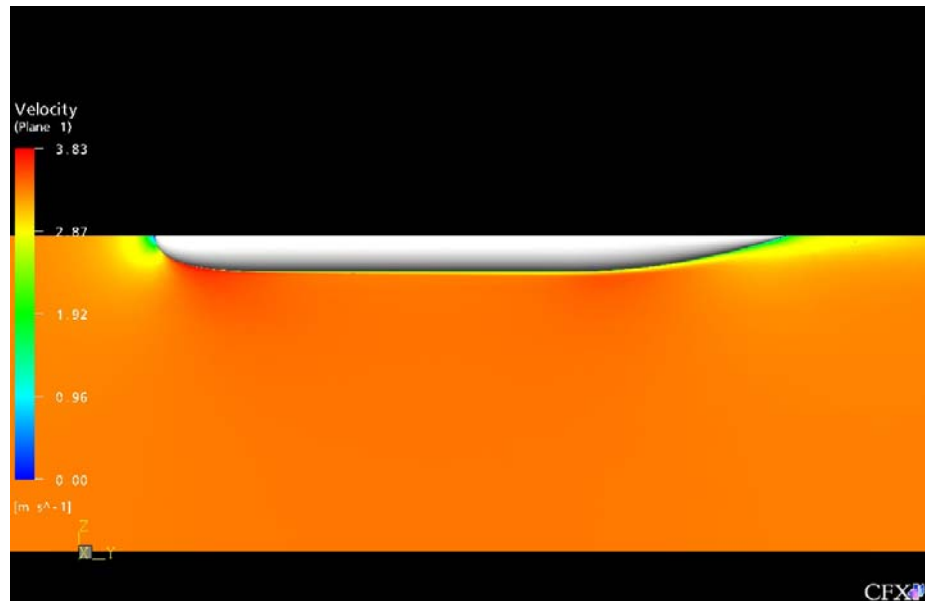


Figure 33 - Centreline Side View Velocity Plot of DREA Submarine Hull at $Re = 23$ Million (3.42 m/s) 556G-Mesh

Figure 34 shows a close up view of the front section of the velocity profile for the submarine hull. Here it is apparent by the colours close to the shape that the no slip boundary condition set for the surface of the hull is in effect. It is also more apparent that the stagnation point is actually a stagnation point with zero velocity (the blue region).

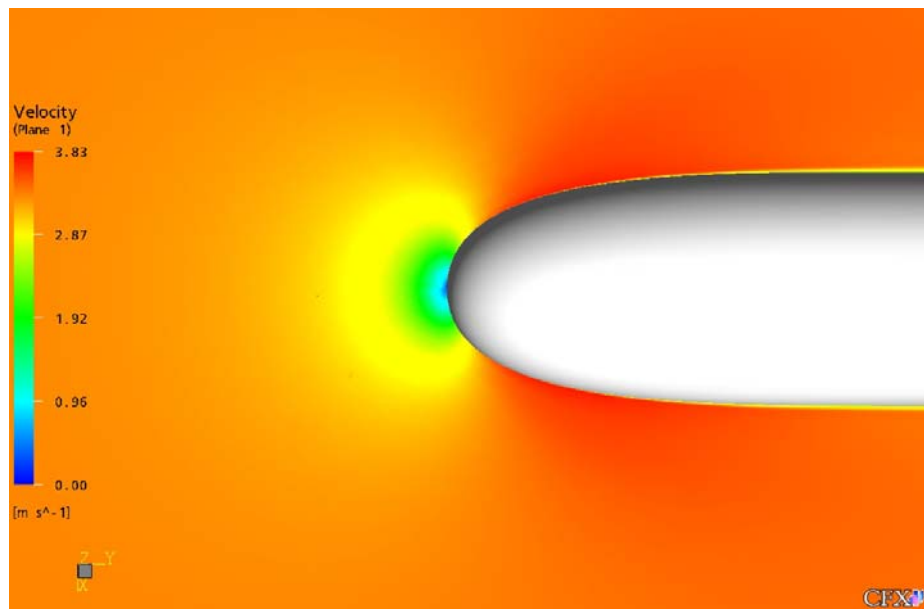


Figure 34 - Top View Velocity Plot of Front Section of DREA Submarine Hull at RE = 23 Million (3.42 m/s) 556G-Mesh

Figure 35 shows a closer look at the tail section of the hull. This shows how the effect of the no slip condition for the surface of the hull has an effect on the flow velocity following the hull.

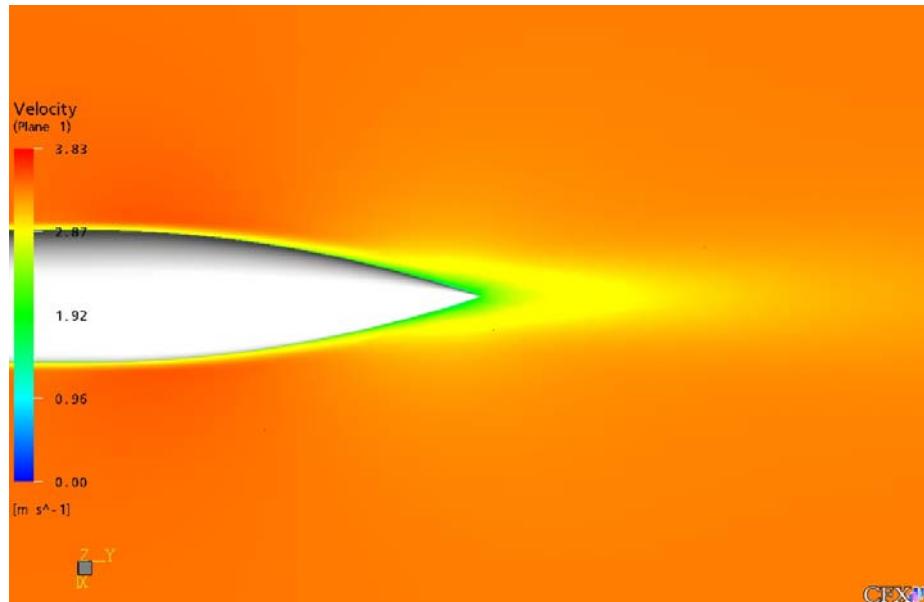


Figure 35 - Top View Velocity Plot of Tail Section of DREA Submarine Hull at Re = 23 Million (3.42 m/s) 556G-Mesh

Figure 36 is another type of velocity plot and can be useful in determining if there is any separation or recirculation. A “velocity v” plot is used here. In this case the absolute velocity is not plotted but the velocity in the y direction only. This allows the operator to look for regions of negative flow velocity to see if there is any recirculation, which is an indication of separation. In this plot there is a small region of dark blue at the very end of the tip, which shows that there is a small amount of separation.

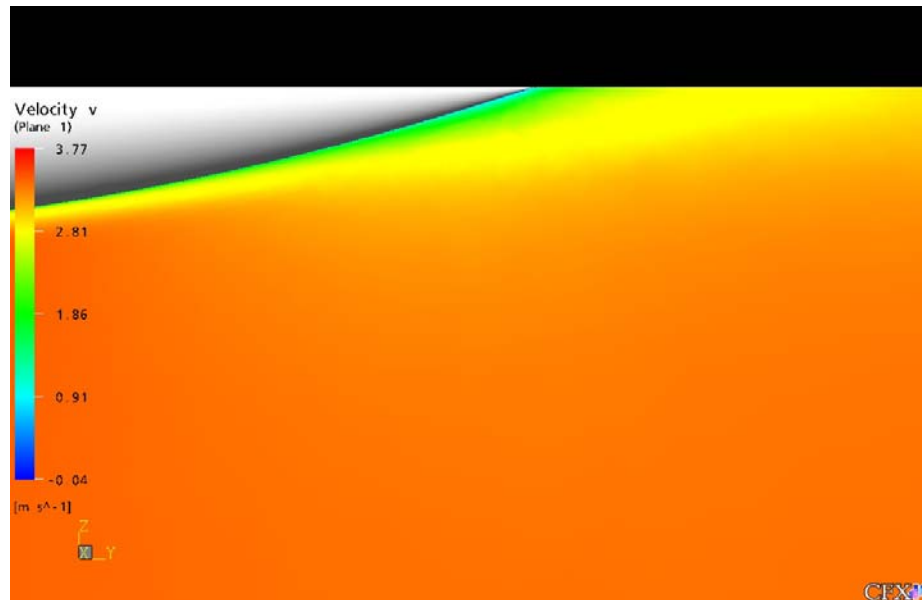


Figure 36 - Centreline Side View “v” Direction Velocity Plot of DREA Submarine Hull at $Re = 23$ Million (3.42 m/s) 556G-Mesh

5.4 Wall Shear Plots

The wall shear plots are a good indication of the viscous drag over the ship. They can also be used to see if there is any separation because the wall shear goes to zero where the boundary layer separates. In *Figure 37* we can see a large wall shear affect in the favourable pressure gradient area at the front section of the hull. This illustrates how this region largely affects the viscous losses. *Figure 38* shows this region closer. The very peak of the front section has a reduced wall shear, which makes sense physically because there is a reduced flow velocity in this region due to the stagnation point.

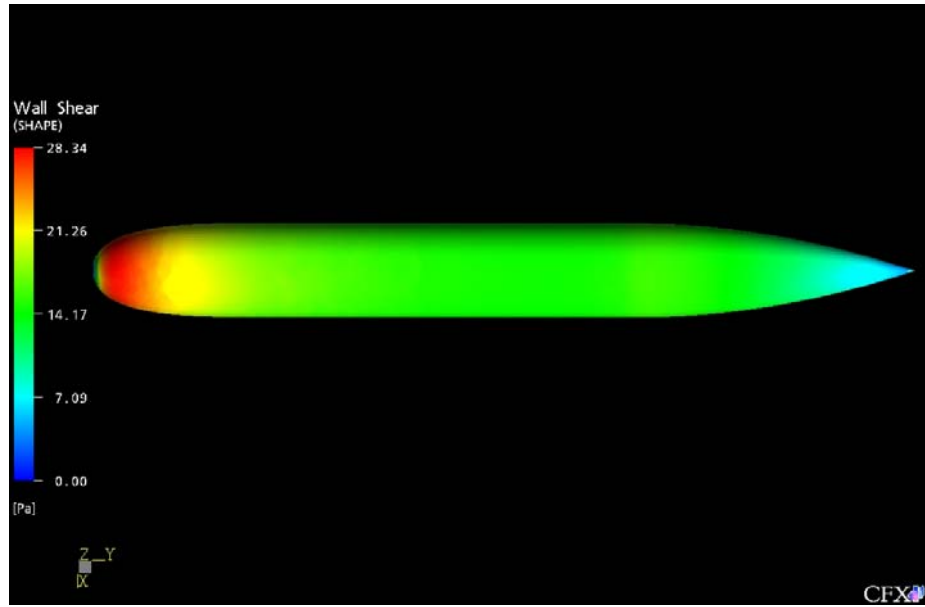


Figure 37 - Top View Wall Shear Plot of DREA Submarine Hull at $Re = 23$ Million (3.42 m/s) 556G-Mesh

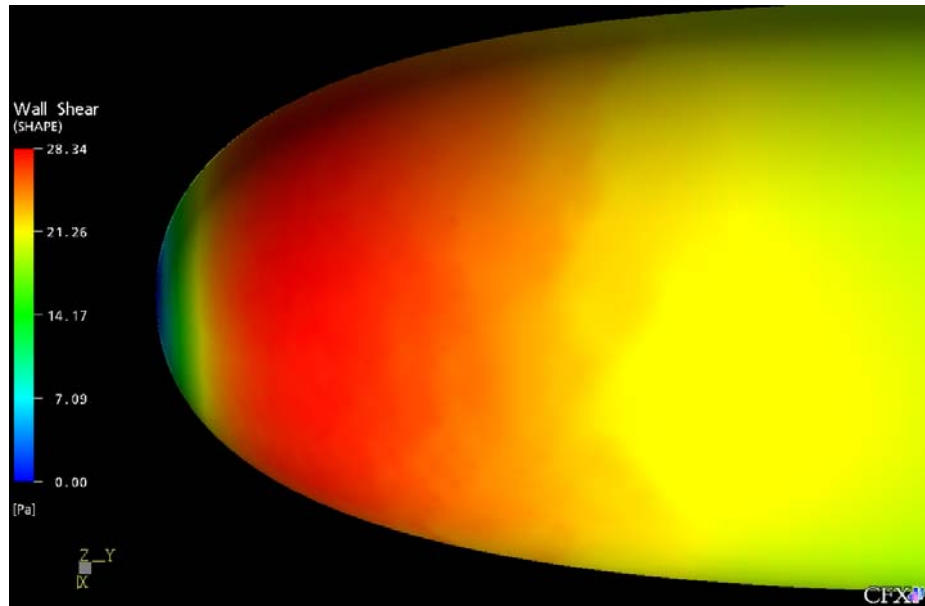


Figure 38 - Top View Wall Shear Plot of Front Section of DREA Submarine Hull at $Re = 23$ Million (3.42 m/s) 556G-Mesh

Figure 39 shows the tail section of the submarine hull. This is where the wall shear plot is beneficial in determining if there is any separation. The wall shear goes nearly to zero but then increases again. This could be the result of one of two things. One possibility is the

boundary layer may have separated and then reattached, which is a common phenomenon. Another possibility is the results could be dependent on the difference in the mesh in that region. Earlier it was noted that the boundary layer did not resolve the smallest part of the tail very well and so tetrahedral elements were used. This change in answer is suspected to be a result of this change, but can only be confirmed by more investigation.

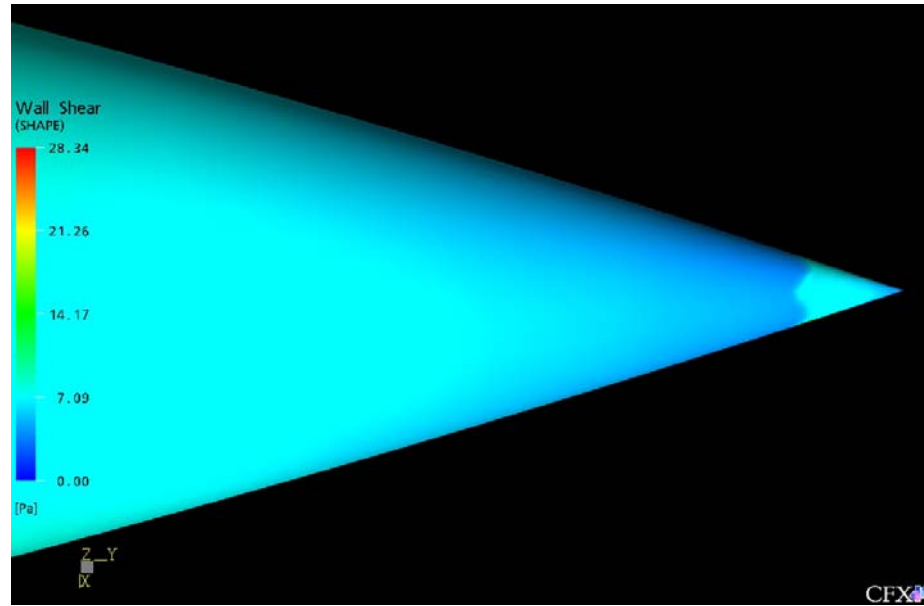


Figure 39 - Top View Wall Shear Plot of Tail Section of DREA Submarine Hull at $Re = 23$ Million (3.42 m/s) 556G-Mesh

5.5 Turbulence Kinetic Energy Plots

Turbulence Kinetic Energy is related to the turbulence model used in this simulation. Turbulence originates from the boundaries of a domain, so in this case the only place for turbulence to be generated is from the shape, since it is the only region with a no slip condition. Turbulence Kinetic Energy is a measure of the energy built up as turbulence. In *Figure 40* the kinetic energy is shown to build up as flow passes along the hull and then propagate from the rear. *Figure 41* shows a close up view of this turbulent energy being dissipated to the free stream.

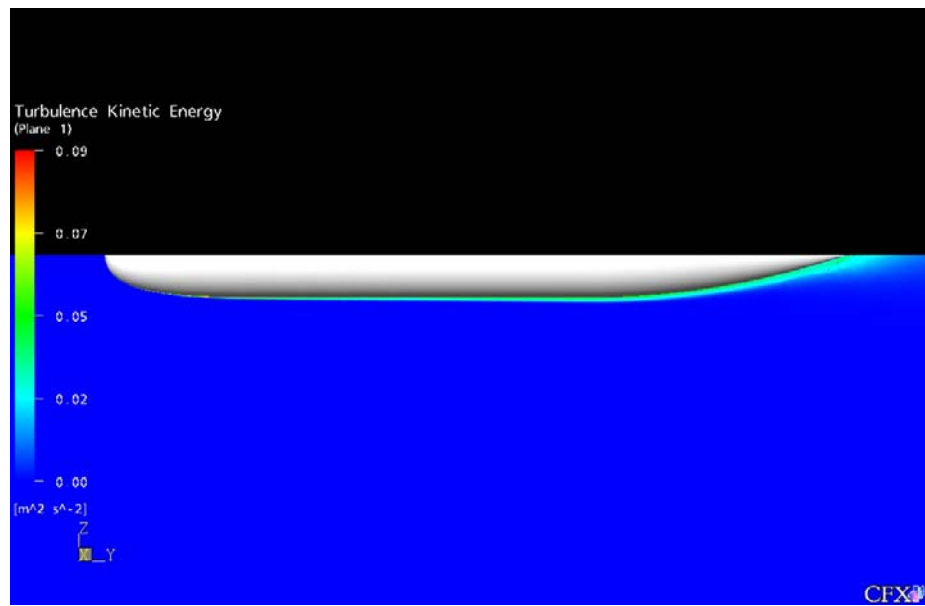


Figure 40 - Centreline Side View Turbulent Kinetic Energy Plot of DREA Submarine Hull at $Re = 23$ Million (3.42 m/s) 556G-Mesh

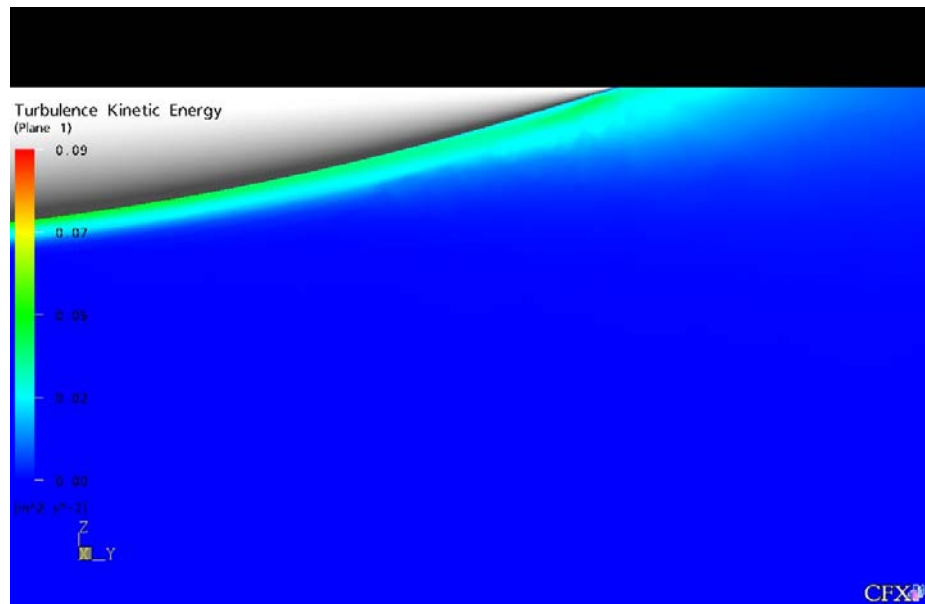


Figure 41 - Centreline Side View Turbulent Kinetic Energy Plot of DREA Submarine Hull at $Re = 23$ Million (3.42 m/s) 556G-Mesh

5.6 Comparison with Experimental Data

As with any CFD simulation, the results should be compared with experimental values to ensure validity. In this case the results are compared to a 1988 wind tunnel test done by DRDC. The results were non-dimensionalized allowing for the comparison between the two fluid mediums. The experiment is subject to errors that lead to a high and low bound for the results. An assumption was made that the error bars would be centred on the calculated value so that the error was equally weighted to either side of the value. *Figure 42* shows the final mesh analysis compared to the high and low bounds for the wind tunnel tests converted to values as if the tests were done using water. The results become closer and closer to the experimental range as the mesh is further refined until the results become mesh insensitive. The final results do not fall within the upper and lower bounds.

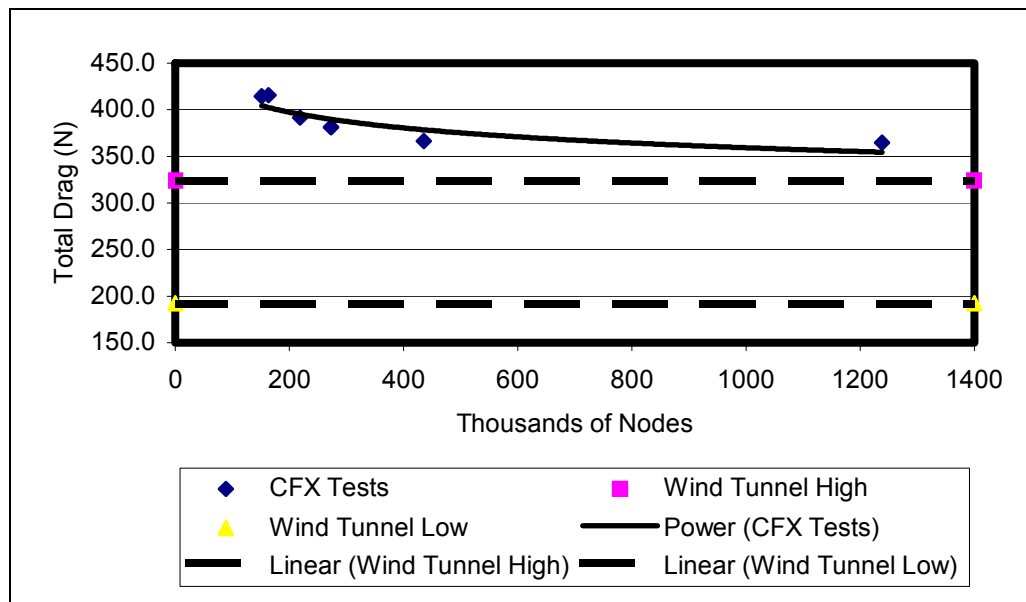


Figure 42 - Standard Bare DREA Hull Drag Values with Changing Mesh Resolution (Final) & Wind Tunnel Tests Error Inclusive Range

The final mesh run at a Reynolds number of 23 million produced a drag force of 350.8 N, which corresponds to a dimensionless drag coefficient (C_D) of 0.00167. The wind tunnel experimental force was found to be 258.2 N +/- 66.1 N, which corresponds to a C_D value of 0.00123 +/- 0.000314. This equates to an approximately 36% difference. However, there are

some solution refinement considerations that have been recommended that may bring these two values into closer agreement. For instance, the advection scheme was changed from the upwind differencing scheme to the high resolution scheme and the pressure drag decreased markedly. The viscous drag remained the same at 176 N while the pressure drag fell to 20 N, resulting in a total drag of 196 N. This places the values at the lower end of the experimental range, but within range nonetheless.

It is also interesting to make a comparison with the flat plate values. Since an appreciable amount of separation is not expected in the flow, the drag values should resemble flat plate values. Flat plate values, based on the same area, indicate a drag force of 175.3 N. This can be compared to two CFX simulation values. First, the total drag was found to be 351 N using the UDS advection scheme and 195 using the high resolution scheme. This results in a 50% and 11% difference, respectively. The viscous drag was found to be 175.6 N using both advection schemes. This makes sense since flat plate drag is primarily viscous in nature.

CHAPTER 6

CONCLUSIONS

Overall the values were found to be of the same order of magnitude but not within the error range of the experimental results. The total drag force on the bare submarine hull was found to be 350.8 N, which corresponds to a dimensionless drag coefficient (C_D) of 0.00167. The wind tunnel experimental force was found to be 258.2 N +/- 66.1 N, which corresponds to a CD value of 0.00123 +/- 0.000314. This equates to an approximately 36% difference. However, there are some solution refinement considerations that have been recommended that may bring these two values into closer agreement.

The exact break up of the drag force was found to be 175.2 N pressure drag and 175.6 N viscous drag. The final mesh used was mesh 556G. The y^+ values were in the proper range of 20 to 100 with the majority below 60. The final mesh had 435 537 nodes and 1 723 342 elements. The elements consisted of 1 393 801 tetrahedral elements, 323 515 prisms, 6029 pyramids. Surface mesh faces numbered 127 531.

The overall project was successful at modeling flow around the bare standard DREA submarine hull at 0° yaw. Further minor adjustments of the parameters may or may not move results closer to the experimental values. Comparing the absolute values is important for verification but the true power of CFD is in qualitative analysis. Comparing the trends produced as the yaw angle changes will be the true test of validation for this overall project. Appreciating this fact, and appreciating the fact the mesh refinement trends moved the results closer to the experimental; it is this author's opinion that the procedure described is a good base for which to continue these calculations.

CHAPTER 7

RECOMMENDATIONS

The following is a list of the recommendations:

- Run simulations using High Resolution advection scheme instead of upwind differencing scheme (UDS). High resolution is a second order advection scheme whereas upwind differencing scheme is first order. This means that with an increase of X nodes, the UDS increases its error reduction by ΔX and the high resolution increases its error reduction by ΔX^2 [2,3].
- Refine mesh in tail region to better determine if separation is occurring, or determine how much of an effect this will have on the final answer and make a judgement call from there.
- Redefine geometry domain so that other yaw angles can be analyzed without the need to rebuild the domain each time. This will be beneficial to the continuation of this project.
- Change the turbulence model to Shear Stress Transport (SST) model and place nodes closer to the surface to better resolve the boundary layer. This should improve results and better resolve separation.

REFERENCES

- [1] White, F., 1999, *Fluid Mechanics*, WCB/McGraw-Hill, Toronto.
- [2] Gerber, A., 2003-02 to 2004-01, Private Communication.
- [3] Versteeg, H.K., Malalasekera, W., 1995, *An Introduction to Computational Fluid Dynamics*, Pearson Prentice Hall, Toronto.
- [4] Holloway, A. G., 2003-08 to 2004-01, Private Communication.
- [5] Department of Research and Development Canada – Atlantic, National Defence, 1988, *Fall 1988 Wind Tunnel Tests of the DREA Six Metre Long Submarine Model – Force Data Analysis*, Ottawa.
- [6] Department of Research and Development Canada – Atlantic, National Defence, 1988, *Flow Visualization Test of DREA Standard Submarine Model October – November 1988*, Ottawa.
- [7] Watt, G. and Knill, K., 1999, “A Preliminary Validation of the RANS Code TASCflow Against Model Scale Submarine Hydrodynamic Data,” *The 7th Annual Conference of the CFD Society of Canada (CFD99)*, Halifax.
- [8] Lin, C., et al., 1995, *Viscous Drag Calculations For Ship Hull Geometry*, Design Evaluation Branch, Hydromechanics Directorate, David Taylor Model Basin, Carderock Division Naval Surface Warfare Center, Bethesda, MD, USA.
- [9] Larson, L., Baba, E., *Advances in Marine Hydrodynamics: Ship Resistance and Flow Calculations*, Computational Mechanics Publications, Boston.
- [10] Holloway, G. 2003-02, ME 3522 Fluid Mechanics II Lecture Notes.

- [11] CFX- Computational Fluid Dynamics Software & Services, <http://www-waterloo.ansys.com/cfx/products/cfx-5/index.html>, Feb. 2003.
- [12] Jones, D.A., et al., 2002, *The Calculation of Hydrodynamic Coefficients for Underwater Vehicles*, DSTO Platforms Sciences Laboratory, Victoria, Australia.
- [13] Larsson, L., et al., “A Method for Resistance and Flow Predictions in Ship Design,” *Trans. Soc. Nav. Arch. Marine Engrs.*, vol. 98, 1990, pp. 495-535.
- [14] Gilbert, D., *Senior Report: Heat Transfer Enhancement Using Wingtip Vortices*, University of New Brunswick, Fredericton, 2002.
- [15] Lingley, S., *Senior Report: The Prediction of Vehicle-Vehicle Flowfield Interaction*, University of New Brunswick, Fredericton, 2002.
- [16] CFX-5.6, *Help Files*, ANSYS Inc., 2003.
- [17] Vennard and Street, *Elementray Fluid Mechanics*, John Wiley and Sons, Inc., Toronto, 1975

APPENDIX A - BOAT HULL

A sample yacht hull was modeled in CFX-5 to demonstrate the potential of CFD in ship hull design. The hull was taken from a ship design package called Prolines and modified for no particular reason other than to learn how to use the software. A starboard side view of the hull can be seen in *Figure 43*. The problem was set up identically to the submarine hull save for the fact the domain was half the size since only half the hull was modeled (one quarter when compared to the one half submarine hull simulation). The hull was six meters long with 12 meters of domain before and after. The simulation was run at an inlet velocity of 3.5 m/s, which corresponds to a Reynolds number of 23.5 million.

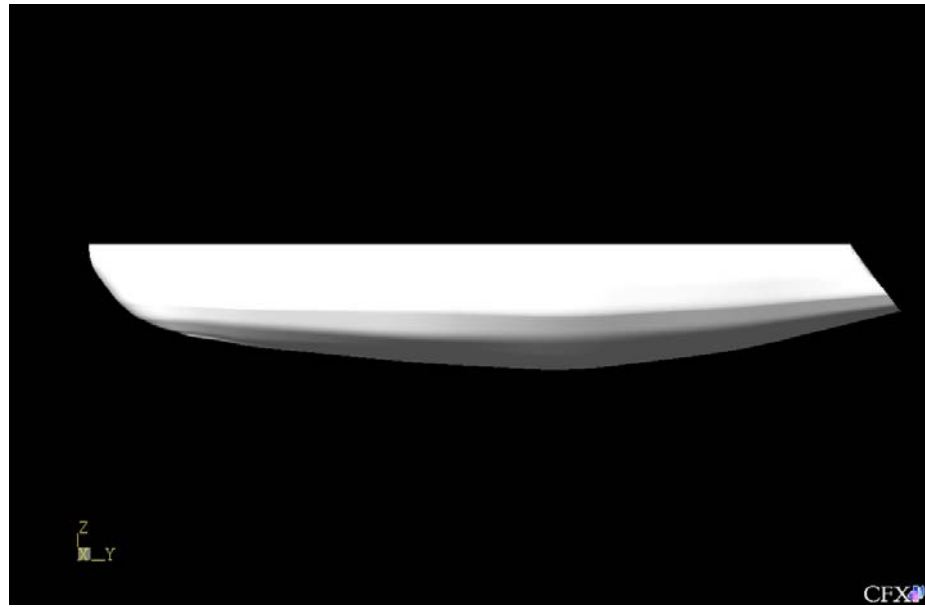


Figure 43 - Side View of Example Boat Hull – Modified Yacht

Figure 44 shows a side view of the mesh used for the simulation. Similar parameters were used for the yacht hull as for the submarine hull. The exact parameters can be found in Appendix C. *Figure 45* shows the top view of the mesh.

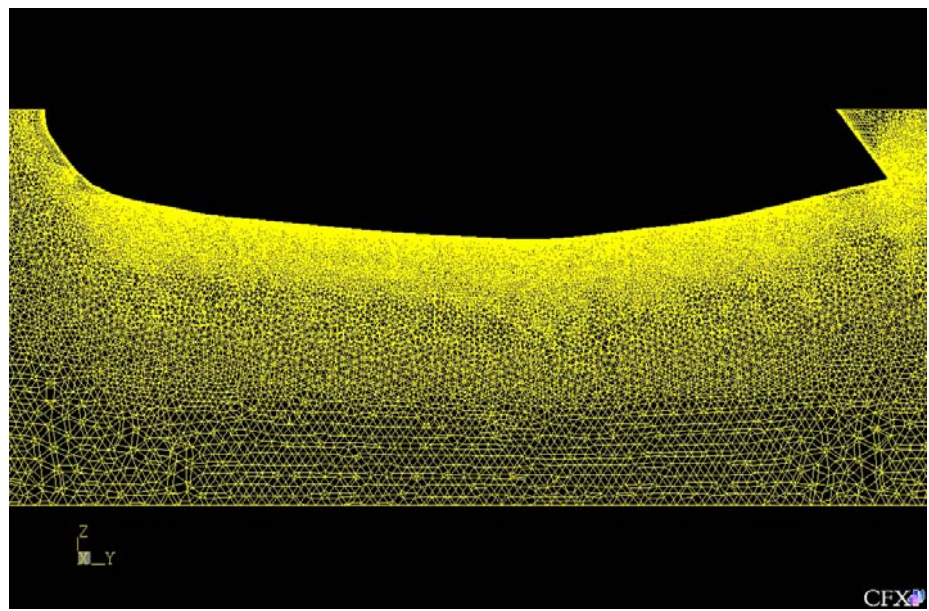


Figure 44 – Side View of Mesh for Example Boat Hull

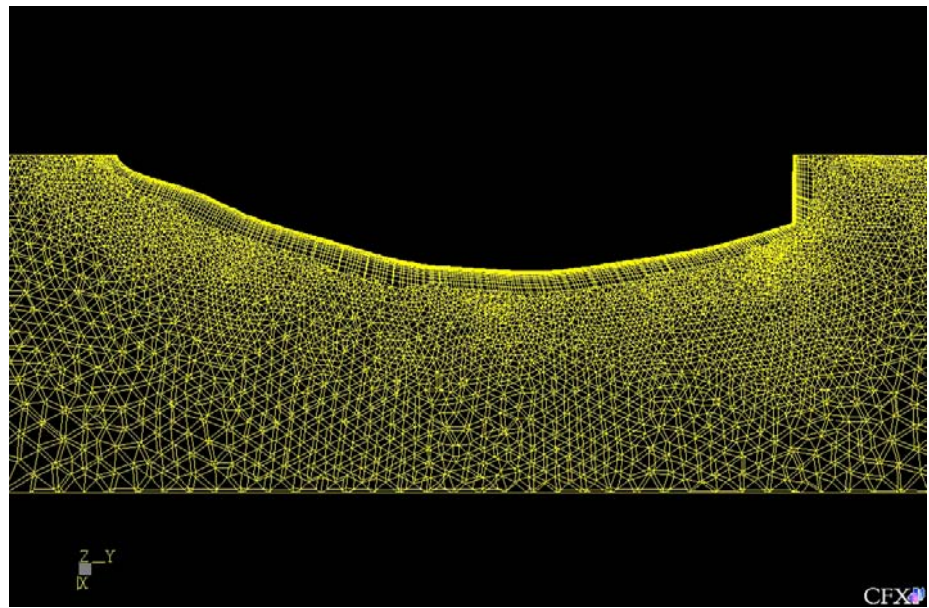


Figure 45 – Top View of Mesh for Example Boat Hull

Figure 46 shows the $y+$ value plot for the simulation. The majority of the values are below 60 with a peak of 61.4, which is well within the range of 20 to 100.

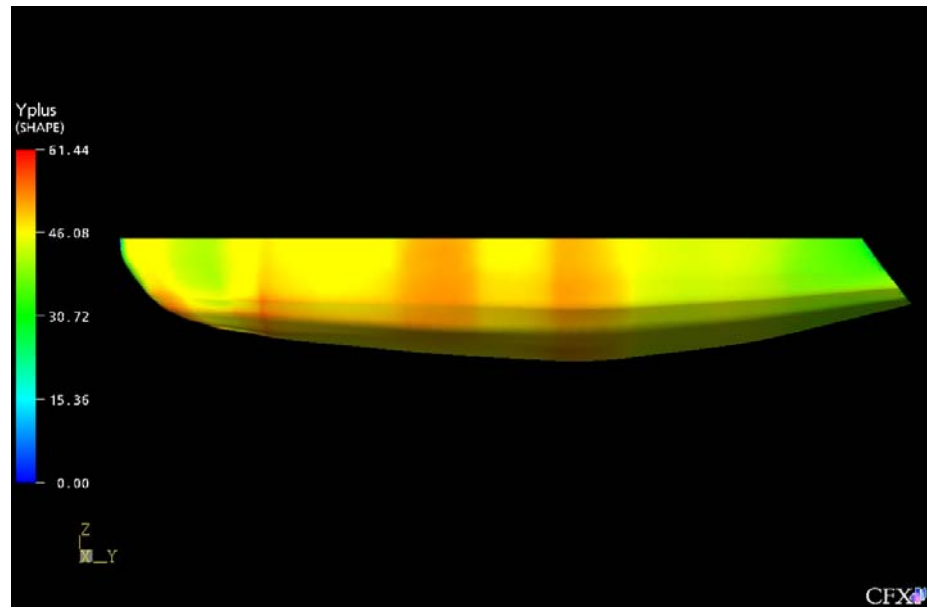


Figure 46 – $y+$ Side View Plot for Example Boat Hull

Figure 47 shows a wall shear plot for the hull. It can be noted that where there is an adverse pressure gradient the wall shear decreases as the boundary layer tends towards separation.

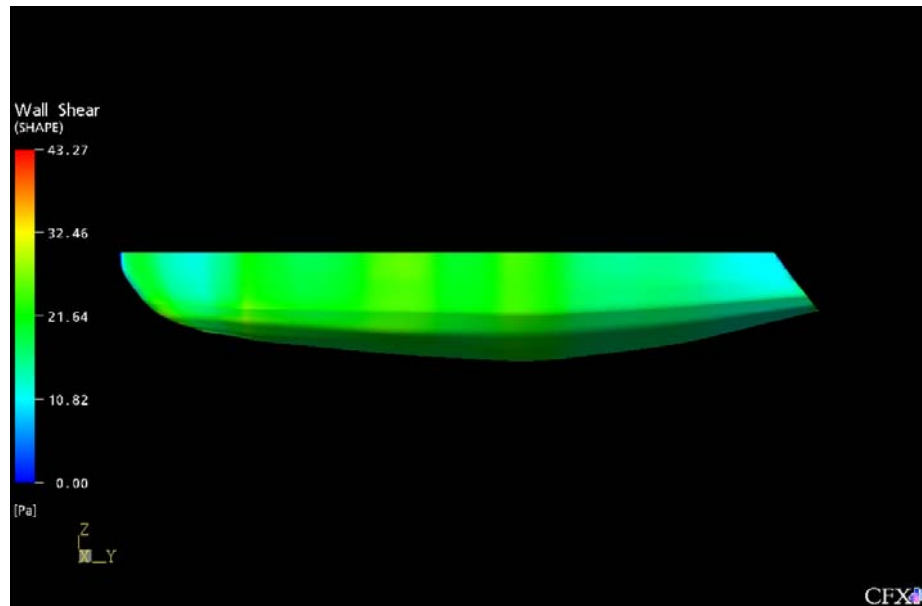


Figure 47 – Wall Shear Side View Plot for Example Boat Hull

Figure 48 shows a side view plot of the pressure distribution around the ship hull. The stagnation point can be noted in red at the front of the hull and a pressure drop is evident at the rear of the hull, most likely indicating flow separation.

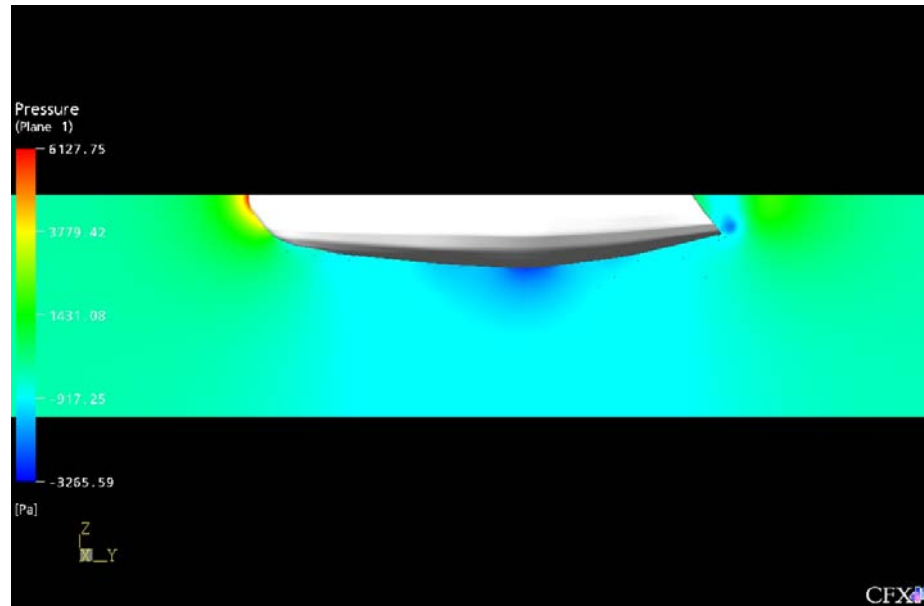


Figure 48 – Pressure Side View Plot for Example Boat Hull

Figure 49 shows a top view velocity v plot. The negative values in the tail section indicate recirculation, which is a result of the boundary layer separation off the blunt body.

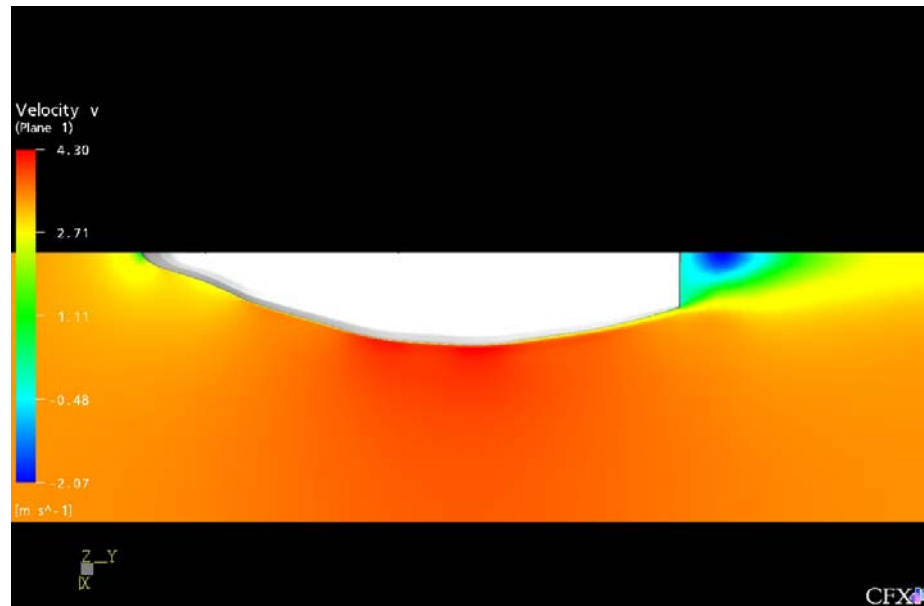


Figure 49 – Velocity v Top View Plot of Example Boat Hull

Figure 50 shows a close up side view of the velocity v plot for the tail section of the hull. The recirculation zone is evident in blue, while the green region indicates flow that passes the vortices.

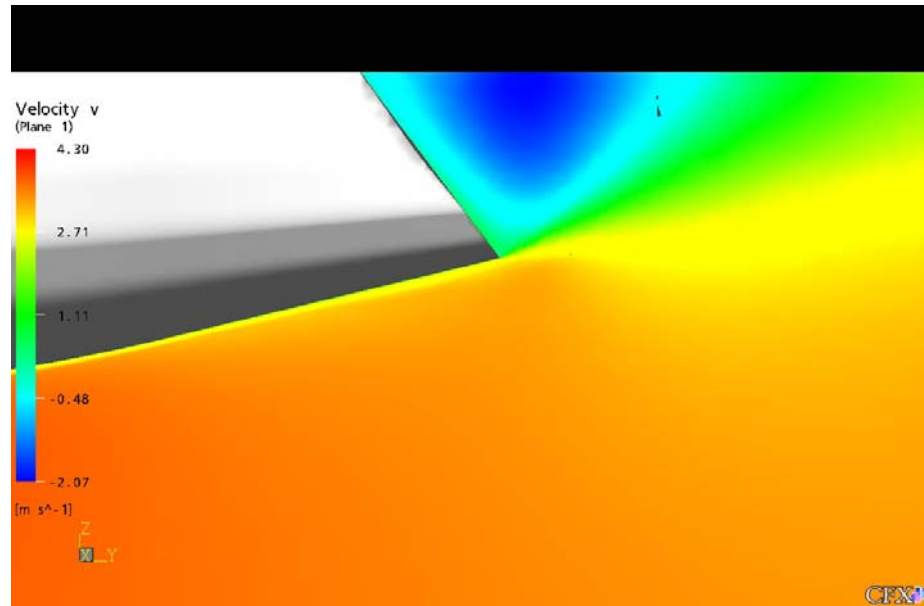


Figure 50 – Velocity v Side View Plot or Rear of Example Boat Hull

Figure 51 shows the absolute velocity in a side view velocity plot.

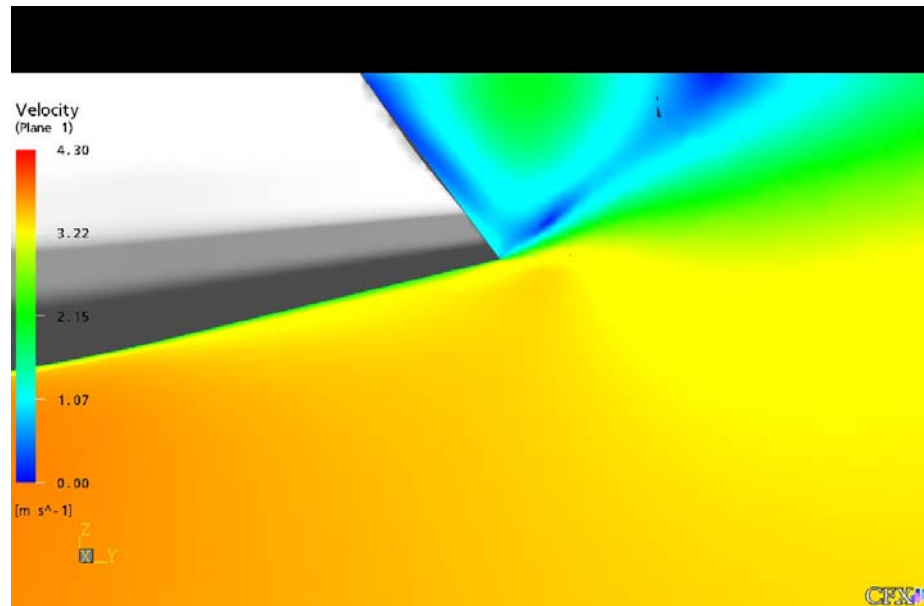


Figure 51 – Velocity Side View Plot of Rear Section of Example Boat Hull

Figure 52 shows the turbulence kinetic energy build up in the swirling vortices at the tail section of the hull.

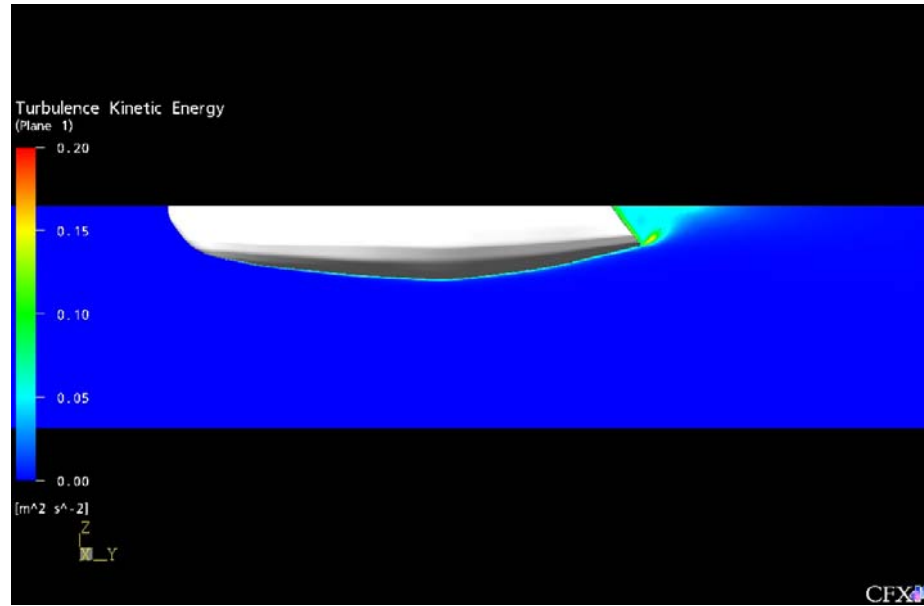


Figure 52 – Turbulence Kinetic Energy for Example Boat Hull

Figure 53 shows another perspective of the flow by showing the streamlines of the flow passing over the hull. Some streamlines get trapped in the recirculation zone at the back of the hull.

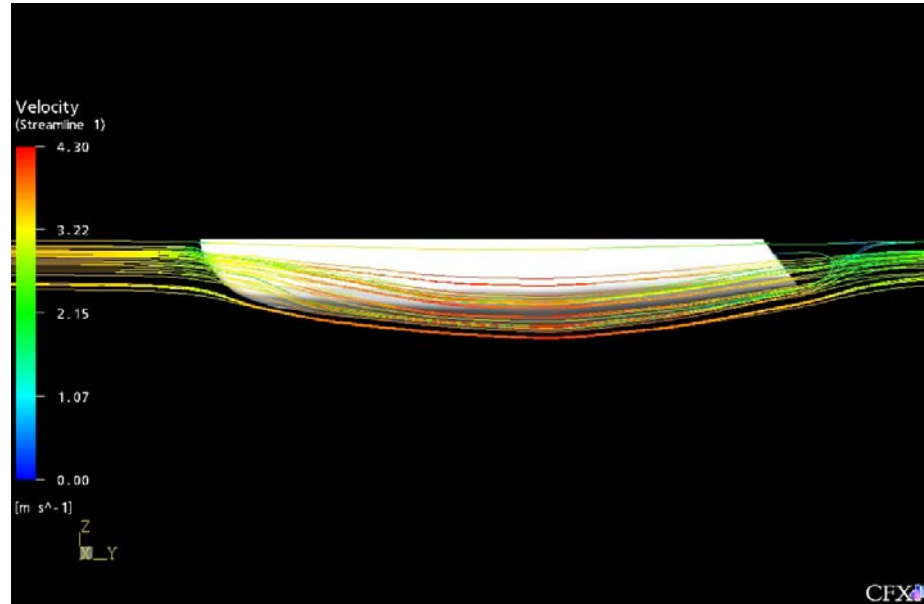


Figure 53 – Streamlines Along Example Boat Hull

Figure 54 shows a close up of the streamlines caught in the recirculation zone at the rear of the hull. The streamlines are a very effective way of visualizing the flow around the hull in this case.

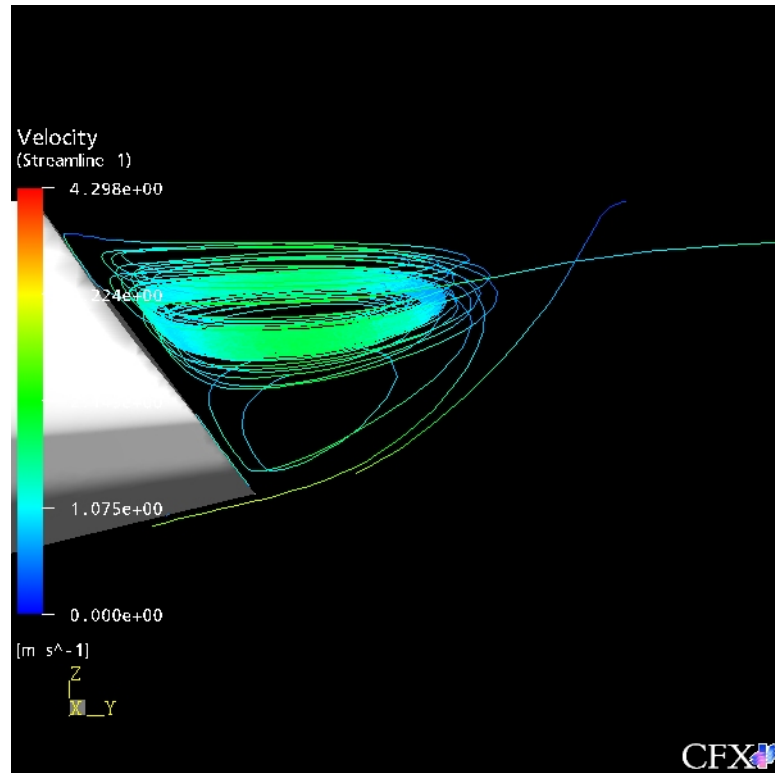


Figure 54 – Streamlines at Rear of Example Boat Hull

APPENDIX B - AXISYMMETRIC MESH AND Y+ SENSITIVITY ANALYSIS

As discussed previously, the reason for using an inflated boundary as a meshing tool is to generate mesh nodes that are close enough to the boundary layer to predict its shape and hence the wall shear. The particular turbulence model and boundary layer model used required $y+$ values between 20 and 100. For this project an axisymmetric shape with a bulbous front and a cone tail section was used during the learning phase. This shape can be seen in *Figure 55*.

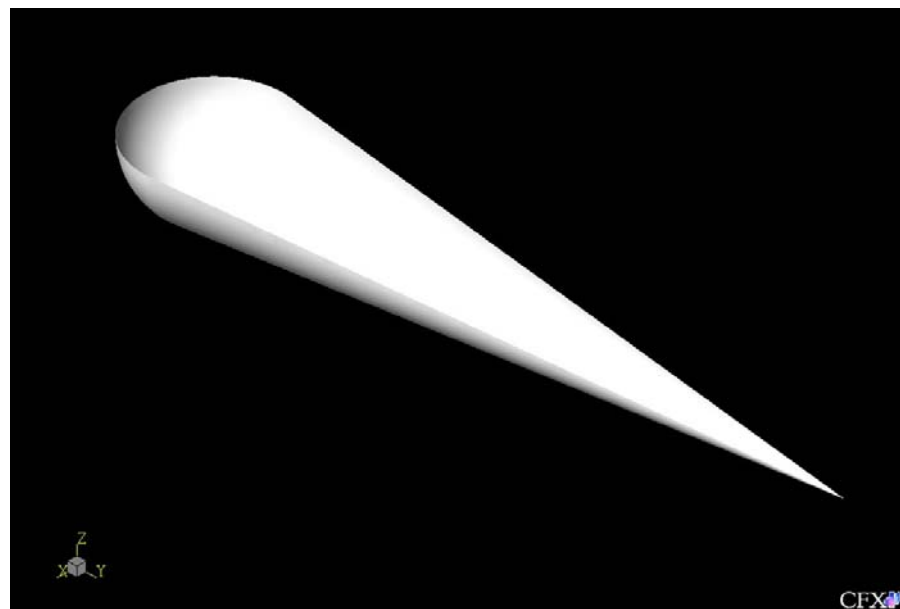


Figure 55 - Axisymmetric Shape Modeled For Trials (Bulbous Front with Tail)

This shape was chosen because it could be created simply and stemmed from a path the project took initially. The trials were run at a very high velocity of 50 m/s which would equate to a Reynolds number associated with an 87 meter long ship if run at 3.5 m/s. In hindsight this was obviously too high. Consequently, the initial $y+$ analysis does not produce $y+$ values in the correct range. However, the time the $y+$ values became within an order of 10 of the required values was the time that the velocity was changed to a more reasonable value, and hence valid $y+$ values dropped to the correct range. At that point, the axisymmetric shape was abandoned and the focus was shifted to the DREA submarine hull.

Table 7 shows the changing output values as the mesh parameters are changed. A complete description of the mesh parameters and the results can be found in Appendix B. Note how the axisymmetric shape simulation 55A is very small compared to the other simulations with only 17 004 nodes compared to 238 118 with simulation 55J. Generally, all the mesh parameters are the same save for one parameter that has been changed. This allows the effect of the change to be determined by comparing it to the previous simulations. *Table 2* tracks the changes made from simulation to simulation.

Name	Number of Nodes	Number of Elements	Pressure Drag (N)	Viscous Drag (N)	Total Drag (N)	Maximum y+
55A	17004	87980	577000	20302	597302	100000
55B	29797	127339	419640	27186	446826	48000
55C	108235	421342	348620	27310	375930	3000
55D	96606	418814	298400	29060	327460	25000
55E	356366	1718464	265340	28478	293818	12000
55F*	167340	570918	314980	26710	341690	2000
55G*	198007	628161	327560	26096	353656	1400
55H*	201108	634758	307000	26896	333896	900
55I*	222699	676134	329880	26186	356066	1500
55J	238118	742518	304000	26490	330490	400

* - y+ peak values actually much higher (~10x) at one small point on crown of bulbous front, reduced by using mesh control at that point

Table 7 - Preliminary Mesh Sensitivity Analysis on Axisymmetric Shape (at 50 m/s)

From these initial tests it can be shown how the inflated boundary affects the y+ value. Simulation 55A shows how with no inflated boundary the y+ values are on the order of 100 000 while with an inflated boundary based on an angular resolution of 18° the y+ values were approximately 48 000. Simulation 55C indicates that it is possible to control the y+ values by controlling the surface mesh parameters and not setting a first prism height. The ancillary effect of this method is that the mesh is made denser throughout the entire domain. By using the first prism height control method the mesh density can be increased in

only the required area, thus saving computational time and giving the desired effect. This can be seen in simulations D to J, as the first prism height drops the $y+$ value follows.

<u>Name</u>	<u>Point of Interest</u>
55A	No inflated boundary (IB) - angular resolution at 18 degrees
55B	Same as 55A but IB dependent on surface mesh only (no 1 st prism height)
55C	Angular resolution at 8 degrees - IB but no 1st prism height
55D	First prism height set to 0.01 m - angular resolution at 7 degrees
55E	First prism height set to 0.005 m - angular resolution at 6 degrees
55F	First prism height at 0.001 m - angular resolution back at 7 degrees
55G	First prism height set to 0.0005 m
55H	First prism height set to 0.0005 m - added mesh control at crown point
55I	First prism height set to 0.0003 m - no mesh control
55J	First prism height set to 0.0003 m - mesh control at crown point

Table 8 - Preliminary Mesh Sensitivity Analysis Changes for Axisymmetric Shape (at 50 m/s)

In *Tables 7 and 8* it notes how simulations F to I have a single point with much higher $y+$ values. An example of this is shown in *Figure 56*. Here nearly the entire surface is dark blue indicating $y+$ values of somewhere in the order a reasonable result. It is difficult to determine the exact values without more investigation because of the extremely high peak values located on the bulbous front. Refining the mesh in that region using a mesh control eliminated these extreme values. *Figure 57* is a similar run using a mesh control. The peak values are eliminated and the rest of the contours are shown.

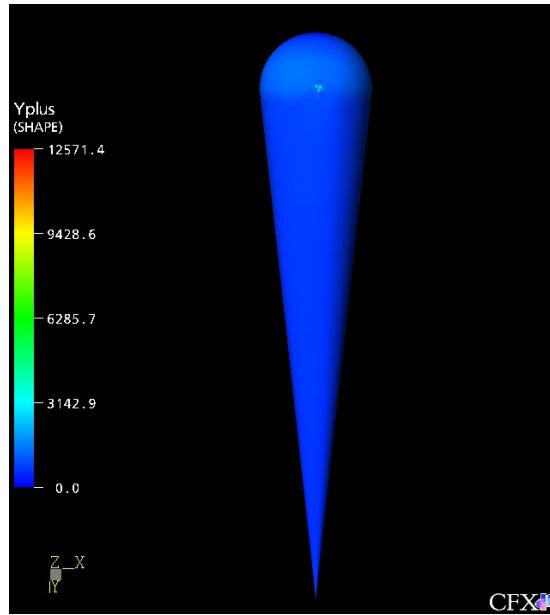


Figure 56 - Example $y+$ Value Plot for Axisymmetric Shape With No Mesh Control

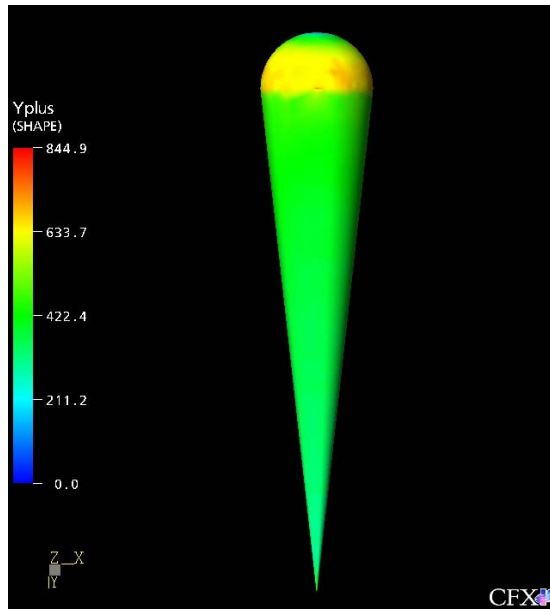


Figure 57 - Example $y+$ Value Plot for Axisymmetric Shape With Mesh Control

As noted before the initial axisymmetric shape simulations were run at 50 m/s compared the more realistic 3.5 m/s. *Table 9* shows a comparison between the two inlet velocities using the final axisymmetric shape mesh. At 50 m/s the $y+$ values were much too high at an approximate value of 400 but when the flow velocity is dropped to 3.5 m/s the $y+$

values are a maximum of 60, which is in the desired range. This makes sense physically since with a lower flow velocity the boundary layer is thicker because of the reduced effects of the pressure gradient. This thicker boundary layer means the distance to the nearest node is reduced.

Name	Velocity (m/s)	Number of Nodes	Pressure Drag (N)	Viscous Drag (N)	Total Drag (N)	Maximum y^+
55J	50	238118	304000	26490	330490	400
55J	3.5	238118	1509	187	1695	60

Table 9 - Comparison of Axisymmetric Bulbous Front Shape Values at 50 m/s and 3.5 m/s

Figure 58 shows the affect of the changing mesh has on the final drag values. As the mesh near the shape is refined, the y^+ value drops to an acceptable range and the drag values become more and more accurate. This preliminary trial shows the trend that the increased mesh density has little effect on the viscous drag estimates but plays a large role in the accuracy of the pressure drag estimate.

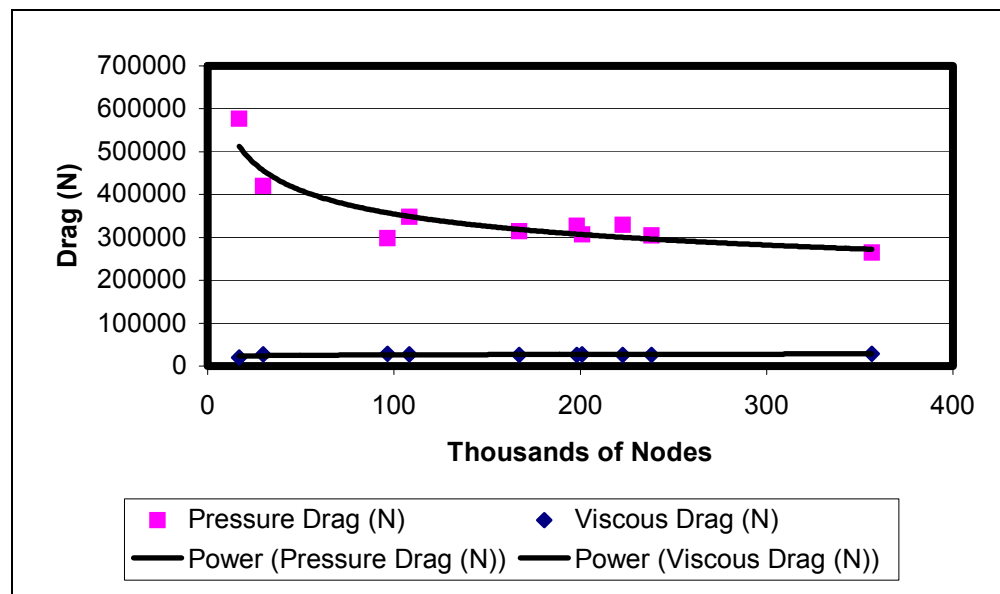


Figure 58 - Axisymmetric Bulbous Front Shape Drag with Changing Mesh Size (at 50 m/s)

APPENDIX C – SIMULATIONS

Summary of Test: AXI6mCFX55a

Geometry: Axisymmetric shape with bulbous front and tapered cone back.

Velocity: 50

Mesh Parameters

Volume Maximum Edge Length: 0.5

Surface Meshing Type: Angular Resolution

Angle: 18°

Maximum Edge Length: 0.5

Minimum Edge Length: 0.05

Expansion Factor: 1.2

Inflated Boundary: on Shape

Number of Layer: N/A

Geometric Expansion Factor: N/A

Inflation Thickness Multiplier: N/A

Max Thickness: N/A

First Prism Height: N/A

Mesh Control: N/A

Length Scale: N/A

Radius: N/A

Expansion Factor: N/A

Mesh Results

Total Number of Nodes: 17 004

Total Number of Element: 87 980

Total Number of Tetrahedrons: 87 980

Total Number of Prisms: 0

Total Number of Pyramids: 0

Total Number of Faces: 7 446

Drag:

Pressure: X = -2.8995 E3

Y = 2.8850 E5

Z = -7.0192 E5

Viscous: X = -1.5156 E1

Y= 1.0151 E4

Z= 1.9861 E2

Moment:

Pressure: X = -9.0795 E6

Y = -8.4280 E2

Z = 3.5287 E4

Viscous: X = 6.5101 E3

Y= -9.9710 E-1

Z= 1.8537 E2

Physical Timestep: 4.88E-2

Computing Time: 0:12

Number of Iterations: 22

Y+ Notes: Below 100 000

Other Notes: Very Coarse Mesh

Summery of Test: **AXI6mCFX55b**

Geometry: Axisymmetric shape with bulbous front and tapered cone back.

Velocity: 50

Mesh Parameters

Volume Maximum Edge Length: 0.5

Surface Meshing Type: Angular Resolution

Angle: 18°

Maximum Edge Length: 0.5

Minimum Edge Length: 0.05

Expansion Factor: 1.2

Inflated Boundary: on Shape

Number of Layer: 5

Geometric Expansion Factor: 1.3

Inflation Thickness Multiplier: 1.0

Max Thickness: 0.5

First Prism Height: N/A

Mesh Control: N/A

Length Scale: N/A

Radius: N/A

Expansion Factor: N/A

Mesh Results

Total Number of Nodes: 29 797

Total Number of Element: 127 339

Total Number of Tetrahedrons: 112 317

Total Number of Prisms: 14 864

Total Number of Pyramids: 158

Total Number of Faces: 11 078

Drag:

Pressure: X = 2.4741 E3

Y = 2.0982 E5

Z = -7.3449 E5

Viscous: X = -7.0474 E1

Y= 1.3593 E4

Z= -3.2062 E2

Physical Timestep: 4.8 E-3

Computing Time: 1:06

Number of Iterations: 75

Moment:

Pressure: X = -9.4635 E6

Y = 5.9001 E1

Z = -3.5579 E4

Viscous: X = 1.2451 E3

Y= 1.6147 E1

Z=1.0772 E3

Y+ Notes: Majority 0-16000, Peak at crown of 48 000

Other Notes:

Summery of Test: AXI6mCFX55c

Geometry: Axisymmetric shape with bulbous front and tapered cone back.

Velocity: 50

Mesh Parameters

Volume Maximum Edge Length: 0.3

Surface Meshing Type: Angular Resolution

Angle: 8°

Maximum Edge Length: 0.3

Minimum Edge Length: 0.01

Expansion Factor: 1.2

Inflated Boundary: on Shape

Number of Layer: 10

Geometric Expansion Factor: 1.3

Inflation Thickness Multiplier: 1.0

Max Thickness: 0.3

First Prism Height: N/A

Mesh Control: N/A

Length Scale: N/A

Radius: N/A

Expansion Factor: N/A

Mesh Results:

Total Number of Nodes: 108 235

Total Number of Element: 421 342

Total Number of Tetrahedrons: 336 844

Total Number of Prisms: 84 196

Total Number of Pyramids: 302

Total Number of Faces: 29 242

Drag:

Pressure: X = 1.1351 E3

Y = 1.7431 E5

Z = -7.3442 E5

Viscous: X = -9.3269 E0

Y= 1.3655 E4

Z= -7.0705 E2

Moment:

Pressure: X = -9.4193 E6

Y = -2.2523 E1

Z = -1.9555 E4

Viscous: X = -3.5011 E3

Y= 1.8549 E1

Z= 9.1911 E1

Physical Timestep: 5 E-3

Computing Time: 2:58

Number of Iterations: 61

Y+ Notes: 0-3000

Other Notes:

Summery of Test: AXI6mCFX55d

Geometry: Axisymmetric shape with bulbous front and tapered cone back.

Velocity: 50

Mesh Parameters

Volume Maximum Edge Length: 0.3

Surface Meshing Type: Angular Resolution

Angle: 7°

Maximum Edge Length: 0.3

Minimum Edge Length: 0.005

Expansion Factor: 1.2

Inflated Boundary: on Shape

Number of Layer: 19

Geometric Expansion Factor: 1.3

Inflation Thickness Multiplier: N/A

Max Thickness: N/A

First Prism Height: 0.01

Mesh Control: N/A

Length Scale: N/A

Radius: N/A

Expansion Factor: N/A

Mesh Results

Total Number of Nodes: 96 606

Total Number of Element: 418 814

Total Number of Tetrahedrons: 378 471

Total Number of Prisms: 38 477

Total Number of Pyramids: 1 866

Total Number of Faces: 33 919

Drag:

Pressure: X = -1.7725 E3

Y = 1.4920 E5

Z = -7.4376 E5

Viscous: X = -1.8761 E1

Y= 1.4553 E4

Z= -2.8891 E2

Moment:

Pressure: X = -9.5164 E6

Y = -1.7967 E1

Z = 2.2024 E4

Viscous: X = 2.1078 E3

Y= -6.2469 E1

Z= 3.4808 E2

Physical Timestep: 5.0 E-3

Computing Time: 3:20

Number of Iterations: 72

Y+ Notes: 0 – 25000

Other Notes:

Summery of Test: AXI6mCFX55e

Geometry: Axisymmetric shape with bulbous front and tapered cone back.

Velocity: 50

Mesh Parameters

Volume Maximum Edge Length: 0.3

Surface Meshing Type: Angular Resolution

Angle: 6°

Maximum Edge Length: 0.1

Minimum Edge Length: 0.001

Expansion Factor: 1.2

Inflated Boundary: on Shape

Number of Layer: 22

Geometric Expansion Factor: 1.3

Inflation Thickness Multiplier: N/A

Max Thickness: N/A

First Prism Height: 0.005

Mesh Control: N/A

Length Scale: N/A

Radius: N/A

Expansion Factor: N/A

Mesh Results

Total Number of Nodes: 356 366

Total Number of Element: 1 718 464

Total Number of Tetrahedrons: 1 637 042

Total Number of Prisms: 79 065

Total Number of Pyramids: 2 357

Total Number of Faces: 145 022

Drag:

Pressure: X = -2.0417 E3

Y = 1.3267 E5

Z = -7.4068 E5

Viscous: X = -8.3974 E0

Y= 1.4239 E4

Z= -4.5869 E2

Moment:

Pressure: X = -8.3974 E0

Y = 1.4239 E4

Z = -4.5869 E2

Viscous: X = -1.1043 E2

Y= 1.6372 E0

Z= 1.1276 E2

Physical Timestep: 5 E-3

Computing Time: 19:51

Number of Iterations: 100

Y+ Notes: 0-12 000

Other Notes:

Summery of Test: AXI6mCFX55f

Geometry: Axisymmetric shape with bulbous front and tapered cone back.

Velocity: 50

Mesh Parameters

Volume Maximum Edge Length: 0.3

Surface Meshing Type: Angular Resolution

Angle: 7°

Maximum Edge Length: 0.3

Minimum Edge Length: 0.001

Expansion Factor: 1.2

Inflated Boundary: on Shape

Number of Layer: 28

Geometric Expansion Factor: 1.3

Inflation Thickness Multiplier: N/A

Max Thickness: N/A

First Prism Height: 0.001

Mesh Control: N/A

Length Scale: N/A

Radius: N/A

Expansion Factor: N/A

Mesh Results

Total Number of Nodes: 167 340

Total Number of Element: 570 918

Total Number of Tetrahedrons: 399 089

Total Number of Prisms: 168 409

Total Number of Pyramids: 3 420

Total Number of Faces: 48 161

Drag:

Pressure: X = -2.7172 E3

Y = 1.5749 E5

Z = -7.2992 E5

Viscous: X = 2.9747 E1

Y= 1.3355 E4

Z= -6.0766 E2

Moment:

Pressure: X = -9.34433 E6

Y = -1.3700 E1

Z = 3.4763 E4

Viscous: X = -2.3167 E3

Y= -1.7091 E1

Z= -4.5660 E2

Physical Timestep: 5 E-3

Computing Time: 21:42

Number of Iterations: 124

Y+ Notes: 0-2000

Other Notes:

Summery of Test: AXI6mCFX55g

Geometry: Axisymmetric shape with bulbous front and tapered cone back.

Velocity: 50

Mesh Parameters

Volume Maximum Edge Length: 0.3

Surface Meshing Type: Angular Resolution

Angle: 7°

Maximum Edge Length: 0.3

Minimum Edge Length: 0.0005

Expansion Factor: 1.2

Inflated Boundary: on Shape

Number of Layer: 30

Geometric Expansion Factor: 1.3

Inflation Thickness Multiplier: N/A

Max Thickness: N/A

First Prism Height: 0.0005

Mesh Control: N/A

Length Scale: N/A

Radius: N/A

Expansion Factor: N/A

Mesh Results

Total Number of Nodes: 198 007

Total Number of Element: 628 161

Total Number of Tetrahedrons: 398 919

Total Number of Prisms: 225 460

Total Number of Pyramids: 3782

Total Number of Faces: 54 202

Drag:

Pressure: X = -3.4046 E3

Y = 1.6378 E5

Z = -7.2205 E5

Viscous: X = -9.9238 E0

Y=1.3048 E4

Z= -5.3372 E2

Moment:

Pressure: X = -9.2405 E6

Y = -7.9095 E0

Z = 4.319 E4

Viscous: X = -1.4889 E3

Y= 3.8896 E0

Z= 1.2324 E2

Physical Timestep: 5 E-3

Computing Time: 7:07

Number of Iterations: 86

Y+ Notes: Majority between 0-1400, peaks at crown of 12000

Other Notes:

Summery of Test: **AXI6mCFX55h**

Geometry: Axisymmetric shape with bulbous front and tapered cone back.

Velocity: 50

Mesh Parameters

Volume Maximum Edge Length: 0.3

Surface Meshing Type: Angular Resolution

Angle: 7°

Maximum Edge Length: 0.3

Minimum Edge Length: 0.0005

Expansion Factor: 1.2

Inflated Boundary: on Shape

Number of Layer: 30

Geometric Expansion Factor: 1.3

Inflation Thickness Multiplier: N/A

Max Thickness: N/A

First Prism Height: 0.0005

Mesh Control: POINT 16

Length Scale: 0.0005

Radius: 0

Expansion Factor: 1.2

Mesh Results

Total Number of Nodes: 201 108

Total Number of Element: 634 758

Total Number of Tetrahedrons: 400 040

Total Number of Prisms: 230 846

Total Number of Pyramids: 3872

Total Number of Faces: 54 746

Drag:

Pressure: X = -9.4415 E2

Y = 1.5350 E5

Z = -7.3426 E5

Viscous: X = -2.3928 E1

Y= 1.3448 E4

Z= -5.6881 E2

Moment:

Pressure: X = -9.3961 E6

Y = 8.8547 E-2

Z = 1.1954 E4

Viscous: X = -1.8130 E3

Y= 6.8339 E0

Z= 2.9783 E2

Physical Timestep: 5 E-3

Computing Time: 11:45

Number of Iterations: 138

Y+ Notes: 0-900 in most places, band of 1200 at crown

Other Notes:

Summery of Test: AXI6mCFX55i

Geometry: Axisymmetric shape with bulbous front and tapered cone back.

Velocity: 50

Mesh Parameters

Volume Maximum Edge Length: 0.3

Surface Meshing Type: Angular Resolution

Angle: 7°

Maximum Edge Length: 0.3

Minimum Edge Length: 0.0003

Expansion Factor: 1.2

Inflated Boundary: on Shape

Number of Layer: 37

Geometric Expansion Factor: 1.3

Inflation Thickness Multiplier: N/A

Max Thickness: N/A

First Prism Height: 0.0003

Mesh Control: N/A

Length Scale: N/A

Radius: N/A

Expansion Factor: N/A

Mesh Results

Total Number of Nodes: 222 699

Total Number of Element: 676 134

Total Number of Tetrahedrons: 401 527

Total Number of Prisms: 270 791

Total Number of Pyramids: 3816

Total Number of Faces: 58 803

Drag:

Pressure: X = -1.5053 E3

Y = 1.6494 E5

Z = -7.2651E5

Viscous: X = 7.1773 E0

Y=1.3093 E4

Z= -4.5683 E2

Moment:

Pressure: X = -9.3019 E6

Y = -1.5035 E1

Z = 1.9083 E4

Viscous: X = -4.5101 E2

Y= -3.7492 E0

Z= -1.2131 E2

Physical Timestep: 5 E-3

Computing Time: 6:38

Number of Iterations: 172

Y+ Notes: 0-1500 with peak of 15 000 at small point on crown

Other Notes:

Summery of Test: AXI6mCFX55j

Geometry: Axisymmetric shape with bulbous front and tapered cone back.

Velocity: 50

Mesh Parameters

Volume Maximum Edge Length: 0.3

Surface Meshing Type: Angular Resolution

Angle: 7°

Maximum Edge Length: 0.3

Minimum Edge Length: 0.0003

Expansion Factor: 1.2

Inflated Boundary: on Shape

Number of Layer: 37

Geometric Expansion Factor: 1.3

Inflation Thickness Multiplier: N/A

Max Thickness: N/A

First Prism Height: 0.0003

Mesh Control: POINT 16

Length Scale: 0.0003

Radius: 0.003

Expansion Factor: 1.2

Mesh Results

Total Number of Nodes: 238 118

Total Number of Element: 742 518

Total Number of Tetrahedrons: 457 367

Total Number of Prisms: 280 898

Total Number of Pyramids: 4253

Total Number of Faces: 60 911

Drag:

Pressure: X = -2.0191 E3

Y = 1.520 E5

Z = -7.3363 E5

Viscous: X = -2.0108 E1

Y= 1.3245 E4

Z= -5.0259 E2

Moment:

Pressure: X = -9.3885 E6

Y = -1.5574 E1

Z = 2.5612 E4

Viscous: X = -1.0786 E3

Y= 5.6988 E0

Z= 2.3077 E2

Physical Timestep: 5 E-3

Computing Time: 7:14

Number of Iterations: 172

Y+ Notes: 0-400 with peak band of ~750 at crown

Other Notes:

Summery of Test: AXI6mCFX55a

Geometry: Axisymmetric shape with bulbous front and tapered cone back.

Velocity: 50

Mesh Parameters

Volume Maximum Edge Length: 0.5

Surface Meshing Type: Angular Resolution

Angle: 18°

Maximum Edge Length: 0.5

Minimum Edge Length: 0.05

Expansion Factor: 1.2

Inflated Boundary: on Shape

Number of Layer: N/A

Geometric Expansion Factor: N/A

Inflation Thickness Multiplier: N/A

Max Thickness: N/A

First Prism Height: N/A

Mesh Control: N/A

Length Scale: N/A

Radius: N/A

Expansion Factor: N/A

Mesh Results

Total Number of Nodes: 17 004

Total Number of Element: 87 980

Total Number of Tetrahedrons: 87 980

Total Number of Prisms: 0

Total Number of Pyramids: 0

Total Number of Faces: 7 446

Drag:

Pressure: X = -2.8995 E3

Y = 2.8850 E5

Z = -7.0192 E5

Viscous: X = -1.5156 E1

Y= 1.0151 E4

Z= 1.9861 E2

Moment:

Pressure: X = -9.0795 E6

Y = -8.4280 E2

Z = 3.5287 E4

Viscous: X = 6.5101 E3

Y= -9.9710 E-1

Z= 1.8537 E2

Physical Timestep: 4.88E-2

Computing Time: 0:12

Number of Iterations: 22

Y+ Notes: Below 100 000

Other Notes: Very Coarse Mesh

Summery of Test: AXI6mCFX55b

Geometry: Axisymmetric shape with bulbous front and tapered cone back.

Velocity: 50

Mesh Parameters

Volume Maximum Edge Length: 0.5

Surface Meshing Type: Angular Resolution

Angle: 18°

Maximum Edge Length: 0.5

Minimum Edge Length: 0.05

Expansion Factor: 1.2

Inflated Boundary: on Shape

Number of Layer: 5

Geometric Expansion Factor: 1.3

Inflation Thickness Multiplier: 1.0

Max Thickness: 0.5

First Prism Height: N/A

Mesh Control: N/A

Length Scale: N/A

Radius: N/A

Expansion Factor: N/A

Mesh Results

Total Number of Nodes: 29 797

Total Number of Element: 127 339

Total Number of Tetrahedrons: 112 317

Total Number of Prisms: 14 864

Total Number of Pyramids: 158

Total Number of Faces: 11 078

Drag:

Pressure: X = 2.4741 E3

Y = 2.0982 E5

Z = -7.3449 E5

Viscous: X = -7.0474 E1

Y= 1.3593 E4

Z= -3.2062 E2

Physical Timestep: 4.8 E-3

Computing Time: 1:06

Number of Iterations: 75

Moment:

Pressure: X = -9.4635 E6

Y = 5.9001 E1

Z = -3.5579 E4

Viscous: X = 1.2451 E3

Y= 1.6147 E1

Z=1.0772 E3

Y+ Notes: Majority 0-16000, Peak at crown of 48 000

Other Notes:

Summery of Test: **AXI6mCFX55c**

Geometry: Axisymmetric shape with bulbous front and tapered cone back.

Velocity: 50

Mesh Parameters

Volume Maximum Edge Length: 0.3

Surface Meshing Type: Angular Resolution

Angle: 8°

Maximum Edge Length: 0.3

Minimum Edge Length: 0.01

Expansion Factor: 1.2

Inflated Boundary: on Shape

Number of Layer: 10

Geometric Expansion Factor: 1.3

Inflation Thickness Multiplier: 1.0

Max Thickness: 0.3

First Prism Height: N/A

Mesh Control: N/A

Length Scale: N/A

Radius: N/A

Expansion Factor: N/A

Mesh Results:

Total Number of Nodes: 108 235

Total Number of Element: 421 342

Total Number of Tetrahedrons: 336 844

Total Number of Prisms: 84 196

Total Number of Pyramids: 302

Total Number of Faces: 29 242

Drag:

Pressure: X = 1.1351 E3

Y = 1.7431 E5

Z = -7.3442 E5

Viscous: X = -9.3269 E0

Y= 1.3655 E4

Z= -7.0705 E2

Moment:

Pressure: X = -9.4193 E6

Y = -2.2523 E1

Z = -1.9555 E4

Viscous: X = -3.5011 E3

Y= 1.8549 E1

Z= 9.1911 E1

Physical Timestep: 5 E-3

Computing Time: 2:58

Number of Iterations: 61

Y+ Notes: 0-3000

Other Notes:

Summery of Test: AXI6mCFX55d

Geometry: Axisymmetric shape with bulbous front and tapered cone back.

Velocity: 50

Mesh Parameters

Volume Maximum Edge Length: 0.3

Surface Meshing Type: Angular Resolution

Angle: 7°

Maximum Edge Length: 0.3

Minimum Edge Length: 0.005

Expansion Factor: 1.2

Inflated Boundary: on Shape

Number of Layer: 19

Geometric Expansion Factor: 1.3

Inflation Thickness Multiplier: N/A

Max Thickness: N/A

First Prism Height: 0.01

Mesh Control: N/A

Length Scale: N/A

Radius: N/A

Expansion Factor: N/A

Mesh Results

Total Number of Nodes: 96 606

Total Number of Element: 418 814

Total Number of Tetrahedrons: 378 471

Total Number of Prisms: 38 477

Total Number of Pyramids: 1 866

Total Number of Faces: 33 919

Drag:

Pressure: X = -1.7725 E3

Y = 1.4920 E5

Z = -7.4376 E5

Viscous: X = -1.8761 E1

Y= 1.4553 E4

Z= -2.8891 E2

Moment:

Pressure: X = -9.5164 E6

Y = -1.7967 E1

Z = 2.2024 E4

Viscous: X = 2.1078 E3

Y= -6.2469 E1

Z= 3.4808 E2

Physical Timestep: 5.0 E-3

Computing Time: 3:20

Number of Iterations: 72

Y+ Notes: 0 – 25000

Other Notes:

Summery of Test: AXI6mCFX55e

Geometry: Axisymmetric shape with bulbous front and tapered cone back.

Velocity: 50

Mesh Parameters

Volume Maximum Edge Length: 0.3

Surface Meshing Type: Angular Resolution

Angle: 6°

Maximum Edge Length: 0.1

Minimum Edge Length: 0.001

Expansion Factor: 1.2

Inflated Boundary: on Shape

Number of Layer: 22

Geometric Expansion Factor: 1.3

Inflation Thickness Multiplier: N/A

Max Thickness: N/A

First Prism Height: 0.005

Mesh Control: N/A

Length Scale: N/A

Radius: N/A

Expansion Factor: N/A

Mesh Results

Total Number of Nodes: 356 366

Total Number of Element: 1 718 464

Total Number of Tetrahedrons: 1 637 042

Total Number of Prisms: 79 065

Total Number of Pyramids: 2 357

Total Number of Faces: 145 022

Drag:

Pressure: X = -2.0417 E3

Y = 1.3267 E5

Z = -7.4068 E5

Viscous: X = -8.3974 E0

Y= 1.4239 E4

Z= -4.5869 E2

Moment:

Pressure: X = -8.3974 E0

Y = 1.4239 E4

Z = -4.5869 E2

Viscous: X = -1.1043 E2

Y= 1.6372 E0

Z= 1.1276 E2

Physical Timestep: 5 E-3

Computing Time: 19:51

Number of Iterations: 100

Y+ Notes: 0-12 000

Other Notes:

Summery of Test: AXI6mCFX55f

Geometry: Axisymmetric shape with bulbous front and tapered cone back.

Velocity: 50

Mesh Parameters

Volume Maximum Edge Length: 0.3

Surface Meshing Type: Angular Resolution

Angle: 7°

Maximum Edge Length: 0.3

Minimum Edge Length: 0.001

Expansion Factor: 1.2

Inflated Boundary: on Shape

Number of Layer: 28

Geometric Expansion Factor: 1.3

Inflation Thickness Multiplier: N/A

Max Thickness: N/A

First Prism Height: 0.001

Mesh Control: N/A

Length Scale: N/A

Radius: N/A

Expansion Factor: N/A

Mesh Results

Total Number of Nodes: 167 340

Total Number of Element: 570 918

Total Number of Tetrahedrons: 399 089

Total Number of Prisms: 168 409

Total Number of Pyramids: 3 420

Total Number of Faces: 48 161

Drag:

Pressure: X = -2.7172 E3

Y = 1.5749 E5

Z = -7.2992 E5

Viscous: X = 2.9747 E1

Y= 1.3355 E4

Z= -6.0766 E2

Moment:

Pressure: X = -9.34433 E6

Y = -1.3700 E1

Z = 3.4763 E4

Viscous: X = -2.3167 E3

Y= -1.7091 E1

Z= -4.5660 E2

Physical Timestep: 5 E-3

Computing Time: 21:42

Number of Iterations: 124

Y+ Notes: 0-2000

Other Notes:

Summery of Test: AXI6mCFX55g

Geometry: Axisymmetric shape with bulbous front and tapered cone back.

Velocity: 50

Mesh Parameters

Volume Maximum Edge Length: 0.3

Surface Meshing Type: Angular Resolution

Angle: 7°

Maximum Edge Length: 0.3

Minimum Edge Length: 0.0005

Expansion Factor: 1.2

Inflated Boundary: on Shape

Number of Layer: 30

Geometric Expansion Factor: 1.3

Inflation Thickness Multiplier: N/A

Max Thickness: N/A

First Prism Height: 0.0005

Mesh Control: N/A

Length Scale: N/A

Radius: N/A

Expansion Factor: N/A

Mesh Results

Total Number of Nodes: 198 007

Total Number of Element: 628 161

Total Number of Tetrahedrons: 398 919

Total Number of Prisms: 225 460

Total Number of Pyramids: 3782

Total Number of Faces: 54 202

Drag:

Pressure: X = -3.4046 E3

Y = 1.6378 E5

Z = -7.2205 E5

Viscous: X = -9.9238 E0

Y=1.3048 E4

Z= -5.3372 E2

Moment:

Pressure: X = -9.2405 E6

Y = -7.9095 E0

Z = 4.319 E4

Viscous: X = -1.4889 E3

Y= 3.8896 E0

Z= 1.2324 E2

Physical Timestep: 5 E-3

Computing Time: 7:07

Number of Iterations: 86

Y+ Notes: Majority between 0-1400, peaks at crown of 12000

Other Notes:

Summery of Test: **AXI6mCFX55h**

Geometry: Axisymmetric shape with bulbous front and tapered cone back.

Velocity: 50

Mesh Parameters

Volume Maximum Edge Length: 0.3

Surface Meshing Type: Angular Resolution

Angle: 7°

Maximum Edge Length: 0.3

Minimum Edge Length: 0.0005

Expansion Factor: 1.2

Inflated Boundary: on Shape

Number of Layer: 30

Geometric Expansion Factor: 1.3

Inflation Thickness Multiplier: N/A

Max Thickness: N/A

First Prism Height: 0.0005

Mesh Control: POINT 16

Length Scale: 0.0005

Radius: 0

Expansion Factor: 1.2

Mesh Results

Total Number of Nodes: 201 108

Total Number of Element: 634 758

Total Number of Tetrahedrons: 400 040

Total Number of Prisms: 230 846

Total Number of Pyramids: 3872

Total Number of Faces: 54 746

Drag:

Pressure: X = -9.4415 E2

Y = 1.5350 E5

Z = -7.3426 E5

Viscous: X = -2.3928 E1

Y= 1.3448 E4

Z= -5.6881 E2

Moment:

Pressure: X = -9.3961 E6

Y = 8.8547 E-2

Z = 1.1954 E4

Viscous: X = -1.8130 E3

Y= 6.8339 E0

Z= 2.9783 E2

Physical Timestep: 5 E-3

Computing Time: 11:45

Number of Iterations: 138

Y+ Notes: 0-900 in most places, band of 1200 at crown

Other Notes:

Summery of Test: AXI6mCFX55i

Geometry: Axisymmetric shape with bulbous front and tapered cone back.

Velocity: 50

Mesh Parameters

Volume Maximum Edge Length: 0.3

Surface Meshing Type: Angular Resolution

Angle: 7°

Maximum Edge Length: 0.3

Minimum Edge Length: 0.0003

Expansion Factor: 1.2

Inflated Boundary: on Shape

Number of Layer: 37

Geometric Expansion Factor: 1.3

Inflation Thickness Multiplier: N/A

Max Thickness: N/A

First Prism Height: 0.0003

Mesh Control: N/A

Length Scale: N/A

Radius: N/A

Expansion Factor: N/A

Mesh Results

Total Number of Nodes: 222 699

Total Number of Element: 676 134

Total Number of Tetrahedrons: 401 527

Total Number of Prisms: 270 791

Total Number of Pyramids: 3816

Total Number of Faces: 58 803

Drag:

Pressure: X = -1.5053 E3

Y = 1.6494 E5

Z = -7.2651E5

Viscous: X = 7.1773 E0

Y=1.3093 E4

Z= -4.5683 E2

Moment:

Pressure: X = -9.3019 E6

Y = -1.5035 E1

Z = 1.9083 E4

Viscous: X = -4.5101 E2

Y= -3.7492 E0

Z= -1.2131 E2

Physical Timestep: 5 E-3

Computing Time: 6:38

Number of Iterations: 172

Y+ Notes: 0-1500 with peak of 15 000 at small point on crown

Other Notes:

Summery of Test: AXI6mCFX55j

Geometry: Axisymmetric shape with bulbous front and tapered cone back.

Velocity: 50

Mesh Parameters

Volume Maximum Edge Length: 0.3

Surface Meshing Type: Angular Resolution

Angle: 7°

Maximum Edge Length: 0.3

Minimum Edge Length: 0.0003

Expansion Factor: 1.2

Inflated Boundary: on Shape

Number of Layer: 37

Geometric Expansion Factor: 1.3

Inflation Thickness Multiplier: N/A

Max Thickness: N/A

First Prism Height: 0.0003

Mesh Control: POINT 16

Length Scale: 0.0003

Radius: 0.003

Expansion Factor: 1.2

Mesh Results

Total Number of Nodes: 238 118

Total Number of Element: 742 518

Total Number of Tetrahedrons: 457 367

Total Number of Prisms: 280 898

Total Number of Pyramids: 4253

Total Number of Faces: 60 911

Drag:

Pressure: X = -2.0191 E3

Y = 1.520 E5

Z = -7.3363 E5

Viscous: X = -2.0108 E1

Y= 1.3245 E4

Z= -5.0259 E2

Moment:

Pressure: X = -9.3885 E6

Y = -1.5574 E1

Z = 2.5612 E4

Viscous: X = -1.0786 E3

Y= 5.6988 E0

Z= 2.3077 E2

Physical Timestep: 5 E-3

Computing Time: 7:14

Number of Iterations: 172

Y+ Notes: 0-400 with peak band of ~750 at crown

Other Notes:

Summery of Test: DREA6mCFX55a

Half standard submarine shape set into box, no appendages

Velocity: 3.5

Mesh Parameters

Volume Maximum Edge Length: 0.3

Surface Meshing Type: Angular Resolution

Angle: 7°

Maximum Edge Length: 0.3

Minimum Edge Length: 0.005

Expansion Factor: 1.2

Inflated Boundary: on Shape

Number of Layer: 22

Geometric Expansion Factor: 1.3

Inflation Thickness Multiplier: N/A

Max Thickness: N/A

First Prism Height: 0.005

Mesh Control: N/A

Length Scale: N/A

Radius: N/A

Expansion Factor: N/A

Mesh Results

Total Number of Nodes: 101 140

Total Number of Element: 405 358

Total Number of Tetrahedrons: 334 466

Total Number of Prisms: 69 402

Total Number of Pyramids: 1490

Total Number of Faces: 30 988

Drag:

Pressure: X = -2.2958 E-1

Y = 1.1677 E2

Z = -1.4203 E3

Viscous: X = -3.3104 E-2

Y= 9.1095 E1

Z= -1.2964 E0

Moment:

Pressure: X = -2.0394 E4

Y = -3.4947 E-4

Z = 2.2559 E0

Viscous: X = 9.3652 E0

Y= 1.6053 E-2

Z= 5.1070 E-1

Physical Time step: 6.976 E-1

Computing Time: 1:25

Number of Iterations: 33

Y+ Notes: 0-200 at front, 790-890 at peak, 590-690 for rest, 200 at tail

Other Notes:

Summery of Test: DREA6mCFX55b

Half standard submarine shape set into box, no appendages

Velocity: 3.5

Mesh Parameters

Volume Maximum Edge Length: 0.3

Surface Meshing Type: Angular Resolution

Angle: 7°

Maximum Edge Length: 0.3

Minimum Edge Length: 0.0003

Expansion Factor: 1.2

Inflated Boundary: on Shape

Number of Layer: 32

Geometric Expansion Factor: 1.3

Inflation Thickness Multiplier: N/A

Max Thickness: N/A

First Prism Height: 0.0003

Mesh Control: N/A

Length Scale: N/A

Radius: N/A

Expansion Factor: N/A

Mesh Results

Total Number of Nodes: 163 856

Total Number of Element: 530 496

Total Number of Tetrahedrons: 345 185

Total Number of Prisms: 183 163

Total Number of Pyramids: 2148

Total Number of Faces: 40 717

Drag:

Pressure: X = 2.2967 E0

Y = 1.1434 E2

Z = -1.4172 E3

Viscous: X = 4.0227 E-2

Y= 9.3474 E1

Z= -1.3740 E0

Moment:

Pressure: X = -2.0337 E4

Y = -4.3127 E-4

Z = -3.0841 E1

Viscous: X = 8.9230 E0

Y= -1.1167 E-2

Z= -5.2652 E-1

Physical Time step: 5E-1 formerly 5E-2

Computing Time: 15:47

Number of Iterations: 239

Y+ Notes: 0-19 at front, 38-57 at body half, 19-38 latter half, 38-57 just before tail, then 19-38

Other Notes:

Summery of Test: **DREA6mCFX55c**

Half standard submarine shape set into box, no appendages

Velocity: 3.5

Mesh Parameters

Volume Maximum Edge Length: 0.15

Surface Meshing Type: Angular Resolution

Angle: 7°

Maximum Edge Length: 0.15

Minimum Edge Length: 0.0003

Expansion Factor: 1.2

Inflated Boundary: on Shape

Number of Layer: 32

Geometric Expansion Factor: 1.3

Inflation Thickness Multiplier: N/A

Max Thickness: N/A

First Prism Height: 0.0003

Mesh Control: N/A

Length Scale: N/A

Radius: N/A

Expansion Factor: N/A

Mesh Results

Total Number of Nodes: 403 090

Total Number of Element: 1 867 774

Total Number of Tetrahedrons: 1 682 433

Total Number of Prisms: 183 163

Total Number of Pyramids: 2148

Total Number of Faces: 81 653

Drag:

Pressure: X = 1.0413 E0

Y = 1.0543 E2

Z = -1.4130 E3

Viscous: X = 1.4516 E-3

Y= 9.2695 E1

Z= -1.3530 E0

Moment:

Pressure: X = -2.0214 E4

Y = -8.7190 E-4

Z = -1.5398 E1

Viscous: X = 8.9364 E0

Y= 7.5313 E-4

Z= 3.5140 E-3

Physical Time step: 5E-2 and 5E-1

Computing Time: 16:58

Number of Iterations: 84

Y+ Notes: 20-40 at tip, 40-60 at first part of body, 20-40 at rear part of body, 10-20 at very rear tip

Other Notes: Very fine mesh.

Summery of Test: **DREA6mCFX55d**

Half standard submarine shape set into box, no appendages

Velocity: 3.5

Mesh Parameters

Volume Maximum Edge Length: 0.3

Surface Meshing Type: Angular Resolution

Angle: 7°

Maximum Edge Length: 0.3

Minimum Edge Length: 0.0003

Expansion Factor: 1.2

Inflated Boundary: on Shape

Number of Layer: 22

Geometric Expansion Factor: 1.3

Inflation Thickness Multiplier: N/A

Max Thickness: N/A

First Prism Height: 0.0004

Mesh Control: N/A

Length Scale: N/A

Radius: N/A

Expansion Factor: N/A

Mesh Results

Total Number of Nodes: 158 176

Total Number of Element: 520 731

Total Number of Tetrahedrons: 346 940

Total Number of Prisms: 171 701

Total Number of Pyramids: 2090

Total Number of Faces: 40 419

Drag:

Pressure: X = 1.3271 E0

Y = 1.1490 E2

Z = -1.4191 E3

Viscous: X = -3.3104 E-2

Y= 9.3231 E1

Z= -1.3988 E0

Moment:

Pressure: X = -2.0365 E4

Y = -1.4120 E-3

Z = -1.7430 E1

Viscous: X = 8.5140 E0

Y= -3.0595 E-3

Z= -4.7218 E-1

Physical Time step: 5E-2 and 5E-1

Computing Time: 4:08

Number of Iterations: 80

Y+ Notes: 36-55 at very tip, 55-73 at front body, 36-55 at rear body, 18-36 at very rear tip

Other Notes: Higher Inflated Boundary first prism height caused higher y+ values

Summery of Test: **DREA6mCFX55e**

Half standard submarine shape set into box, no appendages

Velocity: 3.5

Mesh Parameters

Volume Maximum Edge Length: 0.3

Surface Meshing Type: Angular Resolution

Angle: 7°

Maximum Edge Length: 0.3

Minimum Edge Length: 0.0002

Expansion Factor: 1.2

Inflated Boundary: on Shape

Number of Layer: 32

Geometric Expansion Factor: 1.3

Inflation Thickness Multiplier: N/A

Max Thickness: N/A

First Prism Height: 0.0002

Mesh Control: N/A

Length Scale: N/A

Radius: N/A

Expansion Factor: N/A

Mesh Results

Total Number of Nodes: 172 164

Total Number of Element: 546 859

Total Number of Tetrahedrons: 346 291

Total Number of Prisms: 198 423

Total Number of Pyramids: 2145

Total Number of Faces: 41 936

Drag:

Pressure: X = 2.3119 E0

Y = 1.1631 E2

Z = -1.4156 E3

Viscous: X = 3.4172 E-2

Y= 9.3861 E1

Z= -1.3204 E0

Moment:

Pressure: X = -2.0318 E4

Y = -2.2951 E-4

Z = -3.0798 E1

Viscous: X = 9.7320 E0

Y= -1.1264 E-2

Z= -4.4452 E-1

Physical Time step: 5E-2 and 5E-1

Computing Time: 5:44

Number of Iterations: 82

Y+ Notes: 0-20 at very tip, 20-40 at body, 7-15 at rear tip

Other Notes: Lowering inflated boundary first prism height lowered y+ values, almost too low.

Summery of Test: **DREA6mCFX55f**

Half standard submarine shape set into box, no appendages

Velocity: 3.5

Mesh Parameters

Volume Maximum Edge Length: 0.3

Surface Meshing Type: Angular Resolution

Angle: 6°

Maximum Edge Length: 0.3

Minimum Edge Length: 0.0003

Expansion Factor: 1.2

Inflated Boundary: on Shape

Number of Layer: 32

Geometric Expansion Factor: 1.3

Inflation Thickness Multiplier: N/A

Max Thickness: N/A

First Prism Height: 0.0003

Mesh Control: N/A

Length Scale: N/A

Radius: N/A

Expansion Factor: N/A

Mesh Results

Total Number of Nodes: 191 872

Total Number of Element: 605 547

Total Number of Tetrahedrons: 376 850

Total Number of Prisms: 225 719

Total Number of Pyramids: 2978

Total Number of Faces: 44 683

Drag:

Pressure: X = -4.7709 E-1

Y = 1.1413 E2

Z = -1.4199 E3

Viscous: X = -1.7979 E-2

Y= 9.3285 E1

Z= -1.3483 E0

Moment:

Pressure: X = -2.0381 E4

Y = -1.8550 E-3

Z = 4.6198 E0

Viscous: X = 9.2225 E0

Y= 5.4287 E-3

Z= 3.1073 E-1

Physical Time step: 5E-2 and 5E-1

Computing Time: 6:23

Number of Iterations: 81

Y+ Notes: 35-52 at body, 17-35 at rear tip

Other Notes:

Summery of Test: **DREA6mCFX556a**

Half standard submarine shape set into box, no appendages, Database from 55, now in 56

Velocity: 3.5

Mesh Parameters

Volume Maximum Edge Length: 0.3

Surface Meshing Type: Angular Resolution

Angle: 7°

Maximum Edge Length: 0.3

Minimum Edge Length: 0.005

Expansion Factor: 1.2

Inflated Boundary: on Shape

Number of Layer: 22

Geometric Expansion Factor: 1.3

Inflation Thickness Multiplier: N/A

Max Thickness: N/A

First Prism Height: 0.005

Mesh Control: N/A

Length Scale: N/A

Radius: N/A

Expansion Factor: N/A

Mesh Results

Total Number of Nodes: 151 161

Total Number of Element: 465 259

Total Number of Tetrahedrons: 278 107

Total Number of Prisms: 185 160

Total Number of Pyramids: 1992

Total Number of Faces: 32 474

Drag:

Pressure: X = 7.5886 E-1

Y = 1.1494 E2

Z = -1.4062 E3

Viscous: X = 9.6972 E-3

Y= 9.2215 E1

Z= -1.2548 E0

Moment:

Pressure: X = -2.0182 E4

Y = -3.6774 E-3

Z = -1.1253 E1

Viscous: X = 1.0168 E1

Y= 5.5171 E-3

Z= -1.0839 E-1

Physical Timestep: 0.5 and 0.05

Computing Time: 3:17

Number of Iterations: 53

Y+ Notes: 50-60 at front and part of body, 40-50 at body, 30-40 at tail, 20-30 at very rear tip

Other Notes: Very coarse mesh

Summery of Test: **DREA6mCFX556b**

Half standard submarine shape set into box, no appendages

Velocity: 3.5

Mesh Parameters

Volume Maximum Edge Length: 0.3

Surface Meshing Type: Angular Resolution

Angle: 7°

Maximum Edge Length: 0.3

Minimum Edge Length: 0.0003

Expansion Factor: 1.2

Inflated Boundary: on Shape

Number of Layer: 32

Geometric Expansion Factor: 1.3

Inflation Thickness Multiplier: N/A

Max Thickness: N/A

First Prism Height: 0.0003

Mesh Control: N/A

Length Scale: N/A

Radius: N/A

Expansion Factor: N/A

Mesh Results

Total Number of Nodes: 163 856

Total Number of Element: 530 496

Total Number of Tetrahedrons: 345 185

Total Number of Prisms: 183 163

Total Number of Pyramids: 2148

Total Number of Faces: 40 717

Drag:

Pressure: X = 2.2956 E0

Y = 1.1434 E2

Z = -1.4172 E3

Viscous: X = 4.0181 E-2

Y= 9.3488 E1

Z= -1.3735 E0

Moment:

Pressure: X = -2.0337 E4

Y = -4.3194 E-4

Z = -3.0841 E1

Viscous: X = 8.9349 E0

Y= -1.1165 E-2

Z= -5.2566 E-1

Physical Timestep: 0.5 and 0.05

Computing Time: 3:11

Number of Iterations: 45

Y+ Notes: 49-59 at front part, 39-49 at body part, 29-39 at rear, 19-29 at rear tip

Other Notes:

Summery of Test: **DREA6mCFX556c**

Half standard submarine shape set into box, no appendages

Velocity: 3.5

Mesh Parameters

Volume Maximum Edge Length: 0.1

Surface Meshing Type: Angular Resolution

Angle: 7°

Maximum Edge Length: 0.1

Minimum Edge Length: 0.0003

Expansion Factor: 1.2

Inflated Boundary: on Shape

Number of Layer: 32

Geometric Expansion Factor: 1.3

Inflation Thickness Multiplier: N/A

Max Thickness: N/A

First Prism Height: 0.0003

Mesh Control: N/A

Length Scale: N/A

Radius: N/A

Expansion Factor: N/A

Mesh Results

Total Number of Nodes: 1 030 017

Total Number of Element: 5 441 004

Total Number of Tetrahedrons: 5 252 852

Total Number of Prisms: 185 160

Total Number of Pyramids: 1992

Total Number of Faces: 136 906

Drag:

Pressure: X = 1.0413 E0

Y = 1.0543 E2

Z = -1.4130 E3

Viscous: X = 1.4516 E-3

Y= 9.2695 E1

Z= -1.3530 E0

Moment:

Pressure: X = -2.0214 E4

Y = -8.7190 E-4

Z = -1.5398 E1

Viscous: X = 8.9364 E0

Y= 7.5313 E-4

Z= 3.5140 E-3

Physical Timestep: 5E-2 and 5E-1

Computing Time:

Number of Iterations:

Y+ Notes: 40-65 at tip, 30-50 at body, 21-30 at rear

Other Notes: Partitioned, MeTiS multilevel weighted k-way algorithm

Summery of Test: **DREA6mCFX556d**

Half standard submarine shape set into box, no appendages

Velocity: 3.5

Mesh Parameters

Volume Maximum Edge Length: 0.3

Surface Meshing Type: Angular Resolution

Angle: 7°

Maximum Edge Length: 0.3

Minimum Edge Length: 0.0003

Expansion Factor: 1.075

Inflated Boundary: on Shape

Number of Layer: 32

Geometric Expansion Factor: 1.3

Inflation Thickness Multiplier: N/A

Max Thickness: N/A

First Prism Height: 0.0003

Mesh Control: N/A

Length Scale: N/A

Radius: N/A

Expansion Factor: N/A

Mesh Results

Total Number of Nodes: 218 932

Total Number of Element: 798 143

Total Number of Tetrahedrons: 596 285

Total Number of Prisms: 199 162

Total Number of Pyramids: 2696

Total Number of Faces: 57 606

Drag:

Pressure: X = -1.4083 E0

Y = 1.0518 E2

Z = -1.4026 E3

Viscous: X = -5.1906 E-2

Y= 9.0553 E1

Z= -1.1158 E0

Moment:

Pressure: X = -2.0091 E4

Y = -1.3235 E-3

Z = 1.5802 E1

Viscous: X = 1.1508 E1

Y= 1.2629 E2

Z= 7.0262 E-1

Physical Timestep: 5E-2 and 5E-1

Computing Time: 5:30

Number of Iterations: 56

Y+ Notes: 43-54 at very tip, 54-65 at rest of tip, 33-54 over body, 21-33 at rear end

Other Notes:

Summery of Test: **DREA6mCFX556e**

Half standard submarine shape set into box, no appendages

Velocity: 3.5

Mesh Parameters

Volume Maximum Edge Length: 0.3

Surface Meshing Type: Angular Resolution

Angle: 7°

Maximum Edge Length: 0.3

Minimum Edge Length: 0.0003

Expansion Factor: 1.05

Inflated Boundary: on Shape

Number of Layer: 32

Geometric Expansion Factor: 1.3

Inflation Thickness Multiplier: N/A

Max Thickness: N/A

First Prism Height: 0.0003

Mesh Control: N/A

Length Scale: N/A

Radius: N/A

Expansion Factor: N/A

Mesh Results

Total Number of Nodes: 272 889

Total Number of Element: 1 036 615

Total Number of Tetrahedrons: 807 669

Total Number of Prisms: 225 435

Total Number of Pyramids: 3511

Total Number of Faces: 76 208

Drag:

Pressure: X = 7.2014E-1

Y = 9.9669 E1

Z = -1.4027 E3

Viscous: X = -1.4953 E-2

Y= 9.1025 E1

Z= -9.9880 E-1

Moment:

Pressure: X = -2.0086 E4

Y = -1.0864 E-3

Z = -1.1755 E1

Viscous: X = 1.3162 E1

Y= 6.1491 E-3

Z= 2.2934 E-1

Physical Timestep: 5E-2 and 5E-1

Computing Time: 6:30

Number of Iterations: 56

Y+ Notes: 40-65 at tip, 30-50 at body, 21-30 at rear

Other Notes:

Summery of Test: **DREA6mCFX556f**

Half standard submarine shape set into box, no appendages

Velocity: 3.5

Mesh Parameters

Volume Maximum Edge Length: 0.3

Surface Meshing Type: Angular Resolution

Angle: 7°

Maximum Edge Length: 0.3

Minimum Edge Length: 0.0003

Expansion Factor: 1.05

Inflated Boundary: on Shape

Number of Layer: 32

Geometric Expansion Factor: 1.3

Inflation Thickness Multiplier: N/A

Max Thickness: N/A

First Prism Height: 0.0003

Mesh Control: N/A

Length Scale: N/A

Radius: N/A

Expansion Factor: N/A

Mesh Results

Total Number of Nodes: 272 889

Total Number of Element: 1 036 615

Total Number of Tetrahedrons: 807 669

Total Number of Prisms: 225 435

Total Number of Pyramids: 3511

Total Number of Faces: 76 208

Drag:

Pressure: X = 7.2014 E-1

Y = 9.9669 E1

Z = -1.4027 E3

Viscous: X = -1.4953 E-2

Y= 9.1025 E1

Z= -9.9880 E-1

Moment:

Pressure: X = -2.0086 E4

Y = -1.0864 E-3

Z = -11755 E1

Viscous: X = 1.3162 E1

Y= 6.1491 E-3

Z= 2.6934 E-1

Physical Timestep: 5E-2 and 5E-1

Computing Time: 6:30

Number of Iterations: 56

Y+ Notes:

Other Notes: 40-65 at tip, 30-50 at body, 21-30 at rear

Summery of Test: **DREA6mCFX556g**

Half standard submarine shape set into box, no appendages

Velocity: 3.5

Mesh Parameters

Volume Maximum Edge Length: 0.3

Surface Meshing Type: Angular Resolution

Angle: 7°

Maximum Edge Length: 0.3

Minimum Edge Length: 0.0003

Expansion Factor: 1.03

Inflated Boundary: on Shape

Number of Layer: 32

Geometric Expansion Factor: 1.3

Inflation Thickness Multiplier: N/A

Max Thickness: N/A

First Prism Height: 0.0003

Mesh Control: N/A

Length Scale: N/A

Radius: N/A

Expansion Factor: N/A

Mesh Results

Total Number of Nodes: 435 537

Total Number of Element: 1 723 342

Total Number of Tetrahedrons: 1 393 801

Total Number of Prisms: 323 515

Total Number of Pyramids: 6029

Total Number of Faces: 127 531

Drag:

Pressure: X = 7.1613 E-1

Y = 9.1612 E1

Z = -1.4047 E3

Viscous: X = 2.1026 E-2

Y= 9.1541 E1

Z= -7.9936 E-1

Moment:

Pressure: X = -2.0102 E4

Y = -3.1843 E-4

Z = -9.1846 E0

Viscous: X = 1.5887 E1

Y= -1.1299E-2

Z= -2.8805 E-1

Physical Timestep: 5E-2 and 5E-1

Computing Time: 11:20

Number of Iterations: 56

Y+ Notes: 63 at tip, 43 on body, 21 at rear

Other Notes:

Summery of Test: **DREA6mCFX556h**

Half standard submarine shape set into box, no appendages

Velocity: 3.5

Mesh Parameters

Volume Maximum Edge Length: 0.1

Surface Meshing Type: Angular Resolution

Angle: 7°

Maximum Edge Length: 0.1

Minimum Edge Length: 0.0003

Expansion Factor: 1.05

Inflated Boundary: on Shape

Number of Layer: 32

Geometric Expansion Factor: 1.3

Inflation Thickness Multiplier: N/A

Max Thickness: N/A

First Prism Height: 0.0003

Mesh Control: N/A

Length Scale: N/A

Radius: N/A

Expansion Factor: N/A

Mesh Results

Total Number of Nodes: 1 238 502

Total Number of Element: 6 286 636

Total Number of Tetrahedrons: 5 957 095

Total Number of Prisms: 323 512

Total Number of Pyramids: 6029

Total Number of Faces: 210 795

Drag:

Pressure: X = 2.6148 E-1

Y = 9.0949 E1

Z = -1.4042 E3

Viscous: X = -1.7900 E-3

Y= 9.1501 E1

Z= -9.1643 E-1

Moment:

Pressure: X = -2.0046 E4

Y = -7.9812 E-4

Z = -4.0413 E0

Viscous: X = 1.4194 E1

Y= -2.1973 E-3

Z= 5.3963 E-2

Physical Timestep: 5E-2 and 5E-1

Computing Time: 64:00

Number of Iterations: 90

Y+ Notes: 63 at tip, 43 on body, 21 at rear

Other Notes: Very fine mesh, same results as g

Summery of Test: **DREA6mCFX55a**

Half standard submarine shape set into box, no appendages

Velocity: 50

Mesh Parameters

Volume Maximum Edge Length: 0.3

Surface Meshing Type: Angular Resolution

Angle: 7°

Maximum Edge Length: 0.3

Minimum Edge Length: 0.005

Expansion Factor: 1.2

Inflated Boundary: on Shape

Number of Layer: 22

Geometric Expansion Factor: 1.3

Inflation Thickness Multiplier: N/A

Max Thickness: N/A

First Prism Height: 0.005

Mesh Control: N/A

Length Scale: N/A

Radius: N/A

Expansion Factor: N/A

Mesh Results

Total Number of Nodes: 101 140

Total Number of Element: 405 358

Total Number of Tetrahedrons: 334 466

Total Number of Prisms: 69 402

Total Number of Pyramids: 1490

Total Number of Faces: 30 988

Drag:

Pressure: X = -4.9638 E1

Y = 2.3353 E4

Z = -2.9091 E5

Viscous: X = -4.6156 E0

Y= 1.2907 E4

Z= -1.3787 E2

Moment:

Pressure: X = -4.1756 E6

Y = -5.2395 E-2

Z = 5.0434 E2

Viscous: X = 1.9305 E3

Y= 2.3015 E0

Z= 6.9932 E1

Physical Timestep: 5E-3

Computing Time: 5:30

Number of Iterations: 126

Y+ Notes: 0-5000 at front, 10000 at peak, 7000-8000 at rear

Other Notes:

Summery of Test: DREA6mCFX55b

Half standard submarine shape set into box, no appendages

Velocity: 50

Mesh Parameters

Volume Maximum Edge Length: 0.3

Surface Meshing Type: Angular Resolution

Angle: 7°

Maximum Edge Length: 0.3

Minimum Edge Length: 0.0003

Expansion Factor: 1.2

Inflated Boundary: on Shape

Number of Layer: 32

Geometric Expansion Factor: 1.3

Inflation Thickness Multiplier: N/A

Max Thickness: N/A

First Prism Height: 0.0003

Mesh Control: N/A

Length Scale: N/A

Radius: N/A

Expansion Factor: N/A

Mesh Results

Total Number of Nodes: 163 856

Total Number of Element: 530 496

Total Number of Tetrahedrons: 345 185

Total Number of Prisms: 183 163

Total Number of Pyramids: 2148

Total Number of Faces: 40 717

Drag:

Pressure: X = 4.5933 E2

Y = 2.2825 E4

Z = -2.9037 E5

Viscous: X = 6.2757 E0

Y= 1.3234 E4

Z= -1.6564 E2

Moment:

Pressure: X = -4.1652 E6

Y = -1.2671 E-1

Z = -6.1410 E3

Viscous: X = 1.6530 E3

Y= -1.7567 E0

Z= 8.3605 E1

Physical Timestep: 5 E-3

Computing Time: 13:40

Number of Iterations: 203

Y+ Notes: 0-200 at front, 900-600 at body, 200-400 at tail

Other Notes:

Summery of Test: **DREA6mCFX556g**

Half standard submarine shape set into box, no appendages, Database from 55, now in 56

Velocity: 1

Mesh Parameters

Volume Maximum Edge Length: 0.3

Surface Meshing Type: Angular Resolution

Angle: 7°

Maximum Edge Length: 0.3

Minimum Edge Length: 0.0003

Expansion Factor: 1.03

Inflated Boundary: on Shape

Number of Layer: 32

Geometric Expansion Factor: 1.3

Inflation Thickness Multiplier: N/A

Max Thickness: N/A

First Prism Height: 0.0003

Mesh Control: N/A

Length Scale: N/A

Radius: N/A

Expansion Factor: N/A

Mesh Results

Total Number of Nodes: 435 537

Total Number of Element: 1 723 342

Total Number of Tetrahedrons: 1 393 801

Total Number of Prisms: 323 515

Total Number of Pyramids: 6029

Total Number of Faces: 127 531

Drag:

Pressure: X = 6.3744 E-2

Y = 7.6070 E0

Z = -1.1430 E2

Viscous: X = 1.7517 E-3

Y= 9.0995 E0

Z= -8.7832 E-2

Moment:

Pressure: X = -1.6361 E3

Y = -2.4246 E-5

Z = -8.3409 E-1

Viscous: X = 1.4652 E0

Y= -1.0713 E-3

Z= -2.4103 E-2

Physical Timestep: 0.5 and 0.05

Computing Time: 6:32

Number of Iterations: 85

Y+ Notes: 0-26.5 overall, majority 6-19.87

Other Notes:

Summery of Test: **DREA6mCFX556g**

Half standard submarine shape set into box, no appendages

Velocity: 2.5

Mesh Parameters

Volume Maximum Edge Length: 0.3

Surface Meshing Type: Angular Resolution

Angle: 7°

Maximum Edge Length: 0.3

Minimum Edge Length: 0.0003

Expansion Factor: 1.03

Inflated Boundary: on Shape

Number of Layer: 32

Geometric Expansion Factor: 1.3

Inflation Thickness Multiplier: N/A

Max Thickness: N/A

First Prism Height: 0.0003

Mesh Control: N/A

Length Scale: N/A

Radius: N/A

Expansion Factor: N/A

Mesh Results

Total Number of Nodes: 435 537

Total Number of Element: 1 723 342

Total Number of Tetrahedrons: 1 393 801

Total Number of Prisms: 323 515

Total Number of Pyramids: 6029

Total Number of Faces: 127 531

Drag:

Pressure: X = 3.7238 E-1

Y = 4.6938 E1

Z = -7.1613 E2

Viscous: X = 1.0859 E-2

Y= 4.9226 E1

Z= -4.4402 E-1

Moment:

Pressure: X = -1.0249 E4

Y = -1.5827 E-4

Z = 4.8001 E0

Viscous: X = 8.3477 E0

Y= -5.9981 E-3

Z= -1.4882 E-1

Physical Timestep: 0.5 and 0.05

Computing Time: 13:30

Number of Iterations: 60

Y+ Notes: Maximum 0-62 and majority 25-45.

Other Notes:

Summery of Test: **DREA6mCFX556g**

Half standard submarine shape set into box, no appendages

Velocity: 3

Mesh Parameters

Volume Maximum Edge Length: 0.3

Surface Meshing Type: Angular Resolution

Angle: 7°

Maximum Edge Length: 0.3

Minimum Edge Length: 0.0003

Expansion Factor: 1.03

Inflated Boundary: on Shape

Number of Layer: 32

Geometric Expansion Factor: 1.3

Inflation Thickness Multiplier: N/A

Max Thickness: N/A

First Prism Height: 0.0003

Mesh Control: N/A

Length Scale: N/A

Radius: N/A

Expansion Factor: N/A

Mesh Results

Total Number of Nodes: 435 537

Total Number of Element: 1 723 342

Total Number of Tetrahedrons: 1 393 801

Total Number of Prisms: 323 515

Total Number of Pyramids: 6029

Total Number of Faces: 127 531

Drag:

Pressure: X = 5.3110 E-1

Y = 6.7436 E1

Z = -1.0317 E3

Viscous: X = 1.5535 E-2

Y= 6.8898 E1

Z= -6.0880 E-1

Moment:

Pressure: X = -1.4764 E4

Y = -2.3067 E-4

Z = -6.8246 E0

Viscous: X = 1.1862 E1

Y= -8.4518 E-3

Z= -2.1280 E-1

Physical Timestep: 5E-2 and 5E-1

Computing Time: 12:36

Number of Iterations: 57

Y+ Notes: Maximum 0-73 and majority 25-50.

Other Notes:

Summery of Test: **DREA6mCFX556g**

Half standard submarine shape set into box, no appendages

Velocity: 3.422

Mesh Parameters

Volume Maximum Edge Length: 0.3

Surface Meshing Type: Angular Resolution

Angle: 7°

Maximum Edge Length: 0.3

Minimum Edge Length: 0.0003

Expansion Factor: 1.03

Inflated Boundary: on Shape

Number of Layer: 32

Geometric Expansion Factor: 1.3

Inflation Thickness Multiplier: N/A

Max Thickness: N/A

First Prism Height: 0.0003

Mesh Control: N/A

Length Scale: N/A

Radius: N/A

Expansion Factor: N/A

Mesh Results

Total Number of Nodes: 435 537

Total Number of Element: 1 723 342

Total Number of Tetrahedrons: 1 393 801

Total Number of Prisms: 323 515

Total Number of Pyramids: 6029

Total Number of Faces: 127 531

Drag:

Pressure: X = 6.8506 E-1

Y = 8.7597 E1

Z = -1.3426 E3

Viscous: X = 2.0063 E-2

Y= 8.7806 E1

Z= -7.6915 E-1

Moment:

Pressure: X = -1.9614 E4

Y = -3.0684 E-1

Z = -8.7888 E0

Viscous: X = 1.5205 E1

Y= -1.0830 E-2

Z= -2.7491 E-1

Physical Timestep: 0.005 and 0.05 and 0.5

Computing Time: 16.00

Number of Iterations: 80

Y+ Notes: Maximum 0-82 and 20-60 majority.

Other Notes:

Summery of Test: **DREA6mCFX556g**

Half standard submarine shape set into box, no appendages

Velocity: 3.5

Mesh Parameters

Volume Maximum Edge Length: 0.3

Surface Meshing Type: Angular Resolution

Angle: 7°

Maximum Edge Length: 0.3

Minimum Edge Length: 0.0003

Expansion Factor: 1.03

Inflated Boundary: on Shape

Number of Layer: 32

Geometric Expansion Factor: 1.3

Inflation Thickness Multiplier: N/A

Max Thickness: N/A

First Prism Height: 0.0003

Mesh Control: N/A

Length Scale: N/A

Radius: N/A

Expansion Factor: N/A

Mesh Results

Total Number of Nodes: 435 537

Total Number of Element: 1 723 342

Total Number of Tetrahedrons: 1 393 801

Total Number of Prisms: 323 515

Total Number of Pyramids: 6029

Total Number of Faces: 127 531

Drag:

Pressure: X = 7.1613 E-1

Y = 901612 E1

Z = -1.4047 E3

Viscous: X = 2.1026 E-2

Y= 9.1541 E1

Z= -7.9936 E-1

Moment:

Pressure: X = -2.0102 E4

Y = -3.1843 E-4

Z = -9.1846 E0

Viscous: X = 1.5887 E1

Y= -1.1299 E-2

Z= -2.8805 E-1

Physical Timestep: 5E-2 and 5E-1

Computing Time: 5:40

Number of Iterations: 63

Y+ Notes: 84.1 maximum, 60 majority

Other Notes:

Summery of Test: **DREA6mCFX556g**

Half standard submarine shape set into box, no appendages

Velocity: 4.5

Mesh Parameters

Volume Maximum Edge Length: 0.3

Surface Meshing Type: Angular Resolution

Angle: 7°

Maximum Edge Length: 0.3

Minimum Edge Length: 0.0003

Expansion Factor: 1.03

Inflated Boundary: on Shape

Number of Layer: 32

Geometric Expansion Factor: 1.3

Inflation Thickness Multiplier: N/A

Max Thickness: N/A

First Prism Height: 0.0003

Mesh Control: N/A

Length Scale: N/A

Radius: N/A

Expansion Factor: N/A

Mesh Results

Total Number of Nodes: 435 537

Total Number of Element: 1 723 342

Total Number of Tetrahedrons: 1 393 801

Total Number of Prisms: 323 515

Total Number of Pyramids: 6029

Total Number of Faces: 127 531

Drag:

Pressure: X = 1.1680 E0

Y = 1.5099 E2

Z = -2.3233 E3

Viscous: X = 3.432 E-2

Y= 1.4566 E2

Z= -1.2435 E0

Moment:

Pressure: X = -3.327 E4

Y = -5.3529 E-4

Z = -1.4932 E1

Viscous: X = 2.5662 E1

Y= -1.8142 E-2

Z= -4.7019 E-1

Physical Timestep: 5E-2 and 1E-1

Computing Time: 6:30

Number of Iterations: 57

Y+ Notes: Maximum 0-105.45 and majority 25-80.

Other Notes:

Summery of Test: **DREA6mCFX556g**

Half standard submarine shape set into box, no appendages

Velocity: 10

Mesh Parameters

Volume Maximum Edge Length: 0.3

Surface Meshing Type: Angular Resolution

Angle: 7°

Maximum Edge Length: 0.3

Minimum Edge Length: 0.0003

Expansion Factor: 1.03

Inflated Boundary: on Shape

Number of Layer: 32

Geometric Expansion Factor: 1.3

Inflation Thickness Multiplier: N/A

Max Thickness: N/A

First Prism Height: 0.0003

Mesh Control: N/A

Length Scale: N/A

Radius: N/A

Expansion Factor: N/A

Mesh Results

Total Number of Nodes: 435 537

Total Number of Element: 1 723 342

Total Number of Tetrahedrons: 1 393 801

Total Number of Prisms: 323 515

Total Number of Pyramids: 6029

Total Number of Faces: 127 531

Drag:

Pressure: X = 5.5935 E0

Y = 7.3947 E2

Z = -1.1490 E4

Viscous: X = 1.5984 E-1

Y= 6.4250 E2

Z= -4.9888 E0

Moment:

Pressure: X = -1.6440 E5

Y = -2.6706 E-3

Z = -7.1026 E1

Viscous: X = 1.11989 E2

Y= -8.966 E-2

Z= -2.2004 E0

Physical Timestep: 5E-2 and 5E-1

Computing Time: 6:00

Number of Iterations: 66

Y+ Notes: Maximum 0-218 and majority 54-163.

Other Notes:

Summery of Test: **DREA6mCFX556g**

Half standard submarine shape set into box, no appendages

Velocity: 25

Mesh Parameters

Volume Maximum Edge Length: 0.3

Surface Meshing Type: Angular Resolution

Angle: 7°

Maximum Edge Length: 0.3

Minimum Edge Length: 0.0003

Expansion Factor: 1.03

Inflated Boundary: on Shape

Number of Layer: 32

Geometric Expansion Factor: 1.3

Inflation Thickness Multiplier: N/A

Max Thickness: N/A

First Prism Height: 0.0003

Mesh Control: N/A

Length Scale: N/A

Radius: N/A

Expansion Factor: N/A

Mesh Results

Total Number of Nodes: 435 537

Total Number of Element: 1 723 342

Total Number of Tetrahedrons: 1 393 801

Total Number of Prisms: 323 515

Total Number of Pyramids: 6029

Total Number of Faces: 127 531

Drag:

Pressure: X = 3.4145 E1

Y = 4.5852 E3

Z = -7.1915 E4

Viscous: X = 9.2916 E-1

Y= 3.5552 E3

Z= -2.4354 E1

Moment:

Pressure: X = -1.0289 E6

Y = -1.7106 E-2

Z = -4.3112 E2

Viscous: X = 7.0729 E2

Y= -4.6531 E-1

Z= -1.2873 E1

Physical Timestep: 5E-3 and 5E-2

Computing Time: 14:47

Number of Iterations: 65

Y+ Notes: Maximum 0-509.3 and majority 100-300.

Other Notes:

Summery of Test: **DREA6mCFX556g**

Half standard submarine shape set into box, no appendages

Velocity: 40

Mesh Parameters

Volume Maximum Edge Length: 0.3

Surface Meshing Type: Angular Resolution

Angle: 7°

Maximum Edge Length: 0.3

Minimum Edge Length: 0.0003

Expansion Factor: 1.03

Inflated Boundary: on Shape

Number of Layer: 32

Geometric Expansion Factor: 1.3

Inflation Thickness Multiplier: N/A

Max Thickness: N/A

First Prism Height: 0.0003

Mesh Control: N/A

Length Scale: N/A

Radius: N/A

Expansion Factor: N/A

Mesh Results

Total Number of Nodes: 435 537

Total Number of Element: 1 723 342

Total Number of Tetrahedrons: 1 393 801

Total Number of Prisms: 323 515

Total Number of Pyramids: 6029

Total Number of Faces: 127 531

Drag:

Pressure: X = 8.7101 E1

Y = 1.1697 E4

Z = -1.8424 E5

Viscous: X = 2.2820 E0

Y= 8.5698 E3

Z= -1.0997 E3

Physical Timestep: 5E-3 and 5E-2

Computing Time: 12:40

Number of Iterations: 56

Moment:

Pressure: X = -2.6359 E6

Y = -4.4137 E-2

Z = -1.0997 E3

Viscous: X = 1.7569 E3

Y= -1.1337 E0

Z= 3.1689 E1

Y+ Notes: Maximum 0-788 and majority 200-600.

Summery of Test: **BOAT6mCFX56B**

Velocity: 3.5

Mesh Parameters

Volume Maximum Edge Length: 0.3

Surface Meshing Type: Angular Resolution

Angle: 7°

Maximum Edge Length: 0.3

Minimum Edge Length: 0.0003

Expansion Factor: 1.05

Inflated Boundary: on Shape

Number of Layer: 28

Geometric Expansion Factor: 1.3

Inflation Thickness Multiplier: N/A

Max Thickness: N/A

First Prism Height: 0.0003

Mesh Control: N/A

Length Scale: N/A

Radius: N/A

Expansion Factor: N/A

Mesh Results

Total Number of Nodes: 653 650

Total Number of Element: 2 150 889

Total Number of Tetrahedrons: 1 389 448

Total Number of Prisms: 744 605

Total Number of Pyramids: 16 836

Total Number of Faces: 138 965

Drag:

Pressure: X = 6.7684 E3

Y = 6.2760 E2

Z = -7.0051 E3

Viscous: X = -2.4987 E4

Y= 1.5079 E2

Z= -5.2798 E0

Moment:

Pressure: X = -2.4987 E4

Y = 8.4439 E1

Z = -2.5791 E4

Viscous: X = 9.2429 E1

Y= 2.9862 E-1

Z= 8.1026 E1

Physical Timestep: 0.5 and 0.05

Computing Time: 18 hours

Number of Iterations: 100

Converged: RMS: $5.9(10^{-6})$ and MAX: $7.5(10^{-4})$

Y+ Notes: 20-50 majority, maximum 51.44

APPENDIX D – SAMPLE CALCULATIONS

UNIVERSITY OF NEW BRUNSWICK

FACULTY OF ENGINEERING

Course No. SENIOR PROJECT

Assignment No. — Date JAN 15 / 04

Page

1

Problem No. SAMPLE CALCULATIONS

By CHRIS BAKER

of

6

DRAG COEFFICIENTS

DATA - FALL 1988 WIND TUNNEL TESTS OF THE DREA
 6 METRE LONG SUBMARINE MODEL
 - FORCE DATA ANALYSIS

AIR

 $\rho_{\text{air}} = 0$ $Re = 23$ MILLION $\gamma_{\text{yaw}} = 0$ $U_{\text{ref}} = 54 \text{ m/s}$ $T_{\text{ref}} = 10^\circ\text{C}$ $l = 6 \text{ m}$

$$C_D = 0.00123$$

$$\text{ERROR BAR} = 6.30 (10^{-4})$$

$$C_D = \frac{F}{Q_{\text{ref}} l^2} \quad (\text{FROM REPORT}) \quad Q_{\text{ref}} = \frac{1}{2} \rho U_{\text{ref}}^2$$

$$@ 10^\circ\text{C} \quad \rho = 1.245 \text{ kg/m}^3 \quad \mu = 1.755 (10^{-5}) \frac{\text{Ns}}{\text{m}^2}$$

CHECK U_{ref}

$$Re = 23,000,000 = \frac{\rho U l}{\mu} = \frac{(1.245 \text{ kg/m}^3) U_{\text{ref}} (6 \text{ m})}{1.755 (10^{-5}) \frac{\text{Ns}}{\text{m}^2}}$$

$$U_{\text{ref}} = 54.04 \text{ m/s} \quad \text{OK}$$

$$Q_{\text{ref}} = \frac{1}{2} \rho U_{\text{ref}}^2 = \frac{1}{2} (1.245 \text{ kg/m}^3) (54 \text{ m/s})^2$$

$$Q_{\text{ref}} = 1815.21 \text{ Pa}$$

$$F = C_D Q_{\text{ref}} l^2$$

$$= (0.00123) (1815.21 \text{ Pa}) (6^2 \text{ m}^2)$$

$$F = 80.38 \text{ N} \quad \text{FORCE ON MODEL IN AIR} \\ (\text{WIND TUNNEL})$$

ERROR

$$F = C_{D\text{err}} Q_{\text{ref}} l^2$$

$$= 6.30 (10^{-4}) (1815.21 \text{ Pa}) (6 \text{ m})^2$$

$$F_{\text{err}} = 41.17 \text{ N} \quad \text{so} \quad F_{\text{err}} = \pm 20.58 \text{ N}$$

ASSUMING ERROR BARS ARE CENTERED ON CALCULATED FORCE.

UNIVERSITY OF NEW BRUNSWICK	FACULTY OF ENGINEERING	
Course No. SENIOR REPORT	Assignment No. —	Date JAN 15/04
Problem No. SAMPLE CALCULATIONS	By CHRIS BAKER	Page 2 of

CFX DATA

ROLL = 0°
 Re = 23 MILLION
 VAW = 0°
 WATER

Uref = 3.42 m/s
 Re actual = 23 003 039

DRAG FORCES

	HALF HULL	FULL HULL
VISCOS	88 N	176 N
PRESSURE	88 N	176 N
TOTAL = 352 N		

VALUES FROM CFX LIBRARY:

$$T = 25^\circ\text{C} \quad \rho = 997.0 \text{ kg/m}^3 \quad \mu = 8.899(10^{-4}) \frac{\text{kg}}{\text{m s}}$$

$$Q_{ref} = \frac{1}{2} \rho U_{ref}^2 = \frac{1}{2} (997 \frac{\text{kg}}{\text{m}^3}) (3.42 \text{ m/s})^2$$

$$Q_{ref} = 5830.7 \text{ Pa}$$

$$C_{D_{CFX}} = \frac{F}{Q_{ref} A} = \frac{352 \text{ N}}{(5830.7 \text{ Pa})(6 \text{ m}^2)}$$

$$C_{D_{CFX}} = 0.00167$$

COMPARISON

$$C_{D_{exp}} = 0.00123 \pm 0.000315$$

$$C_{D_{HIGH}} = 0.00155$$

$$C_{D_{LOW}} = 0.00092$$

$$C_{D_{CFX}} = 0.00167$$

ASSUMING ERROR BARS ARE CENTERED ON CALCULATED FORCE

UNIVERSITY OF NEW BRUNSWICK	FACULTY OF ENGINEERING	
Course No. SENIOR REPORT	Assignment No. — Date JAN 15/04	Page 3
Problem No. SAMPLE CALCULATIONS	By CHRIS BAKER	of 6

EQUIVALENT FORCE IF WIND TUNNEL
TEST WAS IN WATER

$$C_D \text{exp} = 0.00123 \pm 0.000315$$

$$T = 25^\circ\text{C}$$

$$\rho = 997 \text{ kg/m}^3$$

$$\mu = 8.898 \times 10^{-4} \text{ kg/ms}$$

} VALUES CFX TEST DONE AT

$$F_{\text{exp}} = C_D Q_{\text{ref}} l^2$$

$$\text{where } Q_{\text{ref}} = 5830.7 \text{ Pa}$$

$$F_{\text{exp}} = (0.00123)(5830.7 \text{ Pa})(6\text{m})^2$$

$$F_{\text{exp}} = 258.18 \text{ N}$$

$$F_{\text{err}} = (0.000315)(5830.7 \text{ Pa})(6\text{m})^2$$

$$F_{\text{err}} = 66.12 \text{ N}$$

$$F_{\text{exp}} = 258.2 \text{ N} \pm 66.1 \text{ N}$$

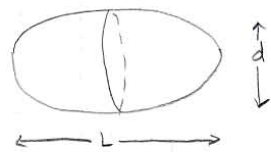
$$F_{\text{HIGH}} = 324.3 \text{ N}$$

$$F_{\text{LOW}} = 192.1 \text{ N}$$

FORCE EXPECTED FROM CFX BASED
ON WIND TUNNEL RESULTS

UNIVERSITY OF NEW BRUNSWICK	FACULTY OF ENGINEERING	
Course No. SENIOR REPORT	Assignment No. —	Date JAN 15/04
Problem No. SAMPLE CALCULATIONS	By CHRIS BAKER	Page 4 of 6

COMPARISON WITH ELLIPSOID



$$l = 6 \text{ m} \quad \frac{l}{D} = 3.50$$

$$D = 1.714 \text{ m}$$

$$C_D \text{ TURBULENT} = 0.1075$$

BASED ON FRONTAL AREA.

$$A_F = \frac{\pi D^2}{4} = \frac{\pi (1.714)^2}{4}$$

$$\rho = 997 \text{ kg/m}^3$$

$$A_F = 2.30734 \text{ m}^2$$

$$U = 3.42 \text{ m/s}$$

$$F = C_D Q_{ref} A_F \quad \text{where } Q_{ref} = \frac{1}{2} \rho U^2$$

$$Q_{ref} = \frac{1}{2} \rho U^2$$

$$= (1/2)(997 \text{ kg/m}^3)(3.42)^2$$

$$Q_{ref} = 5830.66 \text{ Pa}$$

$$F_{DRAG} = C_D Q_{ref} A_F$$

$$= (0.1075)(5830.66)(2.30734 \text{ m}^2)$$

$$F_{DRAG} = 1446.23 \text{ N}$$

SUBMARINE SHAPE WITH C_D BASED ON FRONTAL AREA

$$C_D = \frac{F}{Q_{ref} A_F} = \frac{352 \text{ N}}{(5830.66)(2.30734)}$$

$$C_D = 0.0262$$

COMPARISON $C_D = 0.1075$ ELLIPSOID

$C_D = 0.0262$ SUBMARINE

UNIVERSITY OF NEW BRUNSWICK	FACULTY OF ENGINEERING	
Course No. SENIOR REPORT	Assignment No. — Date JAN 15/04	Page 5
Problem No. SAMPLE CALCULATIONS	By CHRIS BAKER	of 6

BOUNDARY LAYER THICKNESS

$$\frac{\delta}{x} = \frac{0.16}{Re_x^{1/7}} \quad (7.1b) \text{ TURBULENT EQN FROM WHITE}$$

@ x = 1m

$$Re_x = \frac{(\rho)(u)(x)}{\mu} = \frac{(997)(3.422)(1)}{0.0008899}$$

$$\frac{\delta}{1} = \frac{0.16}{\left(\frac{(997)(3.422)(1)}{0.0008899} \right)^{1/7}}$$

$$\delta = 0.0183 \text{ m}$$

@ x = 5m

$$\frac{\delta}{5} = \frac{0.16}{\left(\frac{(997)(3.422)(5)}{0.0008899} \right)^{1/7}}$$

$$\delta = 0.0729 \text{ m}$$

PERCENT DIFFERENCE

$$DRAG_{CFX} = 350.8 \text{ N}$$

$$DRAG_{EXP} = 258.2 \text{ N}$$

$$\begin{aligned} \% \text{ DIFF} &= \frac{|ACTUAL - EXPERIMENTAL|}{ACTUAL} * 100 \\ &= \frac{|258.2 - 350.8|}{258.2} * 100 \end{aligned}$$

$$\% \text{ DIFF} = 36\%$$

UNIVERSITY OF NEW BRUNSWICK	FACULTY OF ENGINEERING	
Course No. SENIOR REPORT	Assignment No. — Date JAN 15, 04	Page 6
Problem No. SAMPLE CALCULATIONS	By CHRIS BAKER	of 6

VOLUME CHECK FOR MODEL

USING POST - DOMAIN VOLUME = 539.121 m^3

HULL VOLUME EQN:

$$\text{VOL}_H = 0.00816191 l^3 \quad l = 6\text{m}$$

$$\text{VOL}_H = 0.00816191 (6)^3$$

$$= 1.76297256 \text{ m}^3$$

VOLUME OF DUCT

$$\text{VOL}_{\text{DUCT}} = \text{BASE} \times \text{WIDTH} \times \text{LENGTH}$$

$$= (6\text{m}) \times (3\text{m}) \times (30\text{m})$$

$$= 540.0 \text{ m}^3$$

$$\text{DOMAIN VOLUME} = \text{VOL}_{\text{DUCT}} - \frac{1}{2} \text{ VOL}_{\text{HULL}}$$

$$= 540 - \frac{1}{2}(1.76297256) \text{ m}^3$$

$$V_{\text{DOMAIN}} = 539.1185137 \text{ m}^3$$

$$\% \text{ DIFF} = \frac{539.119 - 539.121}{1.76297256} \times 2 \times 100$$

$$= 0.28\%$$

UNIVERSITY OF NEW BRUNSWICK	FACULTY OF ENGINEERING	Page
Course No. Senior Project	Assignment No.	Date
Problem No. Sample Calculations	By Chris Baker	of

Flat Plate Drag

C_D FlatPlate Ref [1] (white) Pg 443 Fig 7.6

$C_D = 0.00267$. Assuming all turbulent, smooth plate

$$A_{SA} = 11.2498 \text{ m}^2$$

$$\begin{aligned} F_{\text{DRAG}} &= C_D \left(\frac{1}{2}\right) \rho U^2 A_{SA} \\ &= (0.00267)(0.5)(997 \text{ kg/m}^3)(3.422 \text{ m/s})^2 (11.2498 \text{ m}^2) \\ &= 175.34 \text{ N} \end{aligned}$$

Compared to CFX - with Upwind Differencing Scheme

$$F_{\text{DRAG}} (\text{Viscous}) = 176 \text{ N} \quad \% \text{ Diff} = 0.3\%$$

$$F_{\text{DRAG}} (\text{TOTAL}) = 351 \text{ N} \quad \% \text{ Diff} = 50\%$$

With High Resolution Advection Scheme

$$F_{\text{DRAG}} (\text{Viscous}) = 176 \text{ N} \quad \% \text{ Diff} = 0.3\%$$

$$F_{\text{DRAG}} (\text{TOTAL}) = 195 \text{ N} \quad \% \text{ Diff} = 11\%$$

So

$$F_{\text{Viscous exp}} = 175.3 \text{ N} \quad \% \text{ Diff} = 0.3\%$$

$$F_{\text{Viscous CFX}} = 176 \text{ N}$$

APPENDIX E – DREA STANDARD HULL

DREA Standard Model

Hull

Parent axisymmetric hull form: length ℓ , maximum diameter d , $\ell/d = 8.75$. Profile radii are specified in three regions:

region 1 nose, length: 0.2ℓ

radius: $3 \times$ standard NACA thickness radius $(3.3d^2/\ell)$

profile: Riegels* type D_2 :

$$\frac{r_1(x)}{\ell} = \frac{d}{\ell} \left[2.56905 \sqrt{\frac{x}{\ell}} - 3.48055 \frac{x}{\ell} + 0.49848 \left(\frac{x}{\ell}\right)^2 + 3.40732 \left(\frac{x}{\ell}\right)^3 \right]$$

$$0 \leq \frac{x}{\ell} \leq 0.2.$$

region 2 mid body, circular cylinder:

$$\frac{r_2(x)}{\ell} = \frac{d}{2\ell}, \quad 0.2 \leq \frac{x}{\ell} \leq 1 - \frac{3d}{\ell}.$$

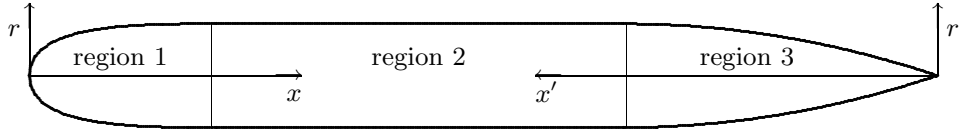
region 3 tail, length: $3d$

profile: parabolic:

$$\frac{r_3(x)}{\ell} = \frac{d}{2\ell} - \frac{\ell}{18d} \left[\frac{x}{\ell} - \left(1 - \frac{3d}{\ell}\right) \right]^2, \quad 1 - \frac{3d}{\ell} \leq \frac{x}{\ell} \leq 1.$$

alternate tail profile specification using $x' = \ell - x$:

$$\frac{r_3(x')}{d} = \frac{1}{2} - \frac{1}{18} \left(3 - \frac{x'}{d} \right)^2, \quad 0 \leq \frac{x'}{d} \leq 3.$$



$$\text{Hull Volume} = 0.00816191\ell^3$$

$$\text{Hull Center of Buoyancy at } x/\ell = 0.444842\ell$$

* Riegels, F.H., *Aerofoil Sections*, London, Butterworths, 1961

Appendages

The appendages all have NACA four digit airfoil thickness profiles, $y_t(x)$, which are given by:^{*}

$$\frac{y_t}{c} = \pm \frac{t}{c} \left[1.4845 \sqrt{\frac{x}{c}} - 0.6300 \frac{x}{c} - 1.7580 \left(\frac{x}{c} \right)^2 + 1.4215 \left(\frac{x}{c} \right)^3 - 0.5075 \left(\frac{x}{c} \right)^4 \right]$$

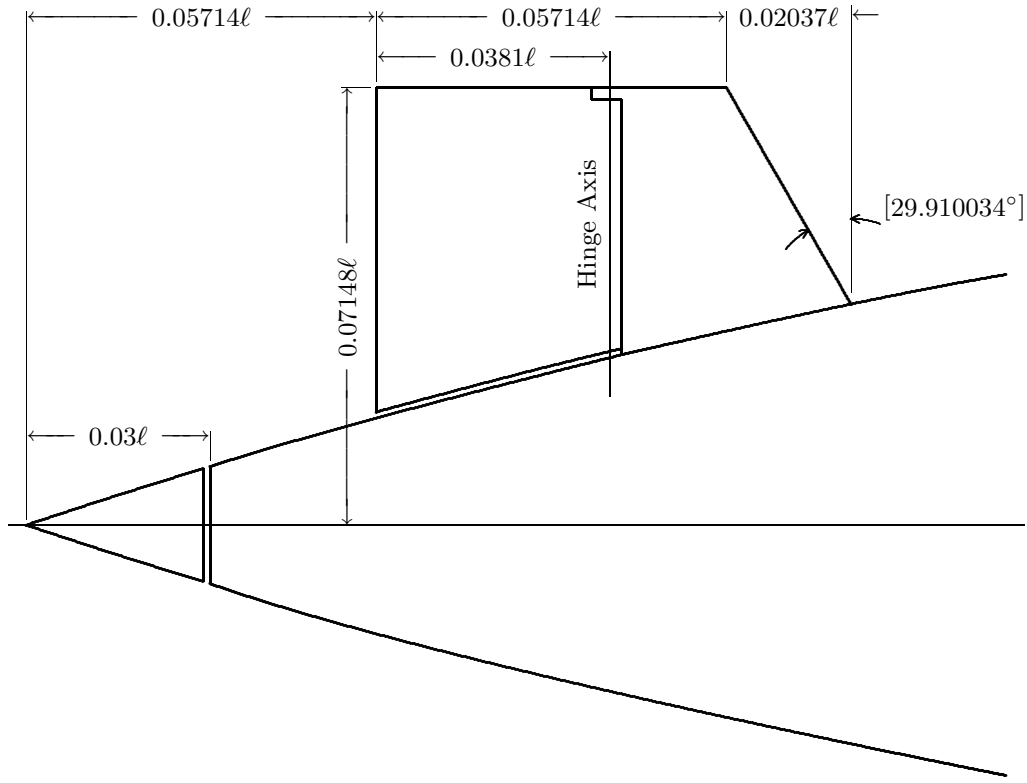
where c is the local chord length and t/c is the maximum thickness to chord ratio. The leading edge is at $x = 0$ and the trailing edge, which has non-zero thickness, is at $x = c$.

Tailplanes

Four identical rudder and sternplane appendages in a symmetrical '+' configuration. Flat tips, NACA 0015 thickness profiles ($t/c = 0.15$).

Propeller Hub

Aft three percent of hull.



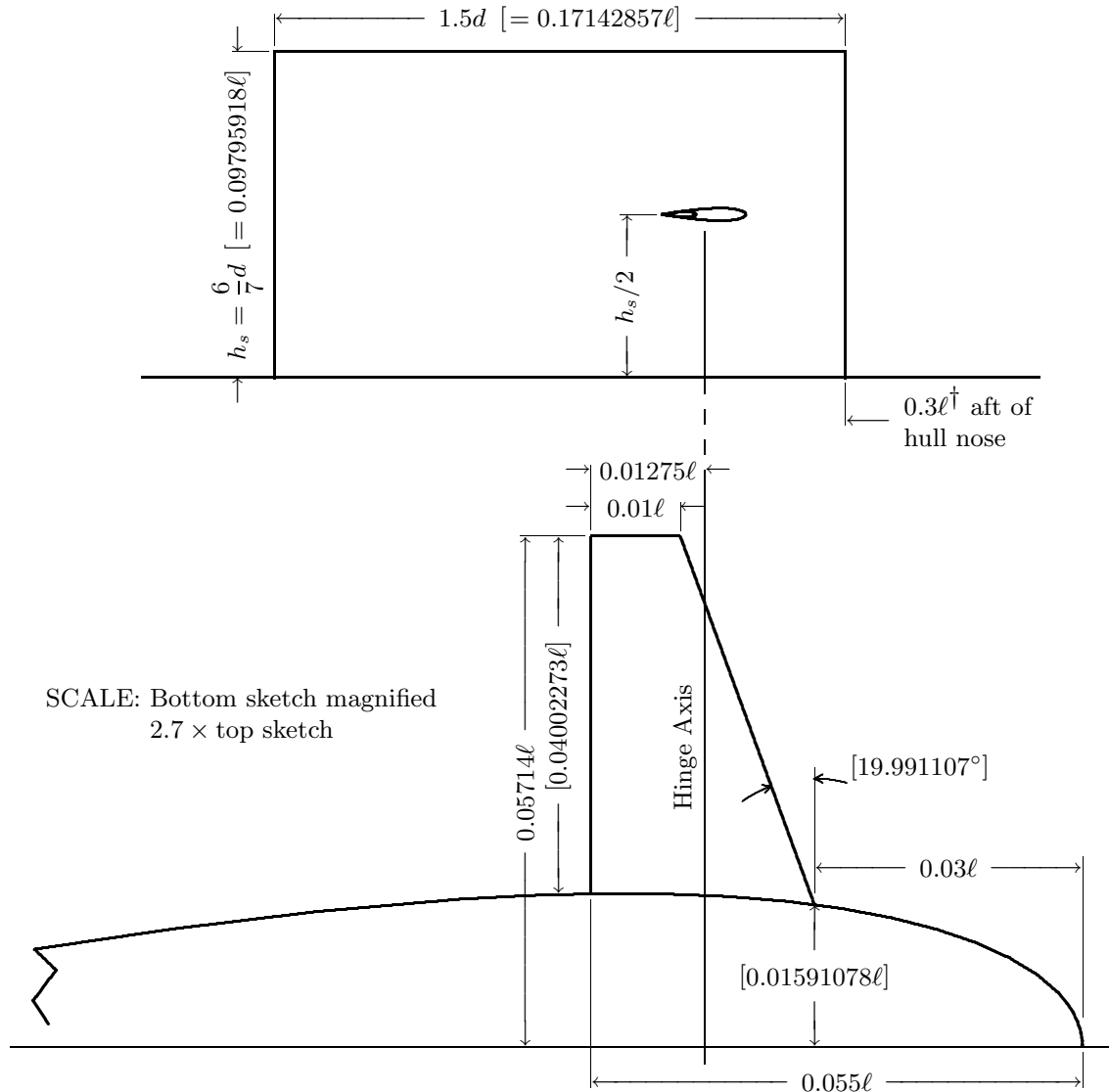
* Abbott, I.H. and von Doenhoff, A.E., *Theory of Wing Sections*, Dover, 1959

Sail

Rectangular planform, flat tip, NACA 0020 thickness profile ($t/c = 0.2$).

Sailplanes

Flat tips, NACA 0015 thickness profiles ($t/c = 0.15$).



Note: Quantities in []'s are calculated from the non-bracketed defining dimensions.

† This value is 0.2867ℓ for the Static Test Rig Mark I model, due to a manufacturing error.

This page intentionally left blank.

DOCUMENT CONTROL DATA

(Security classification of title, body of abstract and indexing annotation must be entered when the overall document is classified)

<p>1. ORIGINATOR (the name and address of the organization preparing the document. Organizations for whom the document was prepared, e.g. Centre sponsoring a contractor's report, or tasking agency, are entered in section 8.)</p> <p>Defence Research and Development Canada – Atlantic P.O. Box 1012, Dartmouth, NS B2Y 3Z7</p>	<p>2. SECURITY CLASSIFICATION (overall security classification of the document including special warning terms if applicable).</p> <p>UNCLASSIFIED</p>	
<p>3. TITLE (the complete document title as indicated on the title page. Its classification should be indicated by the appropriate abbreviation (S,C,R or U) in parentheses after the title).</p> <p>Estimating Drag Forces on Submarine Hulls</p>		
<p>4. AUTHORS (Last name, first name, middle initial. If military, show rank, e.g. Doe, Maj. John E.)</p> <p>Baker, Christopher</p>		
<p>5. DATE OF PUBLICATION (month and year of publication of document)</p> <p>October 2004</p>	<p>6a. NO. OF PAGES (total containing information Include Annexes, Appendices, etc).</p> <p>142</p>	<p>6b. NO. OF REFS (total cited in document)</p> <p>17</p>
<p>7. DESCRIPTIVE NOTES (the category of the document, e.g. technical report, technical note or memorandum. If appropriate, enter the type of report, e.g. interim, progress, summary, annual or final. Give the inclusive dates when a specific reporting period is covered).</p> <p>CONTRACTOR REPORT</p>		
<p>8. SPONSORING ACTIVITY (the name of the department project office or laboratory sponsoring the research and development. Include address).</p> <p>University of New Brunswick Department of Mechanical Engineering Box 440, Fredericton, NB E3B 5A3</p>		
<p>9a. PROJECT OR GRANT NO. (if appropriate, the applicable research and development project or grant number under which the document was written. Please specify whether project or grant).</p>	<p>9b. CONTRACT NO. (if appropriate, the applicable number under which the document was written).</p> <p>W7707-3-2135</p>	
<p>10a ORIGINATOR'S DOCUMENT NUMBER (the official document number by which the document is identified by the originating activity. This number must be unique to this document.)</p> <p>DRDC Atlantic CR 2004-125</p>	<p>10b OTHER DOCUMENT NOS. (Any other numbers which may be assigned this document either by the originator or by the sponsor.)</p>	
<p>11. DOCUMENT AVAILABILITY (any limitations on further dissemination of the document, other than those imposed by security classification)</p> <p>(<input checked="" type="checkbox"/>) Unlimited distribution</p> <p>(<input type="checkbox"/>) Defence departments and defence contractors; further distribution only as approved</p> <p>(<input type="checkbox"/>) Defence departments and Canadian defence contractors; further distribution only as approved</p> <p>(<input type="checkbox"/>) Government departments and agencies; further distribution only as approved</p> <p>(<input type="checkbox"/>) Defence departments; further distribution only as approved</p> <p>(<input type="checkbox"/>) Other (please specify):</p>		
<p>12. DOCUMENT ANNOUNCEMENT (any limitation to the bibliographic announcement of this document. This will normally correspond to the Document Availability (11). However, where further distribution (beyond the audience specified in (11) is possible, a wider announcement audience may be selected).</p>		

- 13. ABSTRACT** (a brief and factual summary of the document. It may also appear elsewhere in the body of the document itself. It is highly desirable that the abstract of classified documents be unclassified. Each paragraph of the abstract shall begin with an indication of the security classification of the information in the paragraph (unless the document itself is unclassified) represented as (S), (C), (R), or (U). It is not necessary to include here abstracts in both official languages unless the text is bilingual).

This report describes a methodology for completing simulations of flow around a standard bare submarine hull using CFX-5. The simple case of zero yaw is used to demonstrate the process used to set up, run and analyze a simulation. The process of creating the geometry, mesh generation, boundary condition application, solution control and post processing is described. Particular emphasis is placed on building a high quality unstructured mesh for resolving boundary layer flows. Subsequently images of the mesh and results are shown to further the understanding of how to model a domain effectively and efficiently. Efforts to ensure a mesh insensitive solution are shown. Final values are validated against wind tunnel testing.

- 14. KEYWORDS, DESCRIPTORS or IDENTIFIERS** (technically meaningful terms or short phrases that characterize a document and could be helpful in cataloguing the document. They should be selected so that no security classification is required. Identifiers, such as equipment model designation, trade name, military project code name, geographic location may also be included. If possible keywords should be selected from a published thesaurus. e.g. Thesaurus of Engineering and Scientific Terms (TEST) and that thesaurus-identified. If it not possible to select indexing terms which are Unclassified, the classification of each should be indicated as with the title).

submarine
unappended hull
CFD drag validation
RANS drag validation

This page intentionally left blank.

Defence R&D Canada

**Canada's leader in defence
and national security R&D**

R & D pour la défense Canada

**Chef de file au Canada en R & D
pour la défense et la sécurité nationale**



www.drdc-rddc.gc.ca